UNIVERSITÀ DEGLI STUDI DI NAPOLI "FEDERICO II"

in consorzio con
SECONDA UNIVERSITÀ DI NAPOLI
UNIVERSITÀ "PARTHENOPE" NAPOLI
in convenzione con
ISTITUTO PER L'AMBIENTE MARINO COSTIERO - C.N.R.
STAZIONE ZOOLOGICA "ANTON DOHRN"

Dottorato in Scienze ed Ingegneria del Mare
XVIII ciclo

Tesi di Dottorato

Optical properties in the Mediterranean open waters
(*running title*)

Candidato:
Dott. Vincenzo Vellucci

Tutor:
Prof. Maurizio Ribera d'Alcalá
Co-Tutor:
Prof. Vincenzo Saggiomo

Il Coordinatore del Dottorato: Prof. Bruno D'Argenio

2007

Introduction

Two weeks ago, while I was drafting this introduction, it came out the news that the Nobel price awarded by the Norwegian Nobel committee to a person, group, etc. who [*... shall have done the most or the best work for fraternity among nations, for the abolition or reduction of standing armies and for the holding and promotion of peace congresses.*, along with the deepest wishes of Alfred Nobel, had been assigned to the Intergovernmental Panel On Climate Change (IPCC) of the United Nations (ONU) for their effort on analyzing and divulgating climate dynamics as a key component for the well-being of human society.

The choice of the committee, though controversial, is nonetheless a sign that the public perception on environmental themes has grown since the Earth Summit held in Rio de Janeiro 15 years ago, and symbolically reflects the demand of society for scientists to make efforts towards the understanding and prediction of ecosystem responses to environmental changes.

To reach these goals the long term monitoring of the ecosystems is crucial to assess the general trends and to understand the interactions of their components. Models, on the other hand, represent an essential complementary tool to simulate and reconstruct the processes which determine Earth System dynamics. Currently the coupling of the two approaches represent the best tool to address key questions on the environment, as the more information derived from observations we put into models the more we should be able to predict scenarios (Iglesias-Rodrıg *et al.*, 2002; Sarmiento *et al.*, 2004; Smyth *et al.*, 2005, among the others).

Atmosphere, land and sea are the three major systems whose processes regulate climate on Earth. Among the three, the ocean is probably the least studied, due to greater difficulties to carry out direct observations. In this context, ocean color offers a powerful solution to the problem and, in fact, its applications are continuously developing.

It is intruiguing to think that, while modern technology is a prerequisite to exploit the information embedded in water color, the idea is very old. I think that nobody could argue if we include in the history of the technique a few old primitive attempts. For example one could trace back the origin of ocean color, though not strictly oceanic, to 206 BC–AD, at the time of the Western Han dynasty, when the river flowing in the actual Quingai Province in China, appears in the Book of Han under the name of Huang He or Yellow River, indicating the perennial ochre-yellow colour of the muddy water in its final tract before flowing into the Bohai Sea. Also ancient Greeks could claim the paternity of the first use of ocean color, when they named Erythra Thalassa

what is now, along that tradition, the Red Sea. It is more likely that it indicated the location of the basin as the red color was used to indicate the South on the compass, and Herodotus on one occasion used Red Sea and Southern Sea interchangeably, but different renditions report that the name referred to the seasonal blooms of the red coloured cyanobacteria *Trichodesmium erythraeum*, *i.e.*, a proper application of ocean color approach.

Besides those issues of "archaelogical oceanography", it is a fact that enormous advances have occurred in the exploitation of the information deriving from the ocean color. Particularly, in the two last decades, remote sensing of ocean color has been demonstrated to be an invaluable tool for ocean sciences from regional to global scales, with spatial resolution for new generation sensors down to 250 m. Sensor on board of satellite platforms cover the whole globe in a relatively short time (quasi-synoptic) respect to standard oceanic cruises. For example the SeaWiFS sensor mounted on the Orbview satellite is able to cover the whole globe in two days. Moreover space technologies are, on the long run, relatively cheap if compared with the huge amount of information that they can give us.

In its pioneering applications satellite ocean color have been devoted to the retrieving of chlorophyll (Gordon *et al.*, 1980), a ubiquitous pigment in marine algae commonly used as a proxy for biomass. Over the years the capacity to utilize the information contained in the ocean colour has increased. For example, by means of satellite chlorophyll fields it has become possible to obtain the first global estimates of primary productivity in the ocean at global scale thus discovering its importance for the biogeochemical balance of planet Earth (Longhurst *et al.*, 1995).

Other applications of ocean color span from the detection of algal blooms dominated by single species such as *Trichodesmium* (Subramaniam *et al.*, 2002) or by groups such as Haptophytes (particularly Coccolithophores), Diatoms, and cyanobacteria (*Prochlorococcus spp.* and *Synechococcus spp.* (Brown and Yoder, 1994; Sathyendranath *et al.*, 2004; Alvain *et al.*, 2005), to the monitoring of harmful algal blooms (Stumpf *et al.*, 2003), the detection of *Sargassum spp.* (Gower *et al.*, 2006), the estimate of particulate organic carbon (Stramski *et al.*, 1999) the absorption coffiecient of coloured dissolved organic matter and phytoplankton (Carder *et al.*, 1999) and so on, till the derivation of optical indexs for phytoplankton physiology (Behrenfeld *et al.*, 2005).

The interpretation of ocean color imagery needs a parallel investigation of *in situ* bio-optical properties. The marine general circulation leads to the formation of biogeochemical provinces (Longhurst, 1995) which may also form bio-optical provinces, in that their optical properties covary differently with the chlorophyll content of the water body (Mueller and Lange, 1989; Siegel *et al.*, 2005a). The most recent example

of such regionality is the Pacific Subtropical Gyre (PSG), where the persistent anti-cyclonic circulation acts as a barrier for the detrital matter of biological origin that accumulates causing an ocean color anomaly (Dandonneau *et al.*, 2003; Claustre and Maritorena, 2003; Grob *et al.*, 2007).

Even though the Mediterranean Sea is not so crucial as the PSG for the global biogeochemical cycles, it is still the most important semi-enclosed basin on the Earth for both geographical and social reasons and displays peculiar bio-optical properties. The Mediterranean Sea is a site where several physical process occur in a relatively small area thus allowing for monitoring the effects of climatic changes on short time scales. Its restricted exchange with the neighboring Atlantic Ocean, the intense urbanization of its coast, the proximity with a large desert, the position between two important atmospheric systems such as North Atlantic Oscillation and Monsoon are among the factors that contribute to determine its complexity and, to a certain extent, its vulnerability (D'Ortenzio, 2003, and references therein). Last but not least, the basin hosts important commercial interests, linked to tourism and fisheries, it is estimated that, in 2006, almost 20 % of the tourists all over the world spent their holidays in the southern Mediterranean Europe (`www.unwto.org`) in places such as the Gulf Of Naples (Golfo di Napoli), the French Riviera (Côte d'Azur) or the South Pontino (Sud Pontino); and the major part of the Bluefin Tuna (*Thunnus thynnus*) catches are made in the basin (`www.fao.org`).

As for what ocean color concerns, different hypotheses (summarized in the chapter 2.5) on its anomalous bio-optical response have been put forward so far, but a definitive answer is still lacking. This study has then been focused on the bio-optical properties of the Mediterranean Sea in the attempt, through an in depth analysis of a sufficiently representative data set, of improving our understanding of what are the drivers of the peculiar bio-optical properties of the Mediterranean.

The underlying hypothesis of the study was that those anomalies might embed information on the functioning of the whole Mediterranean Ecosystem, either within the water column or because of the external forcings and fluxes. And the underlying expectation was that what could be learned on the link among bio-optics and key traits of the ecosystem from the Mediterranean could be of some benefit for other systems as well. Along this path the possibility to further refine retrieval algorithms was considered an important by-product. I structured the text as follows:

- in chapter 1., I made a synthetic review of ocean optics, only for those processes and parameterizations that were relevant for my study.

- in chapter 2., I described the data set and the analyses to derive the IOPs, AOPs and other variables;

- in chapter 3., I reported the current views on why the Mediterranean color is an issue, with first results on regional chlorophyll retrieving algorithm;
- In chapter 4–6, I reported the results of the regional parameterization for IOPs and AOPs;
- In chapter 7–8, I finally synthesized the main implications of my analysis and what conclusions might be drawn from them.

1. Introduction to Optical Oceanography

Historically optical oceanography is considered a branch of Physics being its main focus the radiative transfer in the marine environment. Due to the strong coupling between light and the marine biota, I think it should be better considered a Biophysical discipline. There is no doubt that it is an interdisciplinary science and, nowadays, its many crucial applications are related to answering biological questions at both local and global scale. Light has a crucial role in shaping responses of marine organisms from the evolutionary to the short time scales, and the organisms reciprocally modify, directly or indirectly, the radiant field wich affects the functioning of the whole Earth system. This chapter is far from being an exhaustive synthesis of bio-optics, which would be beyond the scope of my work, and, certainly, beyond my present knowledge. I only selected few topics, starting from the basic aspects, that were relevant for my work. In particular, after introducing light and its physical quantification, I will describe some basic processes and the main optical properties of a water body, generally classified into inherent and apparent optical properties (IOPs and AOPs respectively), focusing especially on the former. A parcel of water, in fact, changes its optical charachteristics (*i.e.* the way it interacts with ligth) due to its content. IOPs are those properties that only depend upon the medium, whereas AOPs depends also upon the structure of the light field.

Because many basic processes are described in textbooks, I omitted, for what them concerns direct reference to the source. Preisendorfer (1976); Kirk (1983); Mobley (1994) are the textbooks I have been using for this section.

1.1 Nature of Light, Radiometry and Interface Processes

After traveling for about 144 Gm through the space, it may happen that a light beam, originated from nuclear fusions on the Sun (known as proton-proton cycle), reaches the Earth atmosphere and, eventually, the Earth surface. Light consists of packets of electromagnectic energy, named photons, running through space with a speed $c = 2.998 \cdot 10^8$ ms^{-1}, having properties of both a particle and a wave but beeing none of them. In fact each photon has an associated wavelength (λ) and frequency (ν) but is a quantic unit too. Wavelength and frequency of a photon are related through its velocity according to the following law:

$$c = \lambda\nu. \tag{1.1}$$

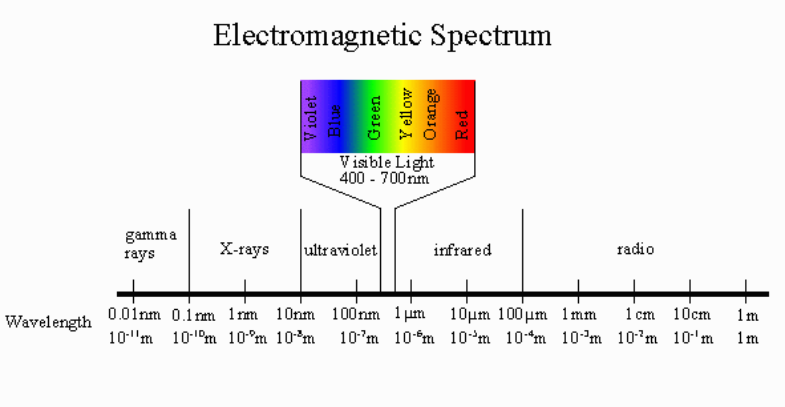

Figure 1.1: Wavelengths of the electromagnetic spectrum of solar radiation and their partitioning into various bands. Picture from http://www.srrb.noaa.gov/.

The discrete energy of a photon (q) depends on its frequency (thus on wavelength too) through the Plank constant $h = 6.626 \cdot 10^{-34}$ Js:

$$q = h\nu = \frac{hc}{\lambda}. \tag{1.2}$$

The amount of solar energy for unit area and time (solar irradiance, E_s) that arrives at the mean Earth–Sun distance is ≈ 1367 Wm^{-2} (Frohlich, 1983). This values is known as *solar constant*, but it undergoes some variations due to solar actvities and to the elliptical trajectory of the Earth around the Sun.

The solar spectrum is usually divided into wavelenght bands **Fig. 1.1**. The visible domain (400–700 nm is that of major interest in optical oceanography (and in the present study), because it provides energy to marine authotrophs to perform phothosynthesis, and it represents about 38 % of solar energy. However the interest of optical oceanography in the near ultraviolet domain (350–400 nm, is rapidly increasing because of its potentiality to damage organisms due to its high energy.

Spectral radiance is one of the basic radiometric quantitities. If we consider the coordinates and angles as established in **Fig. 1.1**, it is defined as the amount of radiant energy per unit area (A), time (t), wavelength and solid angle (Ω) coming from the ξ direction:

$$L(\xi, \lambda) = \frac{\Delta Q}{\Delta A \Delta t \Delta\Omega \Delta\lambda} \qquad (\text{W m}^{-2}\ \text{sr}^{-1}\ \text{nm}^{-1}); \tag{1.3}$$

where Ω is centered on ξ and is defined as the ratio between an area projected onto a sphere and its squared radius, and is measured in steradiants (sr). The dipendence on time and coordinates of measure are omitted for simplicity.

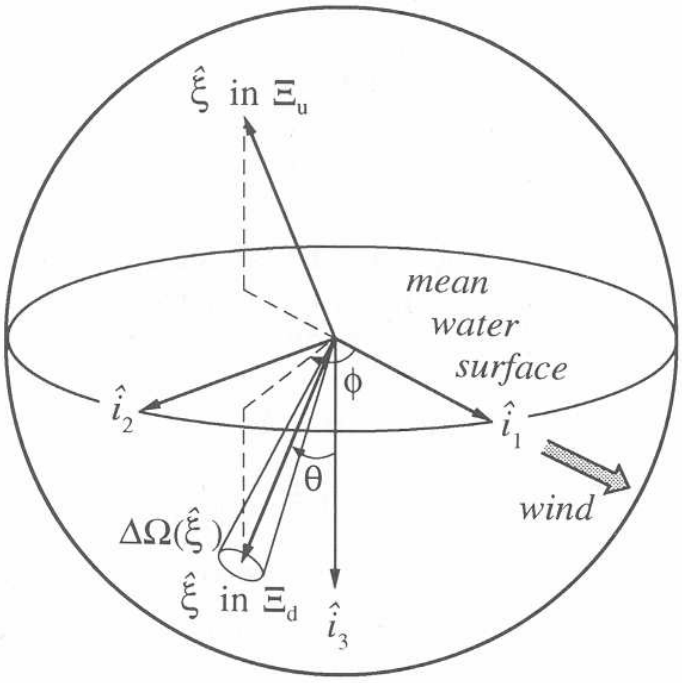

Figure 1.2: Definition of the polar coordinates (θ,ϕ), and of solid angle $\Delta\Omega$ centered on ξ. Ξ_d and Ξ_u are the downward and upward hemispheres of directions. Figure from Mobley (1994).

If we integrate the spectral radiance in all downward directions reaching a certain surface ΔA, we obtain the spectral downward plane irradiance ($E_d(\lambda)$):

$$E_d(\lambda) = \int_{\phi=0}^{2\pi} \int_{\theta=0}^{\pi/2} L(\theta,\phi,\lambda) |\cos\theta| \sin\theta d\theta d\phi \qquad (\text{W m}^{-2}\ \text{nm}^{-1}); \tag{1.4}$$

where the cosine of the angle between the incident beam and the perpendicular to the surface, accounts for the effective area reached by the photon flux $\Delta A|cos\theta|$ (*i.e* the area is projected onto a plane perpendicular to the beam). The spectral upward plane irradiance ($E_d(\lambda)$), instead, is obtained by integrating $L(\xi,\lambda)$ in all upward directions (*i.e.* the second integral in **Eq. 1.4** becomes $\int_{\theta=\pi/2}^{\pi}$).

Finally, if we consider all photons directed to a point or a sphere we may define the spectral total scalar irradiance:

$$E_o(\lambda) = \int_{\phi=0}^{2\pi} \int_{\theta=0}^{\pi} L(\theta,\phi,\lambda) \sin\theta d\theta d\phi \qquad (\text{W m}^{-2}\ \text{nm}^{-1}); \tag{1.5}$$

The scalar irradiance over the visible wavelenghts is a quantity of practical use in

oceanography, especially in the biological domain and has been named photosynthetically available radiation because it is the energy that autothrops may utilize to perform phothosynthesis:

$$PAR = \int_{400}^{700} \frac{\lambda}{hc} E_o(\lambda) d\lambda, \qquad \text{(photons m}^{-2}\text{ s}^{-1}\text{)}. \tag{1.6}$$

PAR is generally is expressed in terms of µE m^{-2} s^{-1}, where 1 Einstein (E) corresponds to 1 mol $(6.023 \cdot 10^{23})$ of photons.

When light reaches the Earth surface, there is 70 % probability to encounter the ocean and then to interact with seawater. At the air-water interface light maybe either reflected (R) or transmitted (T) into the water column according to Fresnel's law for perpendicular ($\perp$) and parallel ($\parallel$) polarization planes of the electromagnetic field respect to the plane of the sea surface (see **Fig. 1.3(a)**):

$$R_\perp = \left[\frac{\sin(\phi_t - \phi_i)}{\sin(\phi_t + \phi_i)}\right]^2 = \left[\frac{n_a \cos(\phi_i) - n_w \cos(\phi_t)}{n_a \cos(\phi_i) + n_w \cos(\phi_t)}\right]^2; \tag{1.7}$$

$$R_\parallel = \left[\frac{\tan(\phi_t - \phi_i)}{\tan(\phi_t + \phi_i)}\right]^2 = \left[\frac{n_a \cos(\phi_t) - n_w \cos(\phi_i)}{n_a \cos(\phi_t) + n_w \cos(\phi_i)}\right]^2; \tag{1.8}$$

$$T_\perp = 1 - R_\perp; \quad T_\parallel = 1 - R_\parallel; \tag{1.9}$$

where the polarization refers to the plane of oscillattion of the electric component of light. Because of the different propagation velocitiy among the two media, the fraction of light that crosses the interface changes its direction (*i.e.* is refracted) according to Snell's law:

$$\frac{\sin(\phi_i)}{\sin(\phi_t)} = \frac{n_w}{n_a}. \tag{1.10}$$

n_a and n_w denote the refractive index of air and sea water whereas ϕ_i and ϕ_t are the angles between the incident and transmitted beams with the perpendicular to the plane of incidence (see **Fig. 1.3(a)**). Snell's law stands in the opposite direction too, *i.e.* when light exits from the water column toward the sky.

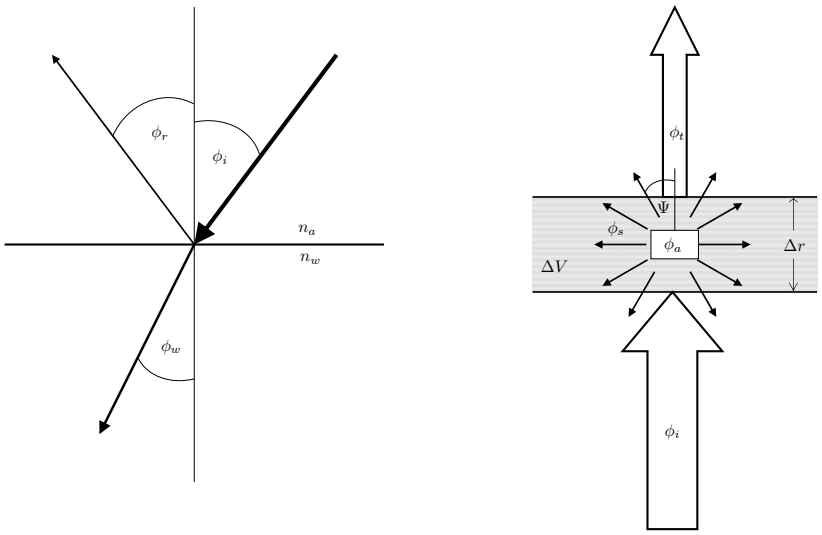

(a) (b)

Figure 1.3: (a) A solar flux, hinting the sea surface with an angle ϕ_i, refracted into seawater with an angle ϕ_w and reflected with an angle ϕ_r. (b) A collimated beam of ligth of intensity ϕ_i enters into a different medium of volume ΔV and pathlenght Δr, part of the light is absorbed (ϕ_a) part is scattered (ϕ_a) at various angles (Ψ) and part is transmitted outside the medium (ϕ_t).

1.2 Inherent and Apparent Optical Properties

Once entered the seawater, light interacts with the particulate and dissolved compounds present in the medium and the medium itself. There are two phenomena that contribute to modify the radiant field underwater: absorption and scattering. Absorption occurr when a photon is captured by a molecule that increases its energy and transforms it in a non radiative form. For a collimated beam of light of spectral radiant power $\phi_i(\lambda)$ ($\mathrm{Wn^{-1}m}$) illuminating a volume of water of thickness Δr, the spectral absorption coefficient is defined as:

$$a(\lambda) = \lim_{\Delta r \to 0} \frac{A(\lambda)}{\Delta r}, \qquad (\mathrm{m^{-1}}), \tag{1.11}$$

where $A(\lambda)$ is the fraction of incident power that is absorbed by the medium, and $\phi_a(\lambda)$ the absolute quantity:

$$A(\lambda) = \frac{\phi_a(\lambda)}{\phi_i(\lambda)} \tag{1.12}$$

Scattering instead takes place when a photon is only deviated either by a particle or by the inhomogeneities of the dielectric constant of seawater; the latter having an effect that is similar to Rayleigh scattering for gases, that means light is scattered half forward and half backward. Moreover scattering maybe elastic or inelastic, in the second case a change of energy (*i.e.* wavelength) takes place too. When there is no loss of radiant energy the scattering is named elastic, when some energy is lost because of transpectral energy transfer, *e.g.* fluorescence or Raman, the scatter is named inelastic. If $B(\lambda)$ is the fraction of incident power that is deviated by the medium, the spectral scattering coefficient is defined as:

$$b(\lambda) = \lim_{\Delta r \to 0} \frac{B(\lambda)}{\Delta r}, \qquad (\mathrm{m}^{-1}). \tag{1.13}$$

In this case $B(\lambda)$ is the fraction of incident power that is lost (*e.g.* do not re-enter the photon flux) deviated by the medium by the beam, but propagates in different directions:

$$B(\lambda) = \frac{\phi_s(\lambda)}{\phi_i(\lambda)}; \tag{1.14}$$

with $\phi_s(\lambda)$ the absolute quantity of light scattered. it is a common practice in optical oceanograpy to divide the scattered light and, therefore, the scattering coefficients into two components perpendicular to a plane parallel to the sea surface:

$$b(\lambda) = b_f(\lambda) + b_b(\lambda). \tag{1.15}$$

The suffix f indicates the forward direction (*i.e.* towards the sea bottom), whereas b indicates the backward direction (*i.e.* towards the sea surface). The latter is of particular interest because it contains the information of the ocean colour. Since scattering is just dispersion of light in different directions, it is important to characterize its angular dependence. To this aim it has been introduced the volume scattering function ($\beta(\psi, \lambda)$, $\mathrm{m}^{-1}\mathrm{sr}^{-1}$), that is the amount of light in proportion to the incident flux for unit distance and unit solid angle (the radiant flux per unit solid angle scattered in the Ψ direction, per unit pathlength, expressed as a proportion of the incident flux). Thus the scattering and backscattering coefficients can be rewritten as:

$$b(\lambda) = 2\pi \int_0^{\pi} \beta(\Psi, \lambda) \sin(\Psi) d\Psi; \tag{1.16}$$

and

$$b_b(\lambda) = 2\pi \int_{\pi}^{\pi/2} \beta(\Psi, \lambda) \sin(\Psi) d\Psi; \tag{1.17}$$

where Ψ is the scattering angle (**Fig. 1.3(b)**). The backscattering efficiency, is instead defined as:

$$\tilde{b}(\lambda) = \frac{b_b(\lambda)}{b(\lambda)}. \tag{1.18}$$

It indicates the probability, for a given optically active components, that a scatterd photon has to be scattered back towards the hemispace of origin.

On those bases, it is introduced the beam attenuation coefficient. *i.e.*, the total loss of radiant energy from the original beam, wich is the sum of the absorption and scattering coefficients:

$$c(\lambda) = a(\lambda) + b(\lambda), \qquad (\mathrm{m}^{-1}). \tag{1.19}$$

It has been demonstrated that absorption and scattering coefficients have additive properties (Preisendorfer, 1961). This means that it is possible to resolve them in various components at our convenience, each of them with its own charachteristics, and with amplitude depending on the concentration of the optically active component in the medium. The optically significant constituents that are the main responsibles of the attenuation coefficients at sea are:

- seawater;
- viruses;
- bacteria;
- colloids;
- phytoplankton;
- non algal particles;
- coloured dissolved organic matter;
- bubbles.

The optical properties of each of these components will be summarized in the following section (1.3). In most of the studies not all the components are resolved and the total absorption ($a_t(\lambda)$) is factorized as (cit, among the others):

$$a_t(\lambda) = a_w(\lambda) + a_{ph}(\lambda) + a_{nap}(\lambda) + a_{ys}(\lambda); \tag{1.20}$$

where $a_w(\lambda)$ is the absorption coeficient of seawater, $a_{ph}(\lambda)$ is the absorption coefficient of phytoplankton, $a_{nap}(\lambda)$ is the absorption coefficient of non-algal particles and $a_{ys}(\lambda)$ is the absorption coefficient of coloured dissolved compounds.

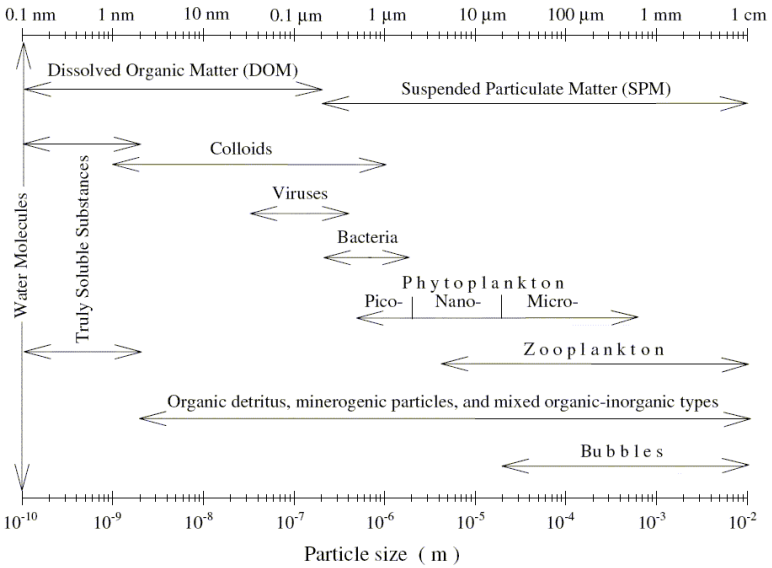

Figure 1.4: Size ranges of various optically active components of marine waters. Figure from (Stramski *et al.*, 2004)

Instead the total scattering and backscattering coefficients (respectively $b_t(\lambda)$ and $b_{bt}(\lambda)$) are factorized as:

$$b_t(\lambda) = b_w(\lambda) + b_p(\lambda); \tag{1.21}$$

and

$$b_{bt}(\lambda) = b_b w(\lambda) + b_{bp}(\lambda); \tag{1.22}$$

where the subscript w again indicates seawater, and $b_p(\lambda)$ and $b_{bp}(\lambda)$ are the scattering and backscattering coefficients of all particulate (with the mechanical definitions of CDOM also dissolved compounds are included, see section 1.3).

If we consider a homogeneous population of N particles suspended in a V volume as the only active components, we can introduce the optical efficiency factors ($Q_a(\lambda)$ and $Q_b(\lambda)$ respectively, the sum being $Q_c(\lambda)$, adimensional) as:

$$a(\lambda) = Q_a(\lambda)\frac{N}{V}s_g; \tag{1.23}$$

$$b(\lambda) = Q_b(\lambda)\frac{N}{V}s_g. \tag{1.24}$$

The cross-sections of a particle for absorption, scattering, backscattering and attenu-

ation are the product of the geometrical cross-section and the corresponding efficiency factor:

$$\sigma_i(\lambda) = Q_i(\lambda)s_g; \tag{1.25}$$

where the suffix i stays for a, b, b_b or c. The optical efficiency factors are the ratio of radiant energy that a particle absorbs or scatters respect to the radiant energy that hints its geometrical cross section s_g. For a spherical particle of diameter d, s_g can be calculated as:

$$s_g = \frac{\pi}{4}d^2. \tag{1.26}$$

If the population of particles has not the same size, as likely to occur in nature, it can be expressed in terms of a size distribution function $N(d)$ (the number N of partcles having a d diameter), then **Eq. 1.23** and **Eq. 1.24** become:

$$a(\lambda) = \int_0^\infty Q_a(\lambda)N(d)\frac{\pi}{4}d^2\mathrm{d}d; \tag{1.27}$$

$$b(\lambda) = \int_0^\infty Q_b(\lambda)N(d)\frac{\pi}{4}d^2\mathrm{d}d. \tag{1.28}$$

In the same way it is also possible to introduce the optical efficiency factor for the backscattering $Q_{b_b}(\lambda)$. The optical efficiency factors for particles can be determined according to Mie-Lorentz theory (Mie, 1908; Van de Hulst, 1957; Bricaud and Morel, 1986), as function of Mie coefficients that depend on the refractive index of the particle, a complex quantity, relative to its embedding medium (m) and the relative size of the particle (α) respect to the wavelength in the surrounding medium (λ_w). m is a complex number composed of a real part (n) and an imaginary part($n^{'}$):

$$m = \left(\frac{n_p}{n_w}\right) - i\left(\frac{k_p}{n_w}\right) = n - in^{'}; \tag{1.29}$$

and

$$\alpha = \frac{\pi d}{\lambda}n_w = \frac{\pi d}{\lambda_w}. \tag{1.30}$$

The real part of the refractive index of particles present in the marine environment is un the range of 0.75 (for air bubbles) to 1.2 for mineral particles. If m is ≈ 1 the anomalous diffraction approximation of Van de Hulst can be adopted and $Q_c(\lambda)$ and

$Q_a(\lambda)$ can be derived from the following equations:

$$Q_c(\rho) = 2 - 4\exp(-\rho\tan\xi)\left[\frac{\cos\xi}{\rho}\sin(\rho-\xi) + \left(\frac{\cos\xi}{\rho}\right)^2\cos(\rho-2\xi)\right] + 4\left(\frac{\cos\xi}{\rho}\right)^2\cos 2\xi; \quad (1.31)$$

$$Q_a(\rho) = 1 + \frac{\exp(-2\rho\tan\xi)(2\rho\tan\xi+1)-1}{2\rho^2\tan^2\xi}; \quad (1.32)$$

where $\rho = 2\alpha(n-1)$ and $\tan\xi = n^{'}/(n-1)$. If we define another parameter $\rho' = 4\alpha n'$ $(= 2\rho\tan\xi)$, **Eq. 1.32** can be rewritten in a simpler form:

$$Q_a(\rho') = 1 + 2\frac{\exp(-\rho')}{\rho'} + 2\frac{\exp(-\rho')}{\rho' 2}. \quad (1.33)$$

Then $Q_b(\lambda)$ can be determined as:

$$Q_b(\rho) = Q_c(\rho) - Q_a(\rho). \quad (1.34)$$

For the estimate of the $Q_{b_b}(\lambda)$ factor the anomalous diffraction approximation cannot be adopted, and the angular scattered intesities $i_1(\theta,\alpha,m)$ and $i_2(\theta,\alpha,m)$ have to be computed first for a given relative size and complex refraction index. The two intensities are the squares of the moduli of the complex amplitude functions relative to the perpendicular and parallel electric fields respect to scattering plane, and are functions of the Mie coefficients. $Q_{b_b}(\lambda)$ can be then obtained from:

$$Q_{b_b}(\alpha,m) = \alpha^{-2}\int_{\pi/2}^{\pi}\frac{i_1(\theta,\alpha,m)+i_2(\theta,\alpha,m)}{2}\sin\theta d\theta. \quad (1.35)$$

The equivalent of $c(\lambda)$ for natural light at sea is the spectral diffuse attenuation coefficient $(K(\lambda))$. While the first is measured both in the lab or at sea by means of an artificial light, the latter can be only measured at sea with ambient light, thus it is an AOP. In fact, with some particular exceptions such as nepheloid layers or bottom reflection, light generally decreases with depth and a $K(\lambda)$, function of depth, can be retrieved by measuring light attenuaton along the water column. This implies that different $K(\lambda)$ can be defined depending on how light is measured to retrieve them. One of them, and most commonly used, is the spectral diffuse attenuation coefficient for downwelling plane irradiance $K_d(\lambda,z)$ and can be defined as:

$$K_d(\lambda,z) = -\frac{d\log E_d(\lambda,z)}{dz}, \qquad (\mathrm{m}^{-1}). \quad (1.36)$$

Other $K(\lambda)$ such as K_u, K_{PAR} and K_{PAR} *etc.* can be similarly defined. $K(\lambda)$ is an extremely important variable in marine ecosistems, having implications on physical processes by regulating heat transfer (Murtugudde *et al.*, 2002; Marzeion *et al.*, 2005; Manizza *et al.*, 2005; Sweeney *et al.*, 2005), and on biological processes by limiting photosynthesis (Gran and Braarud, 1935; Sverdrup, 1953; Nelson and Smith Jr, 1991). Spactral surface reflectance ($R(\lambda)$) and remote sensing reflectance ($R_{rs}(\lambda)$) are two AOPs of particular interest because they can be retrieved with remote sensing tecniques and represent what is generally called the ocean colour. $R(\lambda)$, also called iradiance ratio, is the ratio between upwelling and downwelling plane irradiance just below the sea surface:

$$R(\lambda) = \frac{E_u(0^-, \lambda)}{E_d(0^-, \lambda)}. \tag{1.37}$$

$R_{rs}(\lambda)$ instead is defined as the ratio between the upwelling radiance and downwelling irradiance just above the sea surface:

$$R_{rs}(\lambda) = \frac{L_u(0^+, \lambda)}{E_d(0^+, \lambda)} = \frac{L_w(\lambda)}{E_d(0^+, \lambda)}, \qquad (\mathrm{sr}^{-1}); \tag{1.38}$$

where $L_w(\lambda)$ is the water leaving radiance and is a common way to call the upwelling radiance just above the sea surface. The ratio between upwelling irradiance and upwelling radiance is the $Q(\lambda)$ factor (not to be confused with the efficiency factors):

$$Q(\lambda) = \frac{E_u(\lambda)}{L_u(\lambda)}, \qquad (\mathrm{sr}^{-1}). \tag{1.39}$$

This factor takes into account the anisotropy of the radiant field. If the radiance distribution is homogeneous, as for a completely diffuse radiation, the field is said to be isotropic and $Q = \pi$. Obviously $R(\lambda)$, $R_{rs}(\lambda)$ and $Q(\lambda)$ may also have a dependence on depth, but here I have chosen to omit this dependence as I will use them only at surface in the present work. There are relations between IOPs and AOPs, that will be introduced directly in the text when needed.

1.3 Optically Active Constituents of Marine Waters

Seawater

Seawater is the medium in which all optically active components are suspended. It is a mixture of water and soluble ions, mainly Cl^- and Na^+. Seawater optical properties

are generally considered well known. They are subject only to very slight variations due to temperature, salinity and pressure. Seawater has a high absorption in the red which decreases towards the shorter wavelengths with an absorption minimum between at 415–420 nm (**Fig. 1.5**). However there is still a little level of uncertainty on the absolute values of its absorption coefficients. These uncertainties derive basically from the difficulties to obtain a highly purified laboratory water or to find clear natural waters, and from instrumental limits for eliminating scattering.

Absorption coefficients from Smith and Baker (1981) derived from the analysis of diffuse attenuation coefficients on very clear waters from Sargasso Sea and Crater Lake, has been adopted for a long time. A decade ago Pope and Fry (1997) published absorption coefficients for pure water measured with an integrating cavity sphere, which were significantly lower in the blue domain. Recently Morel *et al.* (2007b), using the same approach of Smith and Baker (1981), reported unexpected low absorption coefficients from the Pacific Subtropical Gyre, where distance from land combined with long residence time for water trapped into the gyre which causes an intense exposure to photobleaching UV radiation, can generate a particularly pure seawater.

Scattering coefficient of this medium exponentially decreases with increasing wavelength (**Fig. 1.5**) and is commonly expressed as:

$$b_w(\lambda) = 5.826 \cdot 10^{-3} \left(\frac{400}{\lambda}\right)^{4.322}; \tag{1.40}$$

whereas the backscattered term ($b_{bw}(\lambda)$) is half of the total scattering (Morel, 1974).

Viruses

Viruses are among the smallest form of organized organic matter. There is still a debate whether they have to be cosidered living forms or not. Certainly viruses are the most abundant biologically related entities in the water column of the world's oceans, and the second largest component of biomass after prokaryotes. Their dimension is between < 0.03–0.75 µm with typical concentrations at sea of the order of 10^{12}–10^{14} m^{-3} and a refractive index $n \approx 1.06$. (Bratbak *et al.*, 1992; Suttle, 2005; Balch *et al.*, 2000).

Until the last decade of the XX century the optical properties of viruses were not known. First theoretical studies indicate a very high backscattering efficiency due to the small dimensions, a small contribution to total scattering (low scattering efficiency) but a not negligible part of $b_{bt}(\lambda)$ at highest concentration (Stramski and Kiefer, 1991; Stramski and Mobley, 1997). Newer laboratory studies, though substan-

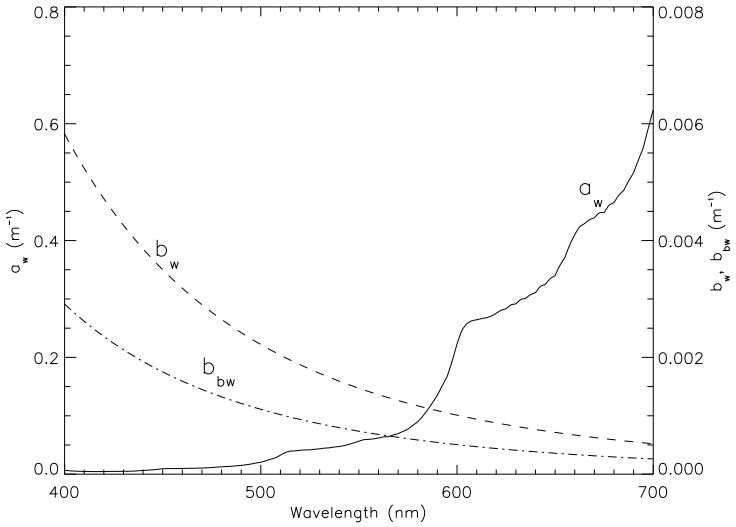

Figure 1.5: Spectral absorption ($a_w(\lambda)$), scattering ($b_w(\lambda)$) and backscattering ($b_{bw}(\lambda)$) coefficients of seawater.

tially confirming previous works, underline that it is unlikely that viruses may have an important role in the bulk backscattering coefficient (Balch *et al.*, 2000). However viruses play an important role in modifying the optical properties of the water through the lysis of microbial populations (Balch *et al.*, 2002; Simis *et al.*, 2005).

Absorption of light by viruses is generally considered negligible and it is not taken into account in optical modelling (Mobley and Stramski, 1997; Stramski and Mobley, 1997; Stramski *et al.*, 2001).

Bacteria

Heterotrophic bacteria (HBAC) are the smallest living organisms on earth (0.2–1 µm, generally peaking in the 0.4–0.7 µm range (Ducklow, 1986)) whose role in the marine food webs has become clearer only in the 80's (Azam *et al.*, 1983). They are part of the picoplankton, and in the marine waters their typical number concentrations are 10^{11}–10^{13} m^{-3}.

Morel and Ahn (1990) and Stramski and Kiefer (1991) reported some estimates on bacterial optical properties. The refractive index was estimated to vary between 1.04 and 1.07 beeing almost wavelength independent. $Q_b(\lambda)$ was shown to change with wavelength in proportion to λ^{-2} with values ranging between 0.25 and 0.7 at 400 nm; whereas $Q_{b_b}(\lambda)$ was approximately wavelength independent ranging between $6 \cdot 10^{-4}$ and $2 \cdot 10^{-3}$. With these characteristics HBAC, at concentrations usually found in

nature, represent a significant source of both scattering and backscattering among microorganisms, especially at low Chl$-a$ concentrations. These results contrasted with previous estimates on the relative importance of HBAC scattering (Kopelevich *et al.*, 1987) mainly due to a low cell abundance, but were substantially confirmed by more recent estimates by Stramski *et al.* (2001), though some lower refractive indexes (1.02) were recorded for some species like *Vibrio sp.* and *Bacillus mycoides* (Kokorin *et al.*, 1994).

Absorption spectra of HBAC show a main peak centered at 412–415 nm and small humps at 515–520 and 555 nm attributable to cytochromes that are likely to be the main absorbing component of these organisms Morel and Ahn (1990). Their contribution to $a_t(\lambda)$ is low but not fully negligible, especially at shortest wavelegths where they can account for 8 % in generic oceanic oligotrophic conditions (Stramski *et al.*, 2001). Carotenoid containing HBAC have also been found in marine environments, showing typical absorption peaks in the blue centered at 432, 458 and 5488 nm, with an absorption cross section in this region at least twice of that of non pigmented HBAC (Stramski and Kiefer, 1998). Pane *et al.* (1996) showed that astaxanthin was the pigment responsible for the absorption of *Bacillus firmus*, isolated from a sea water rock pool. However the absorption spectrum of astaxanthin does not match that described in Stramski and Kiefer (1998), having a unique peak at 479 nm in methanole solution (Jeffrey *et al.*, 1997). So it is likely, that HBAC containing different carotenoids may exist in natural waters (see also Du *et al.* (2006)). The abundance and relative importance of pigmented HBAC and so their possible impact on oceanic optical properties is still unclear. Recently Du *et al.* (2006) reported abundances of pigmented HBAC of the order of 10^9 m^{-3} in the surface waters of the oligotrophic North pacific and China Sea with a few % contribution to total bacterial abundance. If these concentrations of pigmented HBAC are confirmed, it is unlikely that they can have an important impact on the optical properties, namely total absorption coefficients, however an accurate estimate is still needed.

Colloids

Microparticles, macromolecules and aggregates of molecules of dimensions ranging between 0.001–1 µm are generally included in the definition of colloids, i.e. particles large enough to have an interface but not enough to be subjected to settling by gravity. They are the most abundant particles at sea, accounting up to 50 % of the dissolved organic carbon, with residence times of about 10 d. Typical concentrations for small (< 0.02 µm) and large (0.04–1 µm) colloids are of the order of 10^5 and 10^{13}, exceeding in both cases the abundance of microbial particles of the same size class.

(Moran and Buesseler, 1992; Wells, 1998; Stramski and Wozniak, 2005, and references therein).

First theoretical studies indicated that submicron particles could account for a sgnificant part of scattering and in particular in the backward direction (Brown and Gordon, 1974; Gordon, 1974). The major limit of the analyses was the lack of the size distribution and concentration in this range. Once filled this gap, using data covering various oceanic conditions for both small and large sized colloids, Stramski and Wozniak (2005) calculated the optical scattering and backscattering coefficients for various assemblages of colloidal particles with two assumed refractive indexes, $n = 1.04$ and $n = 1.18$ respect to water. Their results show that small colloids undergo large variations in natural assembleges for $Q_b(\lambda)$ (2-3 orders of magnitude) and $Q_{b_b}(\lambda)$ (1-2 orders of magnitude), due to size distribution, number and refractive index. Instead large colloids have sensible variations (2 order of magnitude) for both $Q_b(\lambda)$ and $Q_{b_b}(\lambda)$ only by changing the refractive index. Considering their average conservative estimates (i.e. $n = 1.04$), the resulting bulk scattering coefficients for small particles are comparable to that of pure seawater, whereas large particles are greater of more than an order of magnitude. This means that, while small colloids play a little role, large colloids may give a significative contribution to $b_t(\lambda)$. The estimates for the bulk backscattering coefficients display a more clear pattern. Small colloids have a $b_b(\lambda)$ similar to seawater in the red portion of the spectrum but lower in the blue (about half at 440 nm), whereas for large colloids the average $b_b(\lambda)$ spectrum is almost flat, with lower values in the blue region and higher values at $\lambda > 500$nm respect to seawater. This means that colloids in general may represent an important part of $b_{bt}(\lambda)$.

Little is known about the absorption coefficients of colloids. For the classical measurements protocols, they are usually included within the absorption of coloured dissolved organic matter. The absorption of colloids in the UV domain has been recently investigated (Floge and Wells, 2007). Results show that large sized colloids are positively correlated with $a_{ys}(\lambda)$ in the blu region, suggesting their contribution in the optical signature of CDOM, but it is unclear wether they can influnce the spectral slope cf CDOM or not.

Phytoplankton

Phytoplankton are photosynthetic unicellular (or colonial) algal organisms with a great diversity of species which reflects in a large variability of shape, size and concentration. Their role in the biosphere on Earth is crucial, as they account for about half of the primary production (*i.e.* the fixation of organic carbon at the lowest level

of the marine food web) (Behrenfeld and Falkowski, 1997). Phytoplankton dimensions range between 0.5 µm to more than 200 µm, and they are commonly classified into Pico- (< 2 µm), Nano- (≥ 2 µm and < 20 µm) and Microphytoplankton (≥ 20 µm).

Absorption coefficients of phytoplankton ($a_{ph}(\lambda)$) are mainly related their chlorophyll-a (Chl$-a$) and accessory pigments concentrations within chloroplasts and in oceanic case I waters represent the major source of variability of $a_t(\lambda)$ (Bidigare *et al.*, 1989; Sathyendranath *et al.*, 1987; Hoepffner and Sathyendranath, 1991, 1993; Aguirre-Gomez *et al.*, 2001; Barlow *et al.*, 2002). In general phytoplankton have two main absorption maxima centered in the blu and red whose presence is due to Chl$-a$, and a minimum in the green (**Fig. 1.6**). The so called *package effect* (Duysens, 1956; Kirk, 1975; Morel and Bricaud, 1981), the size spectrum of the algal communities (Ciotti *et al.*, 2002; Bricaud *et al.*, 2004; Devred *et al.*, 2006), light intensity and quality (Vesk and Jeffrey, 1977; Fujiki and Taguchi, 2002; Stomp *et al.*, 2004) nutrients quality and availability (Cleveland and Perry, 1987; Leong and Taguchi, 2005) and circadian rhytms (Bruyant *et al.*, 2005; Ragni and Ribera d'Alcalá, 2007) represent other sources of variability that interplay within oceanic circulation in shaping the absorption spectrum of phytoplankton. One of the commonly adopted empirical model is to express $a_{ph}(\lambda)$ as a function of Chl concentration (Prieur and Sathyendranath, 1981; Morel, 1991; Cleveland, 1995; Bricaud *et al.*, 1995, 1998; Devred *et al.*, 2006):

$$a_{ph}(\lambda) = \alpha(\lambda)\mathrm{Chl}^{\beta(\lambda)}; \tag{1.41}$$

with the range of variation for $a_{ph}(\lambda)$ of the order of $10^{-3} - 10^{-1}$ m^{-1} for Chl spanning between $10^{-2} - 10^{2}$ µg l^{-1}.

Phytoplankton species are very diverse for their optical properties and have been by far the most studied optically active component in marine environments. It is out of the scope of the present work to review all the existing observations on this topic, however general charachteristics may be drawn. The refractive index of phytoplankton displays relatively large variations depending on their metabolite composition. Aas (1996) reviewing n for various species reports values ranging between 1.0045 and 1.095.

The absorption efficency factor for phytoplankton roughly increases with particle diameter and the opposite is for the scattering efficiency factor. Published values for $Q_a(\lambda)$ in corrispondence of the second absorption peack of Chl$-a$ are in the range 0.031–.740, whereas values span between 0.278 and 2.574 for $Q_b(\lambda)$ in the green region of the spectrum (Bricaud *et al.*, 1988; Ahn *et al.*, 1992). $Q_{b_b}(\lambda)$ instead, roughly increases with decreasing diameter of cells with recent reported values ranging

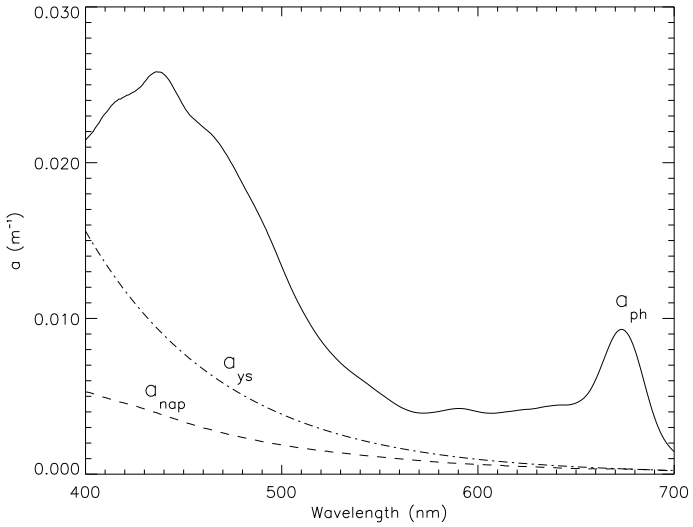

Figure 1.6: Example of absorption spectra of phytoplankton ($a_{ph}(\lambda)$), CDOM ($a_{ys}(\lambda)$) and non-algal particles ($a_{nap}(\lambda)$).

between 0.0029 and 0.0812 in the blue and between 0.0014 and 0.0681 in the green (Vaillancourt *et al.*, 2004).

For what concerns bulk optical properties, Bricaud *et al.* (1998) estimate that phytoplankton on average accounts for more ≈ 73 % of the absorption coefficient of particulate in the blue region, whereas Stramski *et al.* (2001), simulating generic oligotrophic oceanic condition (Chl$-a \approx 0.18$ µg l^{-1}), estimate that the contribution of phytoplankton is ≈ 13 % of $b_p(\lambda)$ and ≈ 2 % of $b_{bp}(\lambda)$ in the visible wavelengths.

Non-Algal Particles

Under the name of non-algal particles (NAP) we indicate organic and inorganic detrital matter of various origins. The main components of this class of optically active compounds are particles derived from biological activity such as faecal pellets, dead cells, or coccoliths and mineral particles from atmospheric deposition, riverine output or bottom resuspension. Their dimensions span from submicrometer to relatively large sizes.

The absorption of NAP ($a_{nap}(\lambda)$) is usually modeled with a decreasing exponential function (see **Fig. 1.6**), with major absorption in the blue, (Yentsch, 1962; Kirk, 1980; Roesler *et al.*, 1989; Bricaud *et al.*, 1998) of the form:

$$a_{nap}(\lambda) = a_{nap}(\lambda_0)e^{[-S(\lambda-\lambda_0)]} \tag{1.42}$$

where λ_0 is a reference wavelength usually set at 440 nm and S is the slope of the function. Bricaud *et al.* (1998) modeled $a_{nap}(440)$ with an empirical relationship from *in situ* data as a power function of Chl concentration:

$$a_{nap}(440) = 0.0124\text{Chl}^{0.724}; \tag{1.43}$$

with a range of variation for $a_{nap}(440)$ of the order of $10^{-4} - 10^{-1}$ m^{-1} for Chl spanning between $10^{-2} - 10^{2}$ µg l^{-1}, and accounting for ≈ 27 % of particulate absorption. The mean slope generally used to model the $a_{nap}(\lambda)$ curve is 0.011 nm^{-1} Roesler *et al.* (1989); Bricaud *et al.* (1998).

Non-algal particles, particularly mineral, are major sources of scattering and especially backscattering at sea. In generic oligotrophic oceanic conditions minerals can account for $\approx 41 - 45$ % to $b_p(\lambda)$ and $\approx 80 - 85$ % to $b_{bp}(\lambda)$. Organic detritus instead can account for ≈ 30 % to $b_p(\lambda)$ and ≈ 9 % to $b_{bp}(\lambda)$ (Stramski *et al.*, 2001).

Coloured Dissolved Organic Matter

The disruption of organic matter in the marine environment and production of exudates by marine organisms leads to the formation of dissolved compounds (DOM) of which the global ocean represent a huge reservoir. In oceanography, the thershold under which matter is considered dissolved is at 0.2–0.4 µm, generally depending on the mesh of the filter that is used to separate it from particulate. Part of DOM is made of cromophoric compounds (*i.e.* optically active) and is generally named as coloured DOM (CDOM) or gilvin or yellow substance (YS) (Thurman, 1985) (here we adopt CDOM in the text and ys for suffixes). The major part of these cromophoric compunds are humic and fulvic acids.

Biological activity represent both a source or a cause of decay for CDOM (Nelson *et al.*, 1998; Steinberg *et al.*, 2004; Nelson *et al.*, 2004). Among these activities there are the production of exudates (at various trophic levels), grazing, and bacterial growth. Photobleaching is another major process for the decay of CDOM, and it occurs in surface waters, especially when well stratified, and general circulation influences its distribution too (Siegel *et al.*, 2002).

CDOM absorbs strongly in the UV and in the short wavelength range of visible spectrum (blue region). For this reasons it plays an important role at sea for regulating the high energy radiation that is potentially harmful for living organisms (Zaneveld, 1975; Zepp *et al.*, 1995). The spectral shape of the absorption coefficient of CDOM ($a_{ys}(\lambda)$) is generally modeled with a decreasing exponential function

(**Fig. 1.6**) of the form:

$$a_{ys}(\lambda) = a_{ys}(\lambda_0)e^{[-S(\lambda-\lambda_0)]}; \tag{1.44}$$

where λ_0 is a reference wavelength and S is the slope of the curve and is independent of λ_0. The latter is usually set at at 440 nm and $a_{ys}(440)$ is modeled as a function of the Chl content (Prieur and Sathyendranath, 1981):

$$a_{ys}(440) = 0.2\left(a_w(440) + 0.06\mathrm{Chl}^{0.65}\right); \tag{1.45}$$

with a range of variation for $a_{ys}(440)$ of the order of $10^{-3} - 10^{-1}$ m^{-1} for Chl spanning between $10^{-2} - 10^{2}$ µg l^{-1}.

The mean value commonly adopted for S is that reported in Bricaud *et al.* (1981) that amounts to 0.014 ± 0.0032 nm^{-1} (with major variation between 0.010-0.020 nm^{-1}, and is considered to be representative for all waters with a reasonable accuracy. However mean values ranging between 0.011 and 0.024, and minima and maxima of 0.004 and 0.036 respectively have been reported for various oceanic regions (Højerslev and Aas, 2001).

Though absorption of CDOM is parameterized as a function of chlorophyll, it has to be considered a rough approximation from a biogeochemical point of view. In fact shifts between phytoplankton concentration and CDOM absorption have been observed (Hu *et al.*, 2006), leading to uncertentains in satellite Chl$-a$ estimates (Siegel *et al.*, 2005b).

Scattering by dissolved compounds is generally considered negligible. However it has to be reminded that the definition of CDOM includes colloids and viruses that are considered separately and may represent an important source of scattering.

Bubbles

Breaking waves at sea surface generate air bubbles. Large bubbles rapidly escape from the water column, whereas microscopic bubbles may be trapped in abundance in the surface layer. They can be found as a background even in flat sea condition, probably remaining after wind events or generated from organisms. There are two typical size distributions found in nature, one exponentially deacreasing with r^{-4} and a second one increasing with r^4 and then decreasing with r^{-4} after a plateau. Their typical concentration is between of 10^5 and 10^7 m^{-3} with a mean diameter of about 100 µm.

Bubbles do not contribute significantly to absorption but it has been demonstrated, from both theorethical and field studies, that they are good scatterers and contribute significally to $b_{bt}(\lambda)$. Moreover the presence of organic microfilms (mainly lipids and proteins, with refractive index $n_l = 1.20$ and $n_p = 1.10$) coating the external surface of bubbles increases their backscattering efficiency though not significantly altering their scattering properties. This enhancement is generally proportional to the refractive index and to the thickness of the film. (Zhang *et al.*, 1998, 2002, and references therein) Wind and sea state condition strongly influence the natural variability of bubbles densities and their effect on the optical properties at short time scales (minutes), especially in surface waters (Terrill *et al.*, 2001).

The effect of bubbles on reflectance is to reduce the B/G ratio especially at low Chl$-a$ concentrations, where simulations show that it can be halved (Zhang *et al.*, 1998; Stramski and Tegowski, 2001).

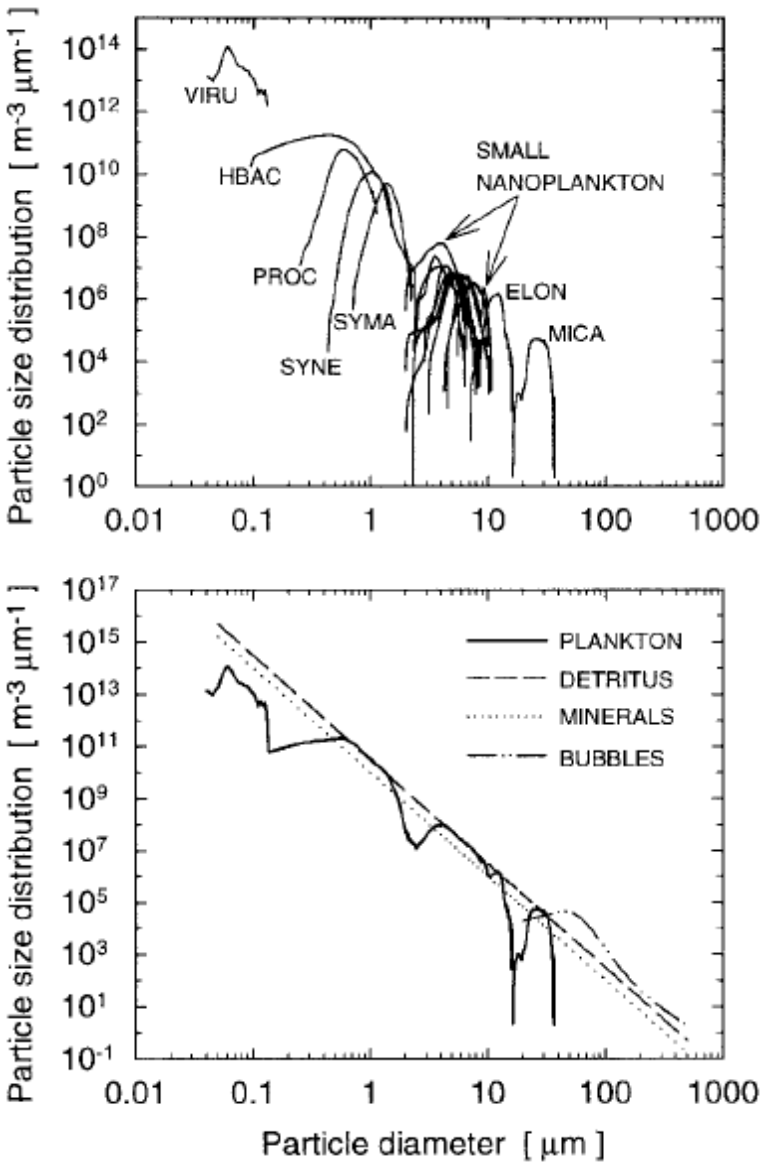

Figure 1.7: The upper figure shows an example of density functions of the particle-size distribution for various planktonic components. The figure on the bottom displays the composite size distribution of all planktonic components, as derived from individual distributions from the above figure, compared with the size distributions of detrital particles, mineral particles, and air bubbles. Figures are taken from Stramski *et al.* (2001).

2. Data and Methods

Bio-optical data used in this study was collected during several cruises in offshore waters of both eastern and western Mediterranean Sea and at an oligotrophic station in the Gulf of Naples (GoN, Southern Tyrrhenian Sea, 220 m isobath). In addiction some data collected during the PROSOPE cruise, available at http://www.obs-vlfr.fr/, were included in this study. Data covers all seasons and almost all trophic conditions generally found in Mediterranean waters, with Chl$-a$ concentrations ranging from 0.05 µg l^{-1} up to 6.00 µg l^{-1}. See **Tab. 2.1** for further details and **Fig. 2.8** for stations location.

In this section an overview of technical procedures for raw data acquisition, the analitycal protocols for their processing and the derivation of the main variables used in this work, are presented. Other deriverd variables here considered will be described when appearing in the text.

At all stations a Seabird CTD probe was deployed together with a SeaTech fluorometer, attached to a general oceanographic rosette equipped with 10 l Niskin bottles for discrete samples collection. Water from Niskin was transferred into polyethylene carboys and then subsampled, filtered under low *vacuum* and stored on board in liquid nitrogen or freezer (-20 °C).

Analyses were made at Laboratory of Biological Oceanography or Environmental Management and Ecology of Temperate and Polar Coastal Areas of the Zoological Station in Naples in few weeks. Since 2001, optical profiles and absorption spectra were collected and analyzed by myself. Pigments were analyzed by Mr. F. Corato,

Year	Month	Cruise	Vessel	Zone	SPMR	ac9	a_p	[Chl]
1999	Apr-May	Emtec	*Urania*	Ion-Aeg	17	-	-	0.03–0.23
1999	Sep-Oct	Prosope	*Thalassa*	Alg-Ion	9	50	-	0.02–0.09
1999	Oct-Nov	Symplex4	*Urania*	Ion	8	-	-	0.05–0.12
2001	Feb-Aug	Dina	*Vettoria*	GoN	11	-	55	0.12–0.84
2001	Dec	Norbal2	*Urania*	GoL-Tyr	11	42	53	0.10–0.28
2002	Sep-Oct	Norbal3	*Urania*	GoL	6	13	13	0.15–0.55
2003	Mar	Norbal4	*Urania*	GoL	14	71	60	0.15–4.30
2003	Apr	Norbal5	*Urania*	GoL	4	44	10	0.96–1.81
2004	Aug	Alt1	*Urania*	Tyr	12	24	31	0.05–0.12

Table 2.1: List of cruises and bio-optical data presented in this paper. N of ac9 and absorption spectra are matched with concurrent Chl samples from bottles. Chl ranges are referred to SPMR data. Data from PROSOPE cruise was downloaded at http://www.obs-vlfr.fr/cd_rom_dmtt/pr_main.htm, and Chl$-a$ was determined with HPLC tecnique. The N of ac9 for this cruise was limited to 50 randomly chosen points.

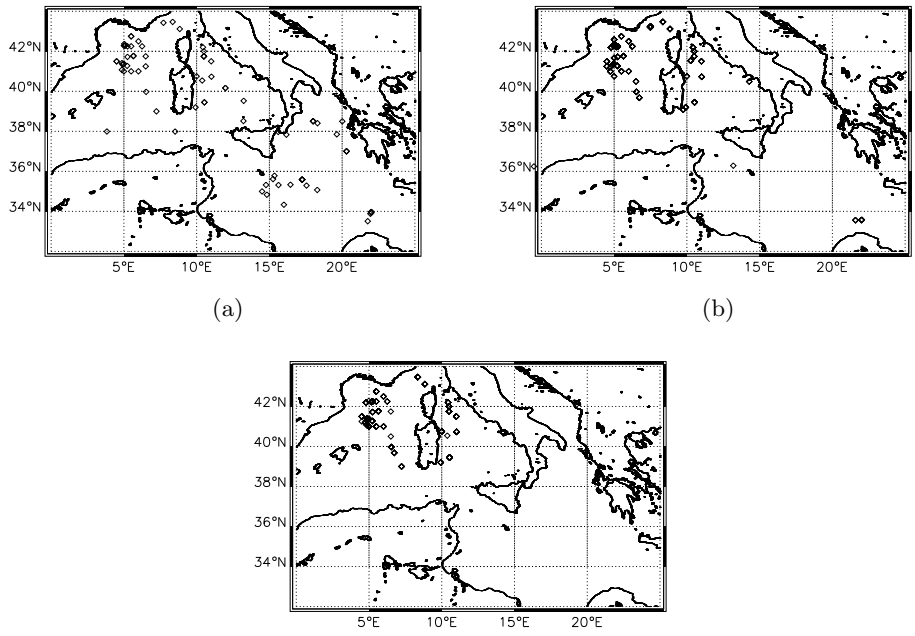

Figure 2.8: (a) Station locations for measurements with SPMR. fig:staz-ac9 station location for measurements with ac9. (c) station location for $a_p(\lambda)$ measurements.

Mr. C. Chiaiese, Dr. F. Margiotta, Mr. A. Passarelli, Dr. I. Santarpia and Mr. F. Tramontano. Hydrological data was acquired processed and made available from Satellite Oceanography group at the Atmospheric Sciences and Climate Institue of the National Research council (ISAC-CNR) in Rome.

2.1 Pigments

Pigment samples were filtered onto GF/F Whatman glass fiber filters (25 mm ⊘, 0.7 µm retention capacity) and then exracted on 90 % $CH_3-CO-CH_3$. Chl$-a$and Phaeo$-a$ were spectrofluorometrically determined with a Spex Fluorolog 1681 (Holm-Hansen *et al.*, 1965; Neveux and Panouse, 1987), and Chl calculated as the sum of the two pigments. For the stations where we lacked pheopigment data, the regional relationship from D'Ortenzio *et al.* (2002) to estimate Chl was used:

$$\text{Chl} = 1.1635\text{Chl}-a + 0.0072. \tag{2.46}$$

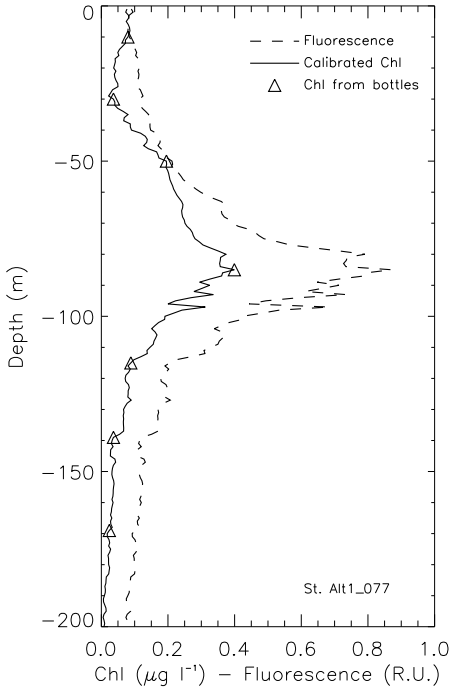

Figure 2.9: Example of fluorescence profile calibrated with discrete Chl samples.

It is known that a systematic overestimate of Phaeo$-a$ is linked to the presence of Chl$-b$ with this method (Gibbs, 1979), otherwise Chl$-b$ concentration in the Mediterranean Sea seems to be not particularly high, especially in surface waters (Claustre, 1994; Vidussi *et al.*, 2000; Casotti *et al.*, 2003; Brunet *et al.*, 2006). Fluorescence profiles are converted into Chl units by regression analysis made on single profiles by using pigment data from discrete samples (**Fig. 2.9**). When pigment data were not available for a single fluorescence profile, specific coefficients for each cruise are used.

Derived Variables

For bio-optical studies it is usual to define a mean Chl concentration for the part of the water column that is optically active in determining the ocean colour (i.e. $z_{pd} = z_{eu}/\ln(100)$ that is the depth where approximately 90 % of the $L_w(\lambda)$ signal comes from, and z_{eu} is the depth reached by the 1 % of the surface PAR). In this study it is calculated in corrispondence of irradiance profiles as:

$$[\text{Chl}] = \frac{1}{z - z_0} \int_{z_0}^{z} \text{Chl}(z)\, dz; \tag{2.47}$$

where z_0 is the first depth with available Chl data and z corresponds to z_{pd}.

A mean concentration weighted for the attenuation of light has been also calculated in the first optical depth as:

$$C_M = \frac{\int_0^{z_{pd}} \mathrm{Chl}(z) \exp(-2Kz)dz}{\int_0^{z_{pd}} \exp(-2Kz)dz}. \tag{2.48}$$

This value is similar to the optically weighted pigment concentration, which is a good proxy for the Chl concentration measured by a remote sensor viewing a stratified ocean Clark (1997).

When optical data was not available the euphotic depth is derived according to the iterative scheme from Morel and Berthon (1989). This scheme consits of progressively integrating the Chl profile with increasing depth (Chl_t) and introducing this value in the following empirical relationship:

$$z_{eu} = 199.85\mathrm{Chl}_t^{-0.435}; \tag{2.49}$$

thus generating a series of decreasing z_{eu}. When the latter becomes less than the integration depth, the loop is closed and so the z_{eu} is finally estimated. The coefficients appearing in **Eq. 2.49** were specifically determined for the Mediterranean Sea (Colella, 2006), thus replacing the original coefficients of Morel and Berthon (1989) and revised in Morel and Maritorena (2001).

2.2 Absorption Spectra

Samples for absorption measurements were filtered onto GF/F Whatman glass fiber filters (25 mm ⌀, 0.7 µm retention capacity), taking care to collect particles upon the homogeneous side of the filter. Absorption coefficients of particulate compounds $a_p(\lambda)$ were determined with filter pad tecnique with an HP 8453E spectrophotometer provided with a Labsphere RSA-HP-8453 integrating sphere in the 400–800 nm wavelength domain. Data were stored in absorbance units and then converted into trasmittance (or reflectance, ρ_t and ρ_r respectively):

$$\rho_T = \frac{1}{10^{A_T}}; \quad \rho_R = \frac{1}{10^{A_R}}. \tag{2.50}$$

Samples treatment procedure was that of Tassan and Ferrari (2002) with few differences due to different design of the integrating sphere. Pigment contribution to $a_p(\lambda)$ was eliminated with 0.1 % active NaClO solution (Ferrari and Tassan, 1999). Absorption coefficients of algal and non-algal particles ($a_{ph}(\lambda)$ and $a_{nap}(\lambda)$ respectively)

were calculated through T-R method (Tassan and Ferrari, 1995a) after optical densities were scaled by 0.72 to take into account for the different response of the Hewlett Packard diode array in respect to traditional units (Mitchell *et al.*, 2000). The T-R method combines light-transmission and light-reflection measurements thus permitting to remove the contribution of sample backscattering to measured absorption. It is based on the equation of radiative balance during a scan:

$$TR + BK + AF + AS = 1 \tag{2.51}$$

where TR is the fraction transmitted into the sphere, BK is the fraction backscattred, AF and AS are the fraction absorbed by the filter and by the sample. The protocol consists of a set of 5 measurements for each sample (see **Fig. 2.10** for reference):

1. ρ_T: reflectance standard on the reflectance holder slide and sample on the trasmittance sample holder.

2. ρ_R: sample on the reflectance sample holder with a black light trap on the back.

3. ρ_{Rf}: blank filter on the reflectance sample holder with a black light trap on the back.

Scan 1.-2. are repeated after bleaching with NaClO for the determination of non algal particles absorption.

A blank is automatically subtracted before each scan: a blank filter treated in the same way of the sample is used as reference in scan 1.-2., whereas a calibrated Spectralon diffuse reflectance standard (95 %) for scan 3. The dummy port is covered with a not calibrated reflectance standard in all scans. The absorption of the sample on filter a_s is then calculated as:

$$a_s = \frac{1 - \rho_T + \rho_{Rf}(\rho_T - \rho_R)}{1 + \rho_{Rf}\rho_T\tau}; \tag{2.52}$$

where:

$$\tau = \frac{1 - T_s^d}{1 - T_s^p}; \tag{2.53}$$

is approximated by the following empirical relationship (Tassan S. personal communication):

$$\tau = 1.171 - 0.2615\ OD_t + 0.00013\ OD_t^2; \tag{2.54}$$

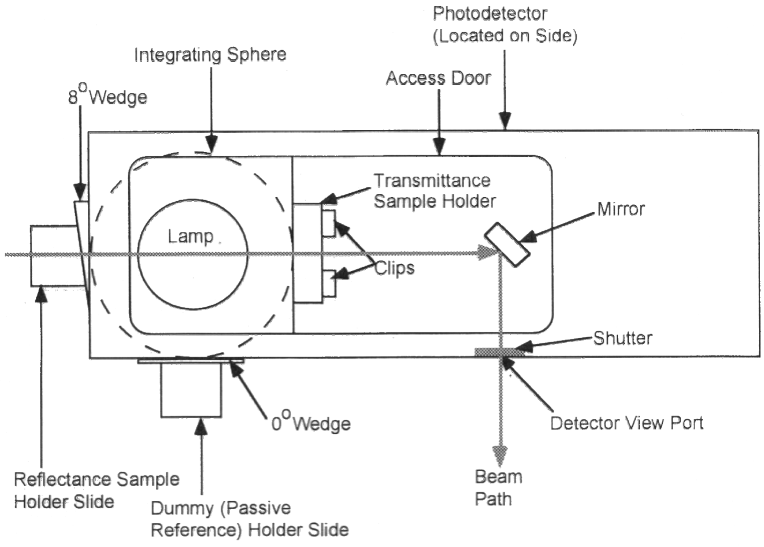

Figure 2.10: Scheme of the Labsphere RSA-HP-8453 integrating sphere used for absorption spectra measurements upon filter. It installed into an HP 8453E spectrophotometer that receive the signal of diffuse light coming out of the sphere.

that is an unpublished previous version of Eq. 7 in Tassan and Ferrari (2002), however not significantly different. Sample absorption is then converted into sample absorbance:

$$A_s = \log\left(\frac{1}{1-a_s}\right); \tag{2.55}$$

and the pathlength amplification due to sample concentration on filter is corrected using the expression found by Tassan and Ferrari (1995a), that has been shown to

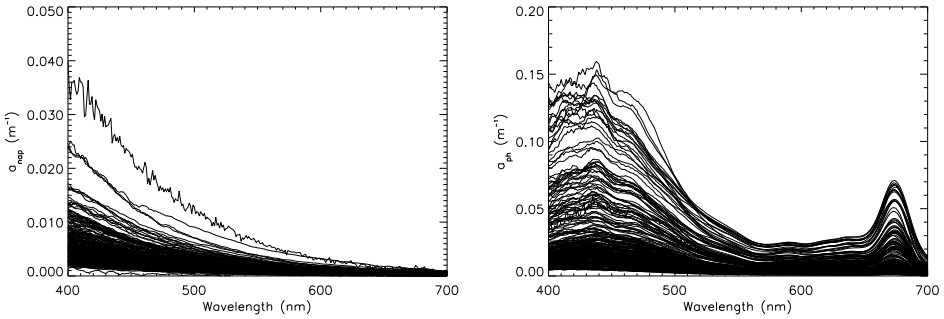

(a) (b)

Figure 2.11: $a_{nap}(\lambda)$ (a) and $a_{ph}(\lambda)$ (b) spectra for the whole data set with concurrent Chl measurements.

performe well on both phytoplankton and detrital particles (Tassan and Ferrari, 1998):

$$OD_s(\lambda) = 0.423 OD_{fp}(\lambda) + 0.479 OD_{fp}(\lambda)^2; \tag{2.56}$$

and the absorption of suspended particulate finally calculated as:

$$a_p(\lambda) = 2.3 OD_s(\lambda) \frac{A}{V}; \tag{2.57}$$

where A is the clearance area of the filter and V is the volume of water filtered. **Eq. 2.52** through **Eq. 2.57** are the same for non algal particles, whereas the phytoplanktonic absorption spectra are obtained as the difference between the two:

$$a_{ph}(\lambda) = a_p(\lambda) - a_{nap}(\lambda). \tag{2.58}$$

Spectra were then set to zero at 750 nm. The specific absorption coefficients ($a^*(\lambda)$) for the three compartments are determined by dividing the absorption spectra by the Chl content.

2.3 Radiance and Irradiance Profiles

Multispectral profiles of downwelling irradiance ($E_d(z, \lambda)$) and upwelling radiance ($L_u(z, \lambda)$) were collected with a factory calibrated (SeaWiFS Profiling Multichannel Radiometer(SPMR, Satlantic Inc.) at 13 wavelengths in the visible domain (400, 412, 443, 470, 490, 519, 532, 555, 590, 620, 665, 683 and 700 nm). In the more recent cruises (2001-2004) a SeaWiFS Multichannel Surface Radiometer (SMSR, Satlantic

Inc.) was deployed during data acquisition.

Thanks to the particular design of the instruments, it was possible to collect data far from the ship ($\approx$ 30 m), thus minimizing the shadowing effect of the ship (Piskozub, 2004) (**Fig. 2.12**). All measurements included in this study were made with good weather conditions (i.e. blue skies or partly cloudy with free sun) and in the central part of the day (solar zenith angle $\leq 60°$, *i.e.* $\leq 30°$ above the horizon). Data was acquired with Satview (Satlantic Inc., various versions) and processed with Prosoft 7.4 software (Satlantic Inc.).

Derived Variables

The diffuse attenuation coefficients for $E_d(z,\lambda)$ (and $L_u(z,\lambda)$) are calculated from profiler data according to derivative method on an interval of 5 m centered at z_m (Ocean Optics Protocols For Satellite Ocean Color Sensor Validation, Revision 4, Vol. III):

$$\ln[E_d(z,\lambda)] = \ln[E_d(z_m,\lambda)] - (z - z_m)K_d(z_m,\lambda). \tag{2.59}$$

A mean attenuation coefficient for $E_d(z,\lambda)$ is computed for the first optical depth:

$$K(\lambda) = \frac{1}{z_{pd}} \ln\left[\frac{E_d(0^-,\lambda)}{E_d(z,\lambda)}\right]; \tag{2.60}$$

then the biogenic contribution to attenuation is derived by subtracting the water term (values tabeled in MM01):

$$K_{bio}(\lambda) = K(\lambda) - K_w(\lambda). \tag{2.61}$$

Surface data, at the water side of the interface, are retrieved by projecting the closest data to surface collected (or that collected with the buoy at $\approx$ 20 cm) by means of the local attenuation coefficients. Then $E_d(0^-,\lambda)$ and $L_u(0^-,\lambda)$ are projected above water according to the following equations:

$$E_d(0^+,\lambda) = E_d(0^-,\lambda)\frac{1}{1-\overline{\rho}}; \tag{2.62}$$

$$L_u(0^+,\lambda) = L_w(\lambda) = L_u(0^-,\lambda)\frac{1-\rho}{n^2}; \tag{2.63}$$

where $\overline{\rho} \cong 0.043$ represents the mean air-water interface Fresnel reflectance for the downward irradiance (or albedo), $\rho \cong 0.021$ is the Fresnel reflectance of the sea and $n \cong 1.345$ is the refractive index of seawater (Austin, 1974; Preisendorfer and Mobley,

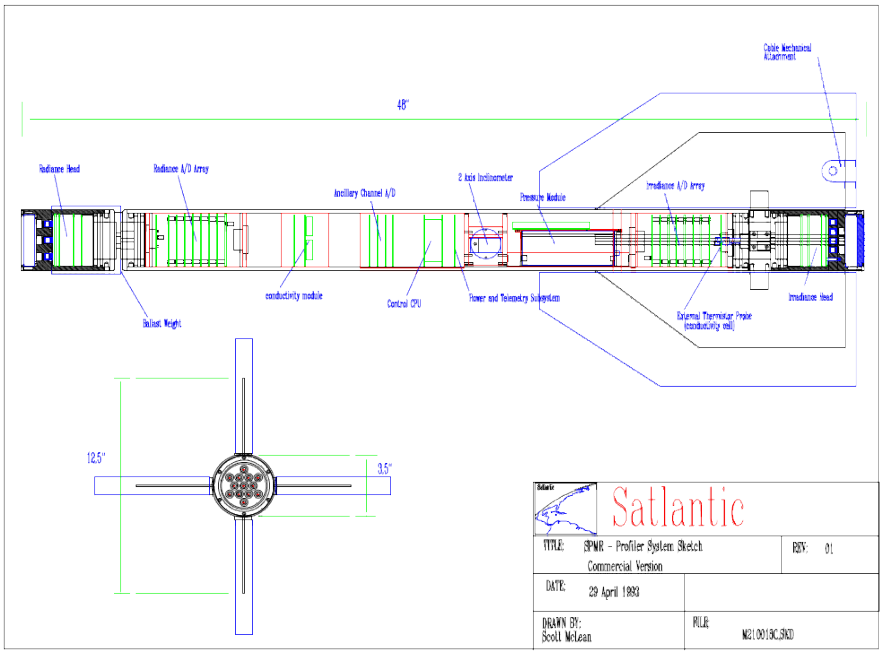

(a)

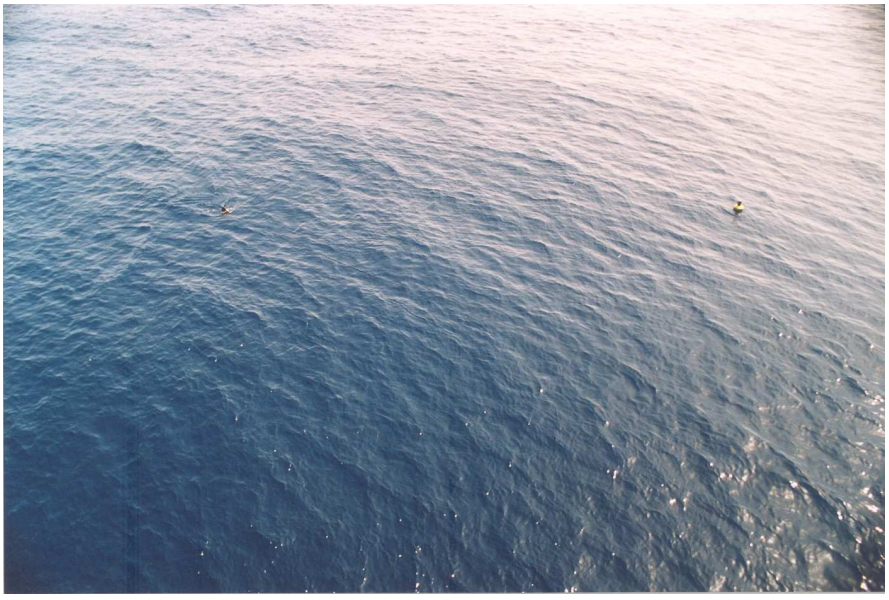

(b)

Figure 2.12: (a) Technical scheme of the SPMR. (b) SPMR and SMSR during typical deployment activities at sea, photo courtesy of C. Luttazzi.

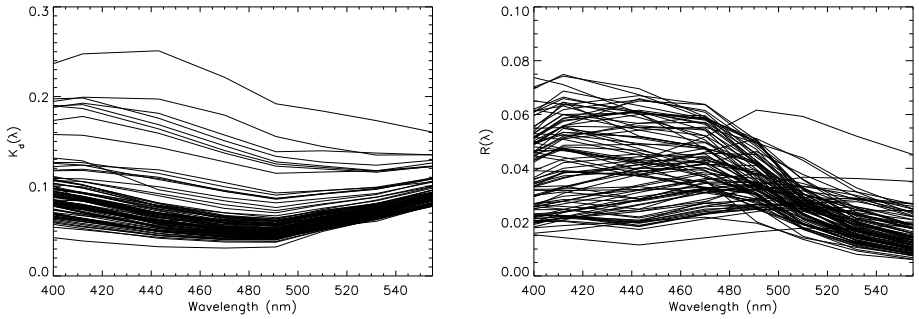

(a) (b)

Figure 2.13: All mean $K(\lambda)$ calculated within z_{pd} (a) and $R(\lambda)$ (b) used in this work.

1986; Gordon *et al.*, 1988; Morel and Gentili, 1996). Surface (in-water) upwelling irradiance ($E_u(0^-, \lambda)$) is obtained from $L_u(0^-, \lambda)$ through **Eq. 1.39**, and $Q(\lambda)$ is tabulated in Morel and Gentili (1996). $R(\lambda)$ and $R_{rs}(\lambda)$ has been determined by means of **Eq. 1.37 Eq. 1.38** and the normalized water leaving radiance is derived as:

$$nL_w(\lambda) = R_{rs}(\lambda)F0(\lambda); \tag{2.64}$$

where $F0$ is the solar radiation at the top of the atmopsphere and is taken from Neckel and Labs (1984).

PAR is assumed to be equal to PAR_d and calculated as:

$$PAR \approx PAR_d = \int_{400}^{700} \frac{\lambda}{hc} E_d(\lambda) d\lambda. \tag{2.65}$$

The resolution of the integrated wavelengths corresponds to the that measured with SPMR.

2.4 Attenuation and Absorption Profiles

Starting from 2001 a 25 cm pathlength ac9 (WETLabs Inc., **Fig. 2.14**) was used during cruises to measure total absorption and attenuation coefficients net of water contribution ($a_{pg}(\lambda)$ and $c_{pg}(\lambda)$ respectively where the suffix pg is used to indicates that it sorresponds to sum of the particulate and dissolved (gylvin) components) at nine wavelengths (412, 440, 488, 510, 532, 555,630, 676 and 715 nm). The instrument was deployed vertically in a handcrafted steel cage from which the instrument was

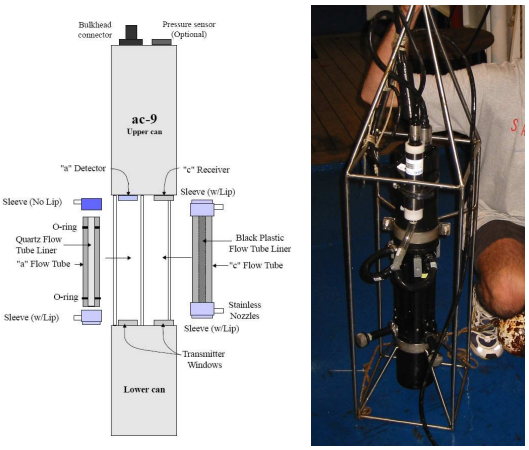

(a) (b)

Figure 2.14: (a) Technical scheme of the ac9. (b) ac9 ready for deployment at sea, photo courtesy of R. Sciarra.

isolated, before or after the CTD cast. Data were acquired through WETView software (WETLabs Inc., various versions) and collected in the first 100 m of the water column.

For each cruise, the instrument was calibrated with a bi-distilled filtered (0.22 µm) water. Cruises were never longer than three weeks and the ac9 was never extensively used and it was carefully cleaned every day, so we assume that intra-cruise instrumental drift is low if not negligible. Salinity and temperature effects were taken into account according to Pegau *et al.* (1997), and correction for possible loss of light due to scattering in the absorption measuring tube was applied by subtracting $a_{pg}(715)$ from $a_{pg}(\lambda)$(Zaneveld *et al.*, 1994). Total scattering (net of water) was then calculated by subtracting absorption from attenuation:

$$b_p(\lambda) = c_{pg}(\lambda) - a_{pg}(\lambda). \tag{2.66}$$

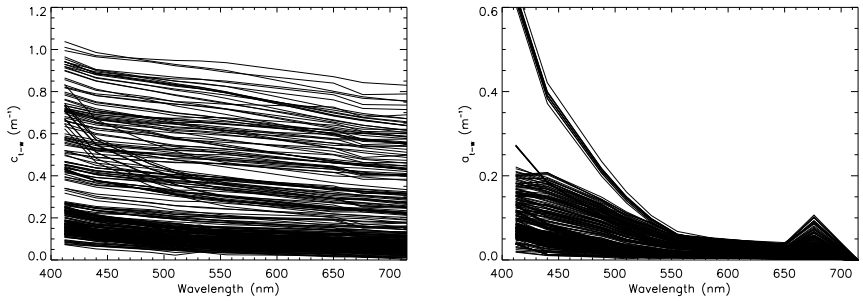

(a) (b)

Figure 2.15: $c_{pg}(\lambda)$ (a) and $a_{pg}(\lambda)$ (b) spectra for the whole data set with concurrent Chl measurements.

2.5 Statistical Parameters

The statistical parameters that will be used in this work are:

- determination coefficient (r^2);
- root mean square (RMS);
- mean relative percentage difference (RPD);
- mean bias error bias (BIAS);
- mean absolute percentage difference (APD);
- Student's t-test (or t-means test);

The r^2coefficient indicates the proportion of variability, in a data set, that is accounted for by a statistical model.

RMS indicates the spread of data respect to the best agreement and was computed as:

$$\text{RMS} = \sqrt{\frac{\sum_{i=1}^{N} Y - X}{N}}; \tag{2.67}$$

The mean bias error was computed as:

$$\text{BIAS} = \frac{1}{N}\sum_{i=1}^{N}(Y - X). \tag{2.68}$$

The mean relative percentage difference was calculated as:

$$\mathrm{RPD} = \frac{1}{N}\sum_{i=1}^{N}\left(\frac{Y-X}{X}\right)\cdot 100. \tag{2.69}$$

In represents the mean relative error generated by the application of a global model to the Mediterranean Sea, if we assume that the results for the regional models are the truth. It gives information on the mean direction of the error, *i.e.* an overestimate of a certain variable derived with a global model over the Mediterranean Sea if it is positive, and an underestimate if negative. Analogous to the RPD but for absolute values is calculated as:

$$\mathrm{APD} = \frac{1}{N}\sum_{i=1}^{N}\left|\frac{Y-X}{X}\right|\cdot 100 \tag{2.70}$$

In the former analysis, the variables X and Y are respectively the results of the application of any statistical model for Mediterranean Sea and the homologous for global ocean.

The t test computes the probability that two sample populations X and Y have significantly different means. The default assumption is that populations have normal distribution and the same variance:

$$p = \frac{\bar{X}-\bar{Y}}{\sqrt{\frac{\sum_{i=0}^{N-1}(X_i-\bar{X})^2+\sum_{i=0}^{M-1}(Y_i-\bar{Y})^2}{N+M-2}\left(\frac{1}{N}+\frac{1}{M}\right)}}. \tag{2.71}$$

3. The Color of the Mediterranean Sea

[Part of this section has been object of a publication I've been involved in (Volpe et al.*, 2007). Only some parts of the paper, functional to the present work will be cited in this chapter. For what not explicitely explained, e.g. missing definitions of some quantities, the reader can refer to the original paper.]*

The Mediterranean Sea is a semi enclosed basin surrounded by South Europe, North Africa and Middle East, and is connected to the North Atlantic Ocean through the Gibraltar Strait and to the Sea of Marmara through the Dardanelles Strait. It spans between $6°E$ and $37°W$, and $30°N$ and $46°N$ approximately. Its surface occupies $\approx 2.51 \cdot 10^6$ km^2 (≈ 0.6 % of the global ocean), and its basin contains ($\approx 3.9 \cdot 10^6$ km^3 of seawater (≈ 0.3 % of world ocean volume). Its coasts are tot km long, so it is characterized by a low surface and volume to coast lenght ratio.

The Mediterranean Sea is divided into two main sub-basins, Eastern and Western Mediterranean by the system of the straits of Sicily, which have two narrow and relatively shallow sills hardly reaching 500 m depth. The two main sub-basins are in turn divided in smaller sub-basins with complex coastlines and different sized islands; the major beeing: Adriatic Sea; Aegean Sea; Alboran Sea; Balearic Sea; Ionian Sea; Levantine Sea; Ligurian Sea and Thyrrenian Sea.

The Mediterranean Sea is considered one of the most complex marine environments on the Earth, because of the variety of physical processes that occur there (Williams, 1998). These processes span from the mesoscale to the basin-scale, and include also deepwater formation. Consequently, the basin has often been considered a "miniature ocean" or a "laboratory basin" (Lacombe *et al.*, 1981; Robinson and Golnaraghi, 1995) because several of the processes controlling the global ocean general circulation are present there, though in reduced temporal and spatial scales.

The Mediterranean Sea is generally considered an oligotrophic basin (Azov, 1991; Antoine *et al.*, 1995; Duarte *et al.*, 1999). However offshore phytoplankton blooms have been regularly observed in limited regions of the basin so that mesotrophic regimes can be found in the basin. For example the North Balearic region is characterized by an intense spring bloom, persistent over 2 months (D'Ortenzio, 2003).

Berman *et al.* (1984a,b) pointed out that oligotrophic waters in the Southeastern Mediterranean Sea showed an anomalaous blue to green reflectance ratio (B/G). In fact this ratio appeared systematically low in respect to the pigment content of the water column as compared to other region of the global ocean. This anomaly has been obseved several times over the years so that the Mediterranean Sea is considered a

separate bio-otpical province and its optical peculiarity was given the name of *green shift*.

As a consequence of this low B/G, when generic algorithms developed to estimate Chl$-a$ content from reflectance ratios were applied to Mediterranean reflectance data, the pigment content was higher than *in situ* observations. For example Gitelson *et al.* (1996) showed that Chl$-a$ was overestimated of more than 40 % for Chl$-a$ unit$>$ 0.1µg l^{-1} and of more than 80 % for Chl$-a<$ 0.06 µg l^{-1} when using Gordon *et al.* (1983) algorithm.

Gitelson *et al.* (1996) proposed that a relatively higher abundance of coccolithophores respect to other groups could explain this *green shift*. This hypothesys was mainly based on previous observation Megard and Berman (1989), who showed that attenuation coefficients were about twice in the Eastern Mediterranean respect to other pelagic regions with a similar trophic regime. This evidence was explained by the presence of *Coccolithus huxlei*, which is a small sized planktonic unicellular organism whose external membrane is covered by calcareous scales (coccoliths). Gitelson *et al.* (1996) also suggested that all extremely oligotrophic regions, characterized by small phytoplankton with high attenuation characteristics (Smith and Baker, 1978) have to be different from that suitable for more productive regions. Then they proposed a new algorithm modifying the coefficients of the two band algorithm of Gordon and Morel (1983) (see **Tab. 3.2**) by fitting regional data, with the aim to apply it to Coastal Zone Color Scanner (CZCS) imagery, addressing the need for calibration and validation of ocean color algorithms on a regional basis.

Several algorithms were then developed to reduce the error in satellite Chl$-a$ estimates over the Mediterranean Sea for the new generation ocean color sensors (*e.g.*: Seaviewing Wide Field-of-view Sensor (SeaWiFS), Moderate-resolution Imaging Spectrometer (MODIS), Medium-resolution Imaging Spectrometer (MERIS)). In fact when the NASA standard algorithm OC4v4 (O'Reilly *et al.*, 2000) is used over the Mediterranean Sea, the retrieved Chl$-a$is generally overestimated. The regional algorithms are summarized in **Tab. 3.2**. In general the efforts made in the calibration and validation activities were accompanied by the attempts to understand the reasons of the observed anomaly in reflectance ratio.

(D'Ortenzio *et al.*, 2002), while proposing two regional algorithms for SeaWiFS (**Fig. 3.16**), analyzed the coccolithophores hypotesis by means of a simple bio-optical model to study the effect of these planktonic organisms upon the B/G, that was previously shown to decrease by increasing the concentration of coccoliths (Gordon and Balch, 1999). In particular, following Tyrrell *et al.* (1999) they expressed the backscattering term as a function of calcite ($CaCO_3$) concentration. They showed that the amount of $CaCO_3$ needed to fit their data set was of about 5 µg l^{-1}, that would corre-

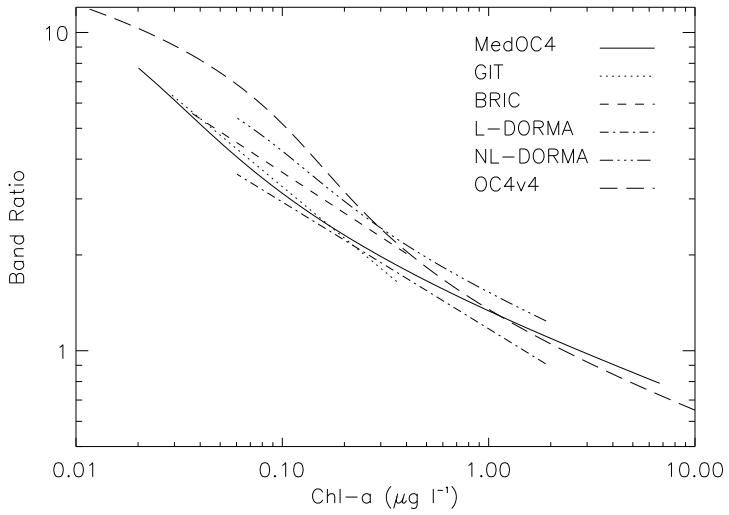

Figure 3.16: Comparison between the OC4v4 and five regional algorithms for Chl$-a$ retrieving from reflectance ratios. Curves are drawn only in the Chl$-a$ range used to retrieve the algorithms.

spond to a coccolithophore concentration between $3 \cdot 10^7$ and $2.5 \cdot 10^8$ cell m^{-3}. This range was almost one order of magnitude higher than the concentration found in the EMED by Rabitti *et al.* (1994); Robarts *et al.* (1996). So they observed that coccolithophores can only partially explain the *green shift*. The authors also underlined that a high concentration of CDOM could also determine a decrease in B/G, but that the low concentrations of dissolved organic matter (DOM) found in the Mediterranean Sea Seritti *et al.* (2000) let them to discard this possibility. So they concluded that the lower value of the measured band ratio was probably due to a phytoplankton community with optical properties different from the average community on which the global ocean color algorithms are based.

Ragni and Ribera d'Alcalá (2004) developed a semi-analytical radiative transfer model, in order to identify specific bands ratios suitable for photoregulative responses in marine algae. They validated the in-water bio-optical model by means of a measured spectral downwelling irradiance profile collected in open waters of the Eastern Mediterranean Sea. Their modelled profiles show some discrepancies in the near-UV blue region, with mean errors of ≈ 10 % in the surface layer (0–20 m). So they improved the model by changing the slope of the semi-logarithmic expression that describes the absorption spectrum of CDOM (**Eq. 1.44**). They found that the slope that best fit the *in situ* data was 0.05 nm^{-1} instead of the often used value of 0.014 nm^{-1} (Bricaud *et al.*, 1981). This choise was mainly based on the evidence that high slope

Name	Equation	ρ	r^2	N	Chl$-a$ range
OC4v4	$\text{Chl}-a = 10^{0.366-3.067\rho+1.930\rho^2+0.649\rho^3-1.532\rho^4}$	$\log_{10}\left\{\frac{\max[R_{rs}(443,490,510)]}{R_{rs}(555)}\right\}$	0.892	2804	0.008–64
GIT	$\text{Chl}-a = 0.914\rho^{-1.86}$	$\frac{R(440)}{R(550)}$	0.83	21	0.028–0.36
L-DORMA	$\text{Chl}-a = 1.49\rho^{-2.51}$	$\frac{R_{rs}(490)}{R_{rs}(555)}$	0.948	45	0.06–1.92
NL-DORMA	$\text{Chl}-a = 10^{0.217-2.728\rho+0.704\rho^2+0.297\rho^3} - 0.035$	$\log_{10}\left[\frac{R_{rs}(443)}{R_{rs}(555)}\right]$	0.941	45	0.06–1.92
BRIC	$\text{Chl}-a = 2.094\rho^{-2.357}$	$\frac{R_{rs}(443)}{R(555)}$	0.952	157	0.034–0.4
MedOC4	$\text{Chl}-a = 10^{0.4424-3.686\rho+1.076\rho^2+1.684\rho^3-1.437\rho^4}$	$\log_{10}\left\{\frac{\max[R_{rs}(443,490,510)]}{R_{rs}(555)}\right\}$	0.84	155	0.02–7

Table 3.2: Acronyms, coefficients, functional forms and band ratio of OC4v4 and five regional algorithms. $\max[R_{rs}(443, 490, 510)]$ is the maximum value of the remote sensing reflectance between the three wavelengths.

of CDOM spectra were reported in the Mediterranean Sea by Ferrari (2000), however these values hardly reached half of the proposed slope and were mainly from shallow waters influenced from Rhône River.

Claustre *et al.* (2002) gave an alternative explanation to the *green shift*. Data collected during a late summer cruise showed that the color shift is caused by both anomalous absorption and backscattering ratios (Mediterranean waters absorb more blue light and backscatter more green light than anticipated), and the particle scattering coefficients, $b_p(555)$, are anomalously high compared to those modeled for a standard ocean. The cruise was held after several Saharan dust events occurred over the Mediterranean Sea, and an enrichment in the concentrations of lithogenic silica in the surface waters was also measured. So they proposed that submicron (< 0.7 µm) brick-red or pink dust coming from Sahara desert during "red rain" storms could be at the origin of the *green shift*. The authors exluded CDOM as possible fonts for the anomalous band ratio, as the first is primarly a by-product of biological activity, which is rather low in the Mediterranean, moreover it is exposed to strong photo-bleaching especially during summer stratification and has not high scattering capabilities to explain the high $b_p(555)$. Bubbles were also excluded because of very good weather conditions during sampling.

Almost at the same time than D'Ortenzio *et al.* (2002), Bricaud *et al.* (2002) developed a regional algorithm that applied to SeaWiFS imagery for the estimate of primary production in the Mediterranean Sea (**Fig. 3.16**). The authors suggested that if the *green shift* originates from Saharan dust inputs, it should not have a continuous and constant effect, and showed that part of their data set (e.g. MINOS cruise in May 1996) was not biased in respect to global relationship between the reflectance ratio and chlorophyll. Antoine and Nobileau (2006) studied the seasonal patterns of Saharan dust transport over the Mediterranen Sea using SeaWiFS observations over the area (years 1998-2004) by means of an algorithm specifically developed to detect blu-absorbing aerosols (Nobileau and Antoine, 2005). They showed an increase of dust load during the years of a factor between 3 and 5 from 1998 to 2004 depending on the considered sub-basin (major increases being in the EMED and WMED and lower in the CMED). From tehir estimates on average monthly spatial coverage of dust inputs, I calculated that the percentage of the area that was interested by dust events ranges between 4 and 19 % of the whole basin.

We recently developed a four band regional algorithm (MedOC4) similar to the OC4v4 (**Fig. 3.16**), using a larger data set for both tuning the algorithm itself and for validating its performances when applied to SeaWiFS archive. Using a data set independent from that used to fit Chl$-a$ and band ratios, we showed that the MedOC4 has best results in diminishing uncertentaines in SeaWiFS Chl$-a$ retrieval

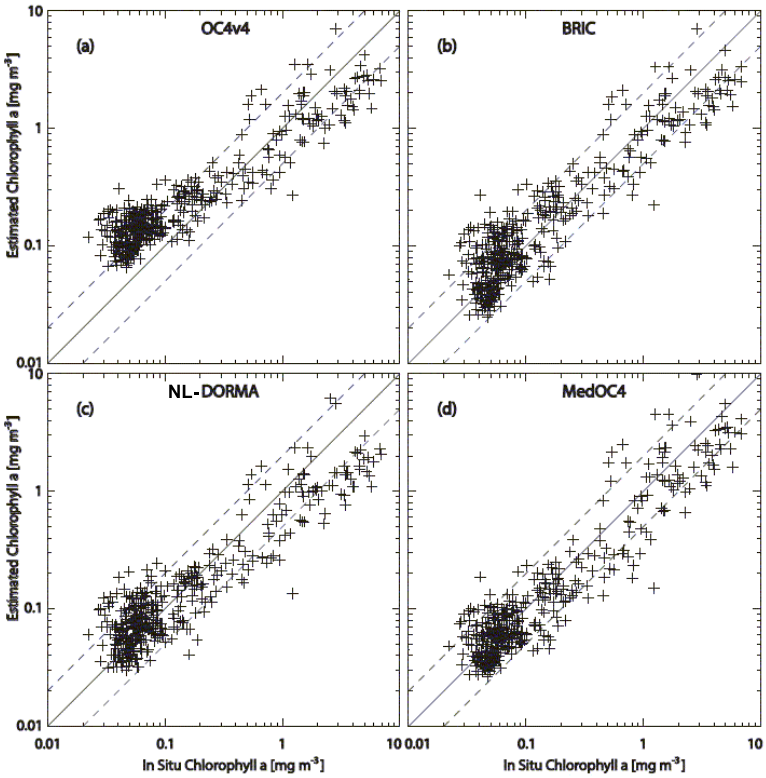

Figure 3.17: Validation of SeaWiFS Chl$-a$ estimates against concurrent in situ Chl$-a$ data (CM). (a) SeaWiFS estimates are obtained applying the OC4v4 algorithm. (b) SeaWiFS estimates are obtained applying the BRIC algorithm. (c) SeaWiFS estimates are obtained applying the DORMA algorithm. (d) SeaWiFS estimated are obtained applying the MedOC4 algorithm. The 1:1 (continuous line) 1:2 (bottom dashed line) and the 2:1 (top dashed line) lines are also plotted.

(**Fig. 2.5**). Considering the large variability in temporal distribution of the data used for the validation (see Tab. 1 in Volpe *et al.* (2007)), it seems unlikely that there are not evident clusters of underestimated Chl$-a$ when using the MedOC4 that could be originated by low dust concentration in the surface waters. In other words, if we enter a band ratio as measured from the SeaWiFS sensor during a free dust period (*i.e.* with a "normal" B/G), we expect that Chl$-a$ is underestimated (*e.g.* for a B/G=4, Chl$-a$ would be less than half of its "true value", ≈ 0.06 instead of ≈ 0.14 µg l^{-1}.

We pointed out that the observed discrepancy between the global and the regional bio-optical algorithms might depend on methodological differences between the datasets used to derive the algorithms coefficients. The OC4v4 algorithm was built on a later version of the SeaBAM bio-optical archive which is prevalently composed of above-water radiance measurements (88 %). On the other hand, the bio-optical

dataset used to develop the MedOC4 was mainly based on in-water radiance measurements (67 %). A recent study by Hooker and Morel (2003) showed that above-water measurements could account up to 4–8 % RPD for the blue-to-green ratios. The comparison of the two MBRs (see **Tab. 3.2** for definition) do show a difference ($\approx$ 65 % in the chlorophyll range 0.01–0.05 µg l^{-1} and $\approx$ 37 % for chlorophyll at 0.2 µg l^{-1}) which is an order of magnitude greater than what found by Hooker and Morel (2003).

A second methodological difference between the datasets, that we considered an other possible source of error, is the utilization of mostly surface chlorophyll concentration (SeaBAM) instead of the optically weighted chlorophyll concentration (MedOC4). In fact Stramska and Stramski (2005) recently demonstrated that a deep chlorophyll maximum (DCM) close to the surface can affect the radiant field by a non-negligible amount. This can quantitatively explain the failure of standard algorithms (OC4v4) on a regional basis, as long as the use of the surface chlorophyll value, as in the OC4v4, assumes a homogeneous distribution of the pigment for the first optical depth. The extent of the uncertainty depends mostly on the depth of the DCM, but also on its amplitude. Therefore we selected among our profiles those with a DCM within the first optical depth. Only 10 % of the profiles fell within this category. Afterwards we modelled our profiles with the Stramska and Stramski (2005) approach, defining a series of coupled values (chlorophyll at surface–DCM depth), and concluded that only 1 to 2 % of them had a chlorophyll value at surface and a DCM depth such to significantly affect the $R_{rs}(\lambda)$. This implies that the influence of the DCM on the surface radiant field is negligible in the Mediterranean Sea. So far it appears that the observed differences are attributable to environmental bio-optical characteristics of the Mediterranean, which ask for further investigations.

We also attempted to characterize the spectral pattern of $R_{rs}(\lambda)$, for the two datasets (SeaBAM and ours) at different Chl$-a$ ranges to highlight the differences in the spectral signatures of the basin versus the global ocean. To this aim, we analyzed the statistical distribution of $R_{rs}(\lambda)$'s values in the blue (numerator of MBR) and green bands (denominator of MBR), in the two datasets in different Chl$-a$ ranges (**Fig. 2.5**). Statistical tests (t-Student, 99 % significance) were performed on sample data to verify whether the two datasets were significantly different. In fact, the Mediterranean Sea looks relatively "greener" for low Chl$-a$ values than the global ocean and this can be either due to the fact that the Mediterranean Sea is less blue and/or effectively greener. The opposite is true for higher Chl$-a$ values in which the global ocean appears slightly greener than the Mediterranean Sea.

Histograms in **Fig. 2.5** show that in the 0.01–0.05 µg l^{-1} Chl$-a$ range the Mediterranean Sea is both less blue and greener than the global ocean. The amount of such a shift has been quantified in $\approx$ 30% RPD for the blue bands and $\approx$ 15% RPD for

the green bands. In the second range, this shift is even more evident: the $R_{rs}(\lambda)$in the blue bands measured in the Mediterranean is $\approx 35\%$ lower than that of the global ocean and the Rrs in the green is $\approx 18\%$ higher than that measured in the global ocean. In the 0.1–0.2 µg l^{-1} Chl$-a$ range the different $R_{rs}(\lambda)$ ratio is due to a blue shift of approximately 32 % while the green bands are not significantly different. The blue and the green in the 0.2–1 µg l^{-1} range are not significantly different. In the last of the considered ranges, even if the two fitting lines appear to be very close to each other **Fig. 3.16**, the datasets are significantly different.

The presence of a bias in the chlorophyll estimates is quite problematic when satellite products are used in primary production models, in validation and tuning of ecosystem modelling and especially in data assimilation systems where an error in satellite estimate can worsen rather than improve the model performance. For example the impact of the new MedOC4 algorithm on primary production estimates of the Mediterranean Sea was quantified to be approximately 10 % less than the same estimate using BRIC (Colella, personal communication). Note that the use of BRIC already reduced the Mediterranean primary production estimate of approximately 30 % with respect to the same calculation vmade using OC4v4 (Bosc *et al.*, 2004; Bricaud *et al.*, 2002). Since primary production models exhibit high sensitivity to the surface chlorophyll concentration then the selection of an adequate bio-optical algorithm becomes critical.

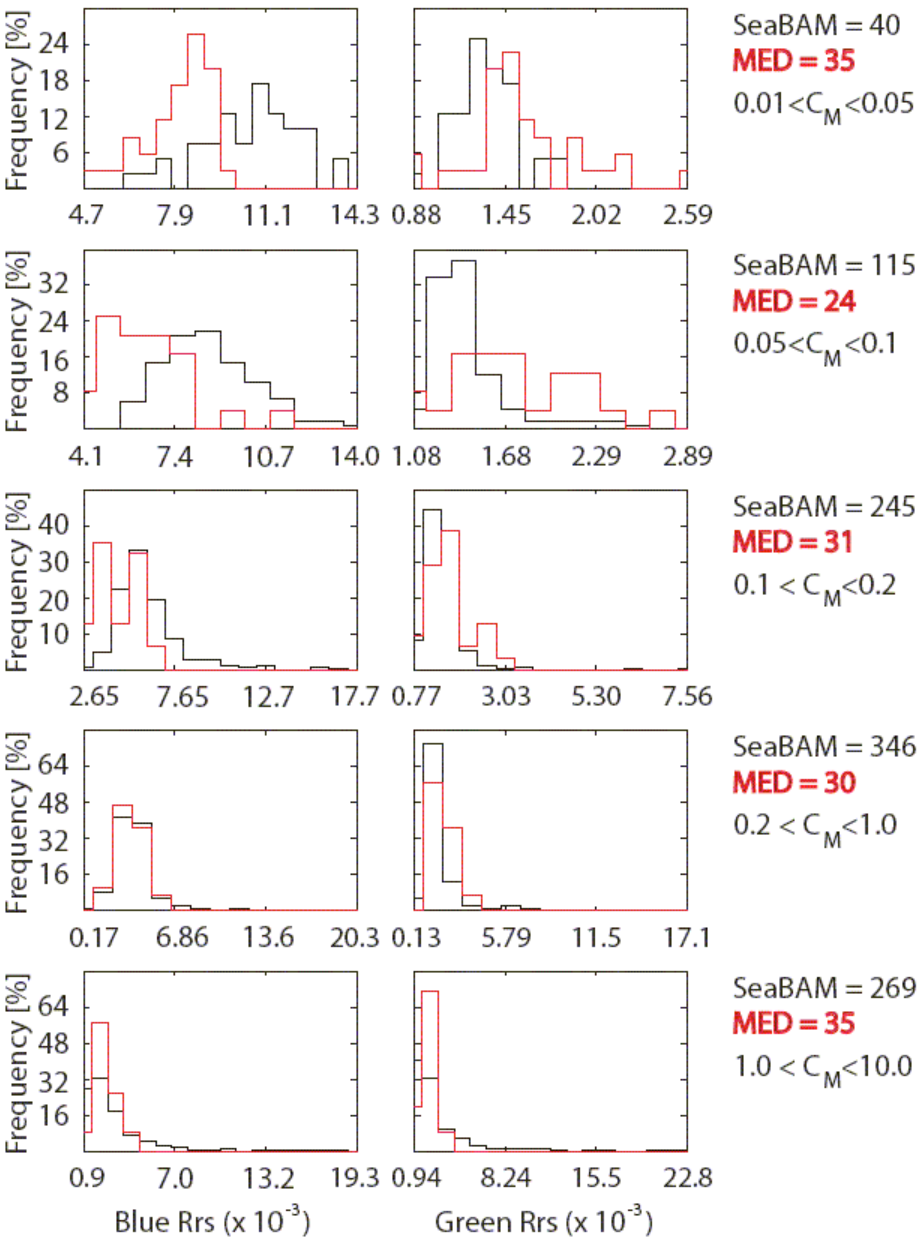

Figure 3.18: Normalized frequency histograms of the $R_{rs}(\lambda)$ for the Mediterranean (red) and SeaBAM global datasets (black) for five different Chl$-a$ ranges. Left panels indicate the maximum value among $R_{rs}(443)$, $R_{rs}(490)$ and $R_{rs}(510)$. Right panels indicate $R_{rs}(555)$. Chl$-a$ ranges are indicated on the right hand side of each row along with the number of points used for each of the two datasets.

4. Parameterization of the AOPs

In this section the study will focus on the parameterization of $K_{bio}(\lambda)$ and $K_d(\lambda)$. Even though semianalytical approaches are continuously developed, and have been demonstrated to be a very powerful tool do derive $K_d(\lambda)$ from remote sensing measurements (Lee *et al.*, 2005a,b), empirical approaches still represent a useful tool to study the bio-optical properties of a water body and to improve the performances of semi-analytical reflectance models and light transfer models, especially at regional scale. Two different parameterizations for $K_{bio}(\lambda)$ and $K_d(\lambda)$ will be presented. In the first case, the parameterization of the $K_{bio}(\lambda)$ is based on the [Chl] concentration. In the second case, the parameterization of $K_d(491)$ is based on $nL_w(\lambda)$. A summary of the results with a preliminary discussion for this section will be also given.

4.1 Estimate of $K_{bio}(\lambda)$ from [Chl] Concentration

Following the approach of Morel (1988) (M88) and Morel and Maritorena (2001) (MM01), $K_{bio}(\lambda)$ and [Chl] are related through a least square fit analysis on log transformed quantities whose results can be expressed as coefficients of the following power low (**Tab. 4.3**):

$$K_{bio}(\lambda) = \chi(\lambda)[\text{Chl}]^{e(\lambda)}. \tag{4.72}$$

For this study I considered only the first eight bands in the yellow-green domain, discarding those wavelengths where the $K_d(\lambda)$ spectrum is flattened by the Raman emission and the measured attenuation coefficients may be less than expected if the attenuation would be only due to water (Morel and Maritorena, 2001).

The results of the least square fit are reported in **Tab. 4.3** and **Fig. 4.19** for three different pairs of data:

N1 [Chl] vs. $K_{bio}(\lambda)$ in the penetration depth (coefficients denoted as $\chi_{pd}(\lambda)$ and $e_{pd}(\lambda)$);

N2 C_M vs. $K_{bio}(\lambda)$ (coefficients denoted as $\chi_{CM}(\lambda)$ and $e_{CM}(\lambda)$);

N3 [Chl] vs. $K_{bio}(\lambda)$ in the illuminated water column (coefficients denoted as $\chi_d(\lambda)$ and $e_d(\lambda)$).

In the first case the choice is made for comparison with the same physical quantities of previous works, the second is made to have coefficients that can be directly applied to

λ	χ_{pd}	e_{pd}	r^2	χ_{md}	e_{md}	r^2	χ_d	e_d	r^2
400	0.12758	0.48491	0.81	0.14126	0.51860	0.81	0.11615	0.32178	0.77
412	0.12708	0.50141	0.83	0.14117	0.53609	0.83	0.11663	0.34604	0.79
443	0.10792	0.55822	0.84	0.12120	0.59626	0.84	0.09862	0.41795	0.83
470	0.08800	0.55450	0.83	0.09868	0.59232	0.82	0.08040	0.44592	0.84
491	0.07257	0.51655	0.79	0.08074	0.55272	0.78	0.06733	0.45079	0.83
510	0.06001	0.45183	0.70	0.06591	0.48429	0.70	0.05546	0.45817	0.82
532	0.05134	0.38140	0.64	0.05557	0.40837	0.64	0.04928	0.40119	0.81
555	0.04687	0.31947	0.54	0.05011	0.34191	0.54	0.04415	0.37183	0.75

Table 4.3: $\chi(\lambda)$ and $e(\lambda)$ coefficients for the three pairs of $K_d(\lambda)$ and Chl concentrations resulting from the least square fit analysis at the selected wavelengths. The r^2 is also reported.

satellite Chl estimates, whereas the third is for possible future applications of optical models.

The regional coefficients resulting from the least square fit analysis are compared to the global coefficients of MM01. Very recently a newer version of these global coefficients has been published (Morel *et al.*, 2007a). Since these new coefficients have been retrieved with the addition of a set of Mediterranean observations, I will refer to them in the present study. They are superimposed in my scatter plots of Chl vs. $K_{bio}(\lambda)$.

N1: Figure 4.20 shows the log-log relation between $K_{bio}(\lambda)$ and [Chl] at 443 nm and 555 nm compared to results of MM01 and their last version (Morel *et al.*, 2007a).

At 443 nm the dispersion of data around the fitted line is low and there is no systematic error at any [Chl] range. The resulting fit is not as good as in MM01, mostly because of the narrower range of measured values and of the reduced number of available data ($r^2 = 0.84$, $N = 92$). However, at this wavelength the difference between the regional and global models is minimal. Instead at 555 nm there are significative differences between the regional and global models especially at low [Chl] concentrations, when $K_d(\lambda)$ is higher for the Mediterranean sea. It can be also noted that at this wavelength the differences between the previous and the updated version of global coefficients are more pronounced than in the blue region.

The spectral shape and amplitude of $\chi_{pd}(\lambda)$ are similar to that of MM01 except for blue and green wavelengths, where regional coefficients are slightly higher. By contrast the exponent $e_{pd}(\lambda)$ is between 15 and 52 % lower and the shape has a sharp decrease in the green domain respect to MM01 (**Fig. 4.19(a)**).

The application of the regional coefficients to estimate $K_{bio}(\lambda)$ are compared to the global model at two [Chl] concentrations (**Fig. 4.21(a)**(b)). 0.10 and 3.00 µg l^{-1} have been chosen as representative for oligotrophic and eutrophic regimes, and are

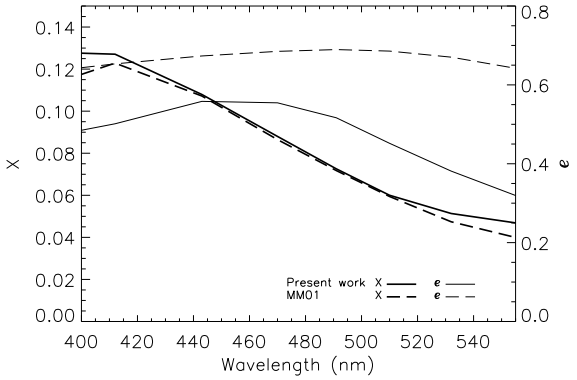

(a)

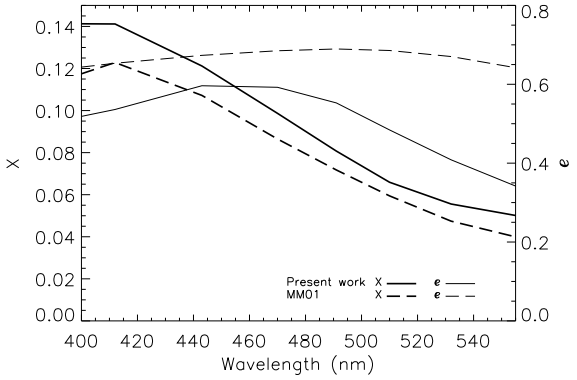

(b)

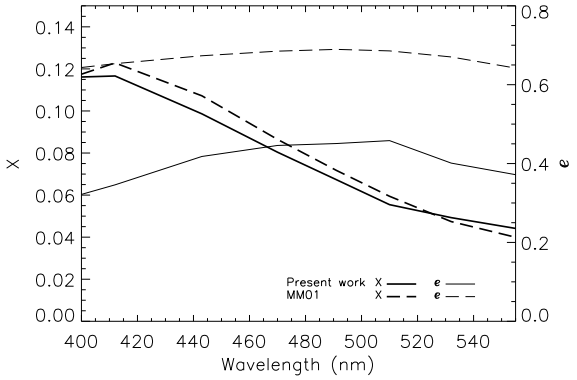

(c)

Figure 4.19: Plot of the $\chi(\lambda)$ and $e(\lambda)$ coefficients for pairs N1 (a), N2 (b) and N3 (c)

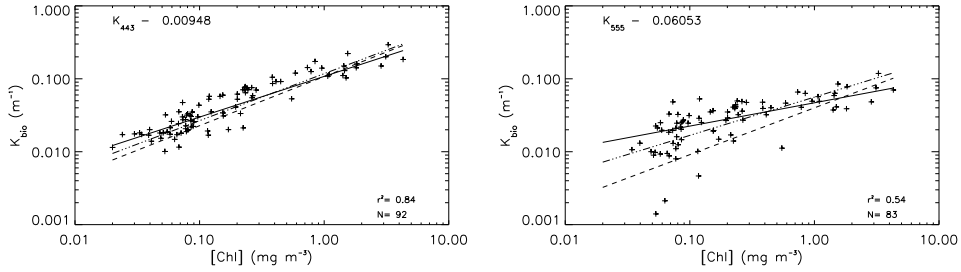

(a) (b)

Figure 4.20: Scatter plot of [Chl] versus $K_{bio}(\lambda)$ at 443 nm (a) and at 555 nm (b) within z_{pd}. Continuous line is the best fit, dotted and dashed-dotted lines are the model of MM01and it's latest version respectively.

well within the lower and upper limits of the data set (but refer to figure 4.19(a) for [Chl]= 1 µg l^{-1}.

At low [Chl] content the $K_{bio}(\lambda)$ spectrum for the Mediterranean displays higher values than for the global ocean. The APD is between 25 and 60 %, with major discrepancies in the green domain and minimum difference at 443 nm. At high [Chl], instead, the regional predicted $K_{bio}(\lambda)$ "s are lower over the whole spectrum, with an APD between 10 and 30 %.

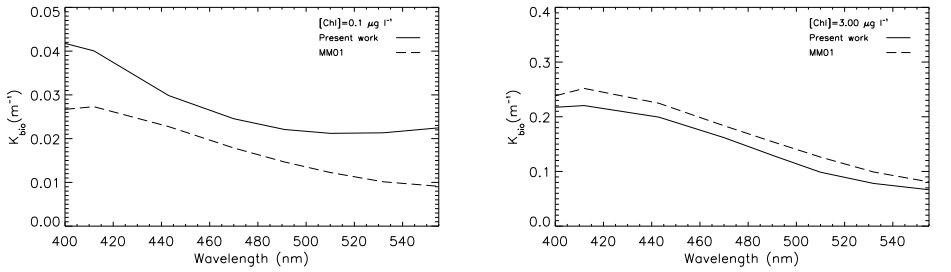

(a) (b)

Figure 4.21: $K_{bio}(\lambda)$ modeled with regional coefficients for the z_{pd} (continuous line) and global coefficients (dashed line) at 0.10 (a) and 3.00 (b) [Chl] concentrations.

N2: The difference of using an optically weighted mean Chl instead of [Chl], is that the range of pigment data for the same $K_{bio}(\lambda)$ is wider at high Chl. This does not cause particular changes in the spectral shape of the coefficients (**Fig. 4.19(b)**). However $\chi_{CM}(\lambda)$ is about 10-25 % higher than $\chi(\lambda)$. At 0.1 µg l^{-1} the $K_{bio}(\lambda)$ is practically the same of case N1, but at 3.0 µg l^{-1} it is very similar to MM01. In

this case, for the blue band, the regional and global models show higher discrepancies, whereas the opposite is true for the green band (see also figure 4.22(a) and figure 4.22(b)).These observation confirms the need of being cautious when applying satellite derived pigment estimates with empirical bio-optical models as uncertainties may be systematically introduced.

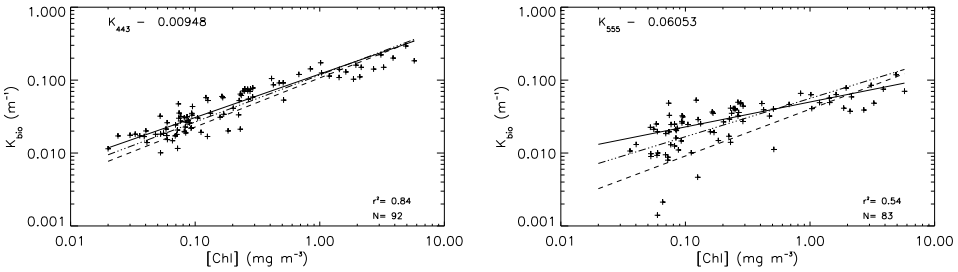

(a) (b)

Figure 4.22: Scatter plot of C_M versus $K_{bio}(\lambda)$ at 443 nm (a) and at 555 nm (b) within z_{pd}. Continuous line is the best fit, dotted and dashed-dotted lines are the model of MM01 and is it's latest version respectively.

N3: Figure 4.24 shows the log-log relation between the mean $K_{bio}(\lambda)$ and [Chl] within the illuminated water column for the two selected bands. At both 443 and 555 nm the dispersion of data around the fitted line is very low ($r^2 = 0.84$ and $r^2 = 0.75$) and there is no systematic error at any [Chl] range. There is a clearly different pattern between the regional and global models. The $K_{bio}(\lambda)(443)$ is higher in the Mediterranean in oligotrophic conditions and is lower in eutrophic conditions. The $K_{bio}(\lambda)(555)$ has a similar pattern but with more pronounced discrepancies especially

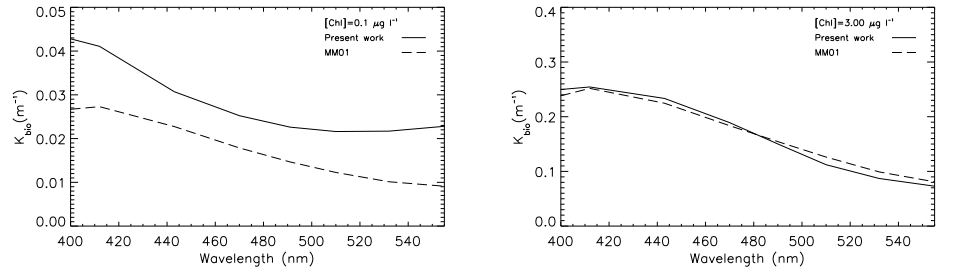

(a) (b)

Figure 4.23: $K_{bio}(\lambda)$ modeled with regional coefficient for the z_{pd} with (continuous line) and global coefficients (dashed line) at 0.10 (a) and 3.00 C_M (b) concentrations.

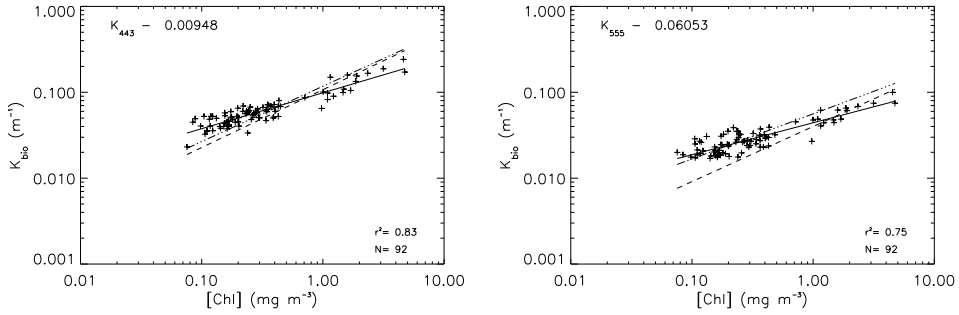

(a) (b)

Figure 4.24: [Chl] versus $K_{bio}(\lambda)$ at 443 nm (a) and at 555 nm (b) within the illuminated water column. Continuous line is the best fit, dotted and dashed-dotted lines are the model of MM01and is it's latest version respectively.

at low [Chl] concentrations. The spectral amplitude of $\chi_{pd}(\lambda)$ is similar to that of MM01 but displays a more flattened shape. The exponent $e_{pd}(\lambda)$ instead, is between 31 and 50 % lower and the shape is more similar respect to MM01 (**Fig. 4.19(c)**).

The regional coefficients to estimate $K_{bio}(\lambda)$ are compared to those of the global model in figure 4.25(a) and figure 4.25(b). At low [Chl] content the $K_{bio}(\lambda)$ spectrum for the Mediterranean displays values higer by between 36 and 56 %, with major differences in the green and violet. At high [Chl] instead, the regional predicted $K_{bio}(\lambda)$ are lower over the whole spectrum, with differences increasing from the green towards the violet between 22 and 52 %.

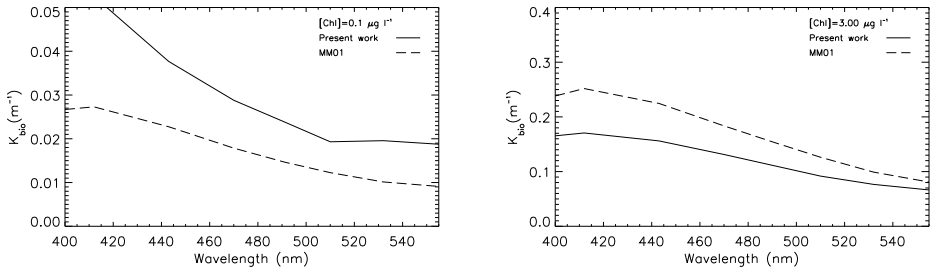

(a) (b)

Figure 4.25: $K_{bio}(\lambda)$ modeled with regional coefficient for the illuminated water column (continuous line) and global coefficients (dashed line) at 0.10 (a) and 3.00 (b) [Chl] concentrations.

4.2 Estimate of $K(490)$ from $nL_w(\lambda)$ measurements

A practical way to estimate the $K_d(\lambda)$ is by means of $nL_w(\lambda)$ ratios. The operational SeaWiFS diffuse attenuation coefficient algorithm for K_d490 is (Mueller, 2000):

$$K_d(490) = K_w(490) + A\left[\frac{L_{wn}(490)}{L_{wn}(555)}\right]^B ; \tag{4.73}$$

where the absorption coefficient for water is derived from the absorption coefficients from Smith and Baker (1981), $A = 0.15645$ and $B = -1.5401$.

Fig. 4.26 shows the scatter plot of the $nL_w(\lambda)$ ratio against the $K_{bio}(491)$ for the Mediterranean data set (the difference of 1 nm for $K_{bio}(\lambda)$ and $nL_w(\lambda)$ is assumed to be not relevant). In this situation discrepancies between the regional (that I will call K_MED1) and global algorithms are observed especially at higher trophic regimes.

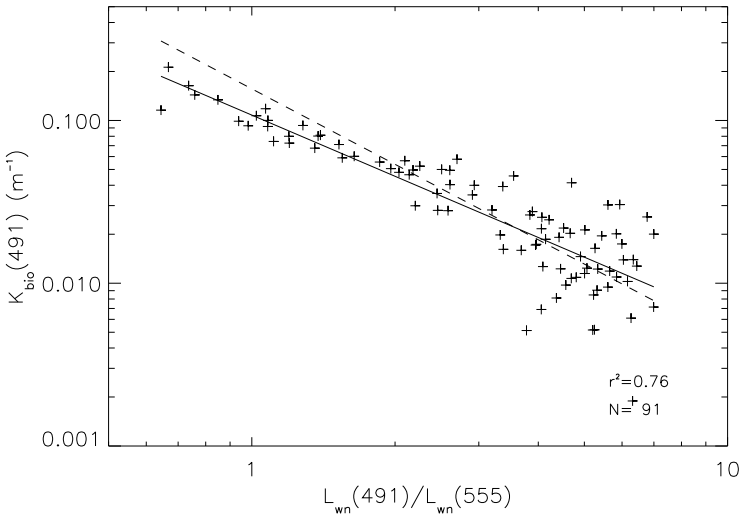

Figure 4.26: Log-log scatter plot for $nL_w(491)/nLw(555)$ and $K_d(491)$. The best fit line (continuous line) and Mueller (2000) algorithm (dashed line) are also plotted.

The new regional coefficients derived from lest square fit are $A = 0.17756$ and $B = -1.8769$, that, using the coefficient of Pope and Fry (1997) for $K_w(491)$ become $A = 0.17957$ and $B = -1.9218$. The high dispersion of data around the fitted line at greater $nL_w(\lambda)$ ratios (low $K_d(491)$ and [Chl]) has been observed by other authors for global ocean data (Werdell and Bailey, 2005). Though not strictly related from a physical point of view, $k_{bio}(443)$ better covaries with the same $nL_w(\lambda)$ ratio (see **Fig. 4.27**), with a determination coefficient $r^2 = 0.91$ respect to $r^2 = 0.74$ for $K_{bio}(490)$.

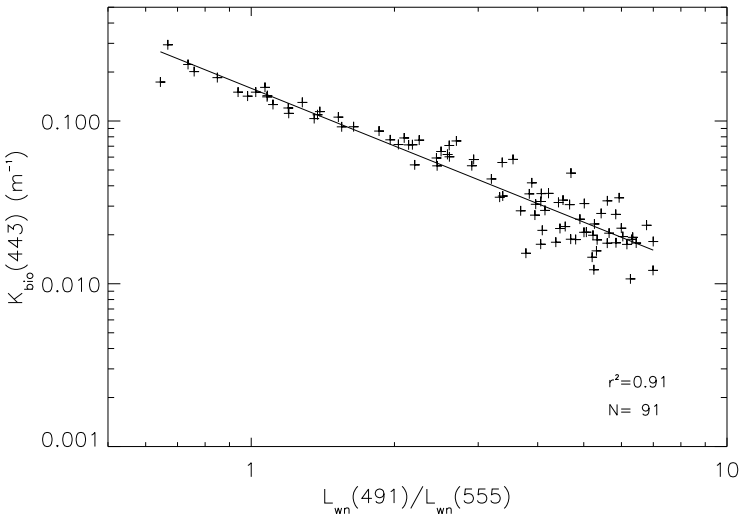

Figure 4.27: Scatter plot between the $nL_w(\lambda)$ ratio at 490 and 555 nm and $K_{bio}(443)$. The $K_w(443)$ with coefficients from Pope and Fry (1997) is subtracted to $K_d(443)$. The coefficients of the least square fit are $A = 0.15881$ and $B = -1.17672$.

The former two relationships can be combined as:

$$K_d(490) = 0.71231 \left\{ K_w(443) + A \left[\frac{L_{wn}(490)}{L_{wn}(555)} \right]^B \right\} + 0.00800. \tag{4.74}$$

The application of this two step algorithm (K_MED2) reduces the uncertainties in the retrieval of $K_{bio}(490)$ from water leaving radiance measurements. All the considered statistical parameters improve (**Tab. 4.4**). In particular, APD and RPD decrease from more than 40 and 30 % to less than 20 and 15 %.

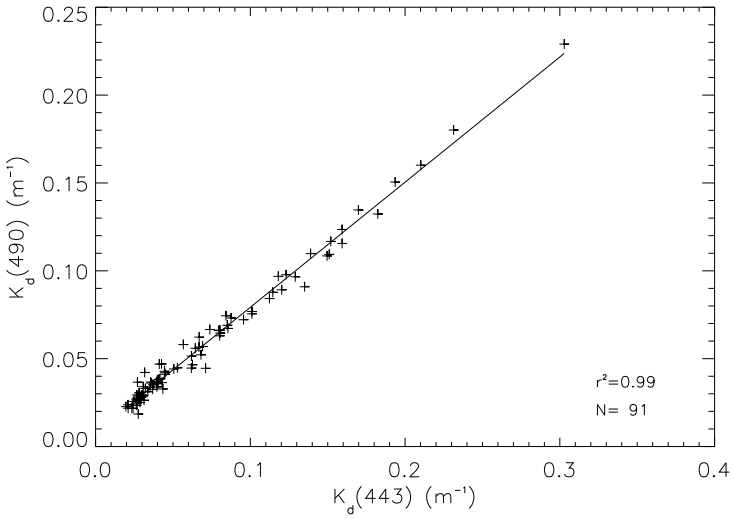

Figure 4.28: Scatter plot and best fit line for $k_{bio}(443)$ and $k_{bio}(490)$. The least square fit for log-transformed data yelds: $K_d(490) = 0.71231 K_d(443) + 0.00800$.

	Mueller (2000)	K_MED1	K_MED2
r^2	0.89	0.90	0.90
APD	44.07	40.76	19.27
RPD	-31.40	-39.72	-13.39
$BIAS$	-0.0065	-0.0180	-0.0065
RMS	0.0315	0.0219	0.0142

Table 4.4: Results of the statistical analysis performed upon the global and the two regional algorithms for $K_d(490)$.

4.3 Summary and Preliminary Discussion

In this section $K_{bio}(\lambda)$, in the blue to green wavelengths, and $K_d(491)$ have been parameterized for the Mediterranean Sea. The results have been compared to existing homologous global algorithms, showing differences between regional and global parameterizations.

Ss anticipated above, on average, the $K_{bio}(\lambda)$ in the Mediterranean Sea is considerably higher at low [Chl] concentrations, especially in the green bands. At high [Chl] concentration, instead, the $K_{bio}(\lambda)$ is slightly lower than the global ocean. Bricaud *et al.* (2002) suggested that [...the possible presence of dust in surface waters is expected to affect not only the surface reflectances, but also the euphotic depth (via the diffuse attenuation coefficient in the water column), and therefore the primary production estimate]. By means of this study, I can confirm the hypothesis that, for a given [Chl] concentration, the z_{eu} is affected by the optical characteristics of the

Mediterranean Sea but I cannot assess which is/are the optical component/s. In fact, though the spectral shape of $K_{bio}(\lambda)$ for the regional and global models differ, it is not simple to associate the different behavior to any of the optical components. A more detailed study of the single optical components is needed to better understand why the Mediterranean Sea have this characteristics.

The implications on satellite primary production estimate (*sensu* Morel (1991)), cannot be throughly assessed for two main reasons. First: the effect on z_{eu} should produce lower estimates at low [Chl] concentrations but also higher estimates at high [Chl] concentrations. Second: other factors that are critical in the computations of primary production estimates, such as the vertical distribution of phytoplankton and their photosynthetic efficiency, may be affected by the light field. Colella (2006) proposed a regional model for primary production estimates, tuning, among other parameters, a regional parameterization for z_{eu} and for vertical Chl distribution. The results of the application of the regional model to satellite imagery gives lower estimates respect to a global model.

The results also suggest that attention is needed in the use of a mean attenuation coefficient for the prediction of light decay in the water column. If the use of C_M instead of [Chl] results in minor differences in the modeled $K_d(\lambda)$, the use of $\chi_{pd}(\lambda)$ and $e_{pd}(\lambda)$ instead of $\chi_d(\lambda)$ and $e_d(\lambda)$ changes significantly the results at both high and low [Chl] concentrations.

The utilization of the $nL_w(491)/nL_w(555)$ ratio to derive K_d491 shows less discrepancies between the K_MED1 and Mueller (2000) models respect to the [Chl] based model. However the results, for both models, are not optimal, especially at low [Chl] concentrations. I proposed a new model based on algorithm that makes use also of the $nL_w(443)$. The K_MED2 has been demonstrated to give better results in reproducing the *in situ* measurements, reducing the high dispersion of data observed at low [Chl].

This dispersion of data could be attributed to the variability of the absorption of carotenoid pigments respect to that of Chl$-a$ content (Barlow *et al.*, 2002), or to the variability of the absorption and/or backscattering by other substances not directly linked to Chl$-a$ concentration at that wavelength. The 443 nm band, introduced in the new algorithm, corresponds to the absorption peak of Chl$-a$, that, at this wavelength, is likely to play a major role in determining the variability of the $K_{bio}(\lambda)$ respect to absorption and scattering of other constituents, thus resulting in a better log-linear response.

5. Parameterization of the IOPs

This section is focused on the regionalization of the parameterizations of various measured or derived IOPs. Most of them are modeled similarly to $K_d(\lambda)$ (**Eq. 4.72**), with coefficients ($\alpha(\lambda)$) and exponents ($\beta(\lambda)$) of the fitting power function derived with regression analysis on log transformed data:

$$IOP_i(\lambda) = \alpha(\lambda)\mathrm{Chl}^{\beta(\lambda)} \tag{5.75}$$

The results of the least square fit are reported in **Tab. 4.3** for three different pairs of data:

N1: Chl vs. one of the IOPs, collected within the z_{pd};

N2: Chl vs. one of the IOPs, collected within the z_{eu};

N3: Chl vs. one of the IOPs, for the whole data set (*i.e.* with data collected outside the z_{eu} or during the night, z_n).

When a different model is adopted it will be described in the dedicated subsection. The results of the regional models are compared to the most representative homologous for the global ocean. The section is divided in six subsections for different IOPs, with the exception of starting with the IOPs that have been directly measured and concluding with those that have been derived with the aim to build a regional semi-analytical reflectance model. A summary of the results with a preliminary discussion for this section will be also given.

5.1 Absorption of Particulate, Phytoplankton and Non-Algal Particles

$\alpha(\lambda)$ and $\beta(\lambda)$ derived from the three subsets for $a_p(\lambda)$ and $a_{ph}(\lambda)$ coefficients are shown in **Fig. 5.29** together with the determination coefficients. Their values are also reported in the appendix (section 6.1) at 2 nm resolution.

The spectral shape of the coefficients are similar between the three data set, whereas their values increase from subset N3 to N1.

The determination coefficient in all cases has a maximum in correspondence of the red absorption of Chl$-a$ between 650 and 700 nm. In this region Chl$-a$ is the major responsible of the absorption coefficient for both particulate and phytoplankton, and in fact in this region the difference between the r^2 for the two components are close. Moreover, these values are similar among the three subset.

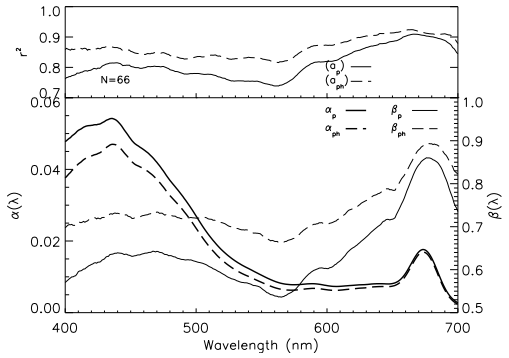

(a)

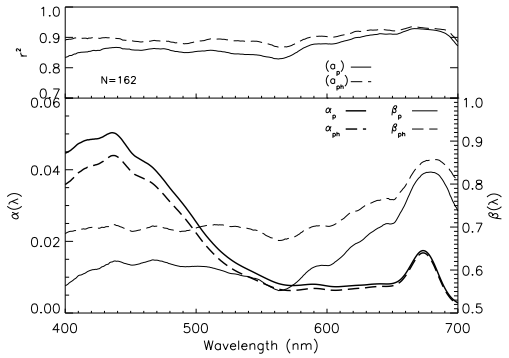

(b)

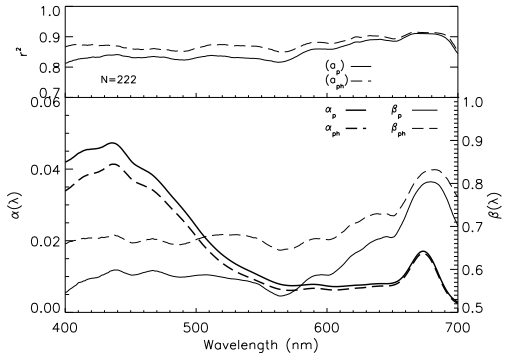

(c)

Figure 5.29: For each panel the lower box represents the coefficients for the log-log relationship for Chl versus $a_p(\lambda)$ (continuous line) and $a_{ph}(\lambda)$ (dashed line) α (left axis, thick line) and β (right axis, thin line); while the top box represents the determination coefficients for $a_p(\lambda)$ (continuous line) and $a_{ph}(\lambda)$ (dashed line). In panel (a) are the coefficients derived for case N1 (values are reported in **Tab. 9.17**, **Tab. 9.18**, **Tab. 9.19**); in panel (b) are the coefficients derived for case N2 (values are reported in **Tab. 9.14**, **Tab. 9.15**, **Tab. 9.16**); in panel (c) are the coefficients derived for case N3 (values are reported in **Tab. 9.20**, **Tab. 9.21**, **Tab. 9.22**).

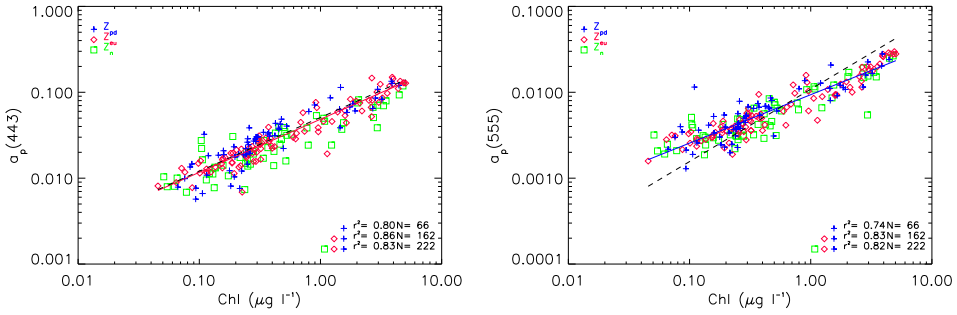

(a) (b)

Figure 5.30: Scatter plot of Chl versus $a_p(443)$ (a) and $a_p(555)$ (b). Crosses indicates data for case N1, diamonds are used for data added in case N2, and squares are used for data added for case N3. Continuous line is the best fit on log-transformed data for case N2 and dashed line is the model of BR98.

In the remaining part of the spectra the r^2 is always greater for $a_{ph}(\lambda)$ as expected, thus confirming a good partitioning of the two components with the $NaClO$ technique. In general r^2 is lower for case N1 due to the more limited number of available data, but the highest values are for case N2 as the circadian variability is more limited than case N3. Finally the difference between the r^2 of $a_p(\lambda)$ and $a_{ph}(\lambda)$ are more pronounced within the z_{pd}, thus indicating a higher variability of particulate optically active components non directly linked to Chl$-a$.

$\beta_{a_p}(\lambda)$ and $\beta_{a_{ph}}(\lambda)$ have similar shape. But, their values differ remarkably all over the spectrum if compared to what observed in BR98, except in the red Chl$-a$ absorption domain. This means that absorption by non-algal particles is not proportional to total particle absorption. Moreover the relative contribution of phytoplankton to particulate absorption varies with pigment content.

In particular at low (0.10 µg l^{-1}) and high (3.00 µg l^{-1}) Chl content, $a_{ph}(\lambda)$ is respectively 57 % and 81 % of $a_{ph}(\lambda)$ at 400 nm (88 and 96 % at 675 nm). BR98 found a nearly constant $a_{ph}(\lambda)$ to $a_p(\lambda)$ ratio of 0.55 and 0.88 for the 400 and 675 nm bands. This implies that, for the Mediterranean data set the absorption of light by phytoplankton in respect to total particulate absorption behaves similarly to global ocean only at low trophic regimes, and increases with increasing biological activity.

$\alpha_{a_p}(\lambda)$ values are similar to those found in BR98 whereas $\beta_{a_p}(\lambda)$ values are generally lower. The spectral shape of the $\alpha(\lambda)$ coefficients appear similar to the global model except in the violet where the mean Mediterranean spectrum is more flattened.

At the blue absorption peak (443 nm) there are not significant differences for both $a_p(\lambda)$ and $a_{ph}(\lambda)$ between regional and BR98 models (**Fig. 5.30(a)**,**Fig. 5.31(a)**).

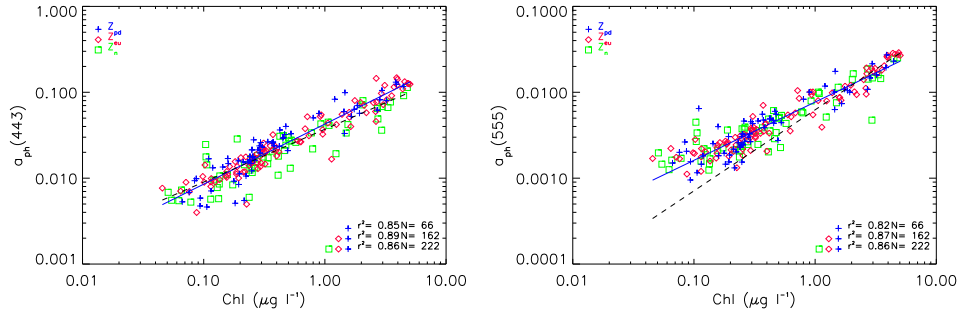

(a) (b)

Figure 5.31: Scatter plot of Chl versus $a_{ph}(443)$ (a) and $a_{ph}(555)$ (b). Symbols are the same **Fig. 5.30**. Continuous line is the best fit on log-transformed data for case N2 and dashed line is the model of BR98.

On the contrary, at the green absorption minimum, $a_{ph}(555)$ becomes relatively higher with decreasing pigment content (**Fig. 5.31(b)**). This pattern is similar for $a_p(555)$ at Chl$<$ 1 µg l^{-1}, while it becomes relatively lower with increasing pigment content (**Fig. 5.30(b)**).

$a_{nap}(\lambda)$ has an extremely low correlation with Chl at all wavelengths **Fig. 5.32**. Practically the absorption of non algal particles is approximately constant at all trophic conditions, being "insensitive" to changes in living phytoplankton content.

An extended data set of $a_{nap}(\lambda)$ spectra was fitted with equation **Eq. 1.42** to derive the slope of the spectra. The data set is larger (N=606) as this analysis was not limited by the number of available Chl data. The resulting mean slope is 0.011 ± 0.003 nm^{-1}, that is identical to values found from previous authors (*i.e.* 0.011 ± 0.002 nm^{-1} for both BR98 (N=267) and Roesler *et al.* (1989)) with a mean $r^2 = 0.98$.

BR98 found the ratio of non-algal absorption to total particulate matter at 440 nm to vary between 0.07 and 0.80, with most of cases falling between 0.15 and 0.60, with extreme values found in tropical-equatorial and Mediterranean ecosystems respectively. They did not found any general regular pattern linked to the Chl content. On the contrary the Mediterranean data set under study shows a clear negative trend, with $\alpha_{a_{nap}}(440)/\alpha_{a_p}(440)$ exponentially decreasing with increasing Chl ($r^2 = 0.68$ on log transformed quantities). The range of variability within our data set is between 0.01 and 0.48 with values well distributed through the whole range. We did not observe the high values found by BR98 in the Mediterranean Sea, however the ratios are similar in the same Chl range.

The specific absorption coefficients of phytoplankton ($a^*_{ph}(\lambda)$) account for the

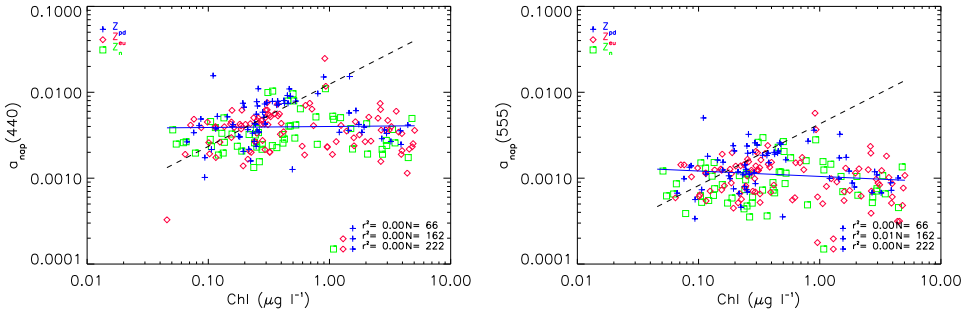

(a) (b)

Figure 5.32: Scatter plot of $a_{nap}(443)$ (a) and $a_{nap}(555)$ (b) versus Chl. Crosses indicates data sampled in the penetration depth, diamonds are further data sampled within the euphotic depth and squares represent data sampled outside the z_{eu} or during the night. Continuous line is the best fit on log-transformed data within the penetration depth and dashed line is the model of BR98.

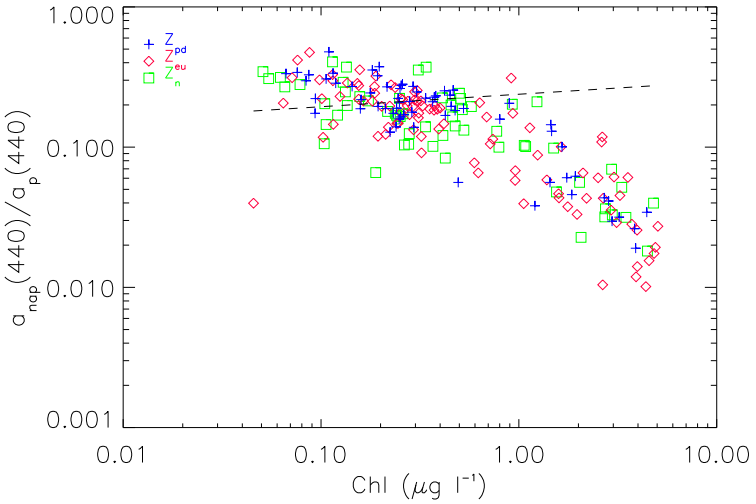

Figure 5.33: Ratio of non-algal particles and total particles absorptions against Chl concentration at 440 nm. Symbols are the same of **Fig. 5.30**. The same ratio derived from BR98 models is also plotted.

major part of the specific absorption coefficient of particulate ($a_p^*(\lambda)$) at Chl> 3 µg l^{-1}. The relative importance of the specific absorption coefficients of non-algal particle ($a_{nap}^*(\lambda)$) increases with decreasing [Chl] concentrations and is almost half of $a_p^*(\lambda)$ for [Chl]= 0.03 µg l^{-1} in the violet and green bands (**Fig. 5.34**).

In **Fig. 5.35** the specific absorption coefficients of the three components for the

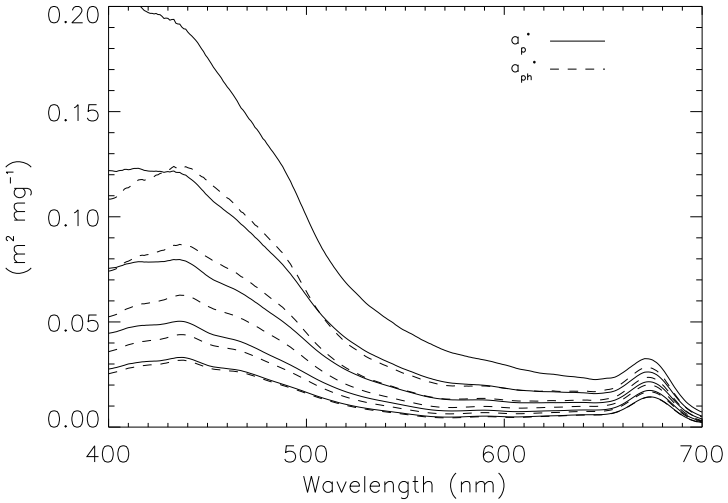

Figure 5.34: Specific absorption coefficients for particulate (continuous line) and phytoplankton (dashed line) at five Chl concentrations for the regional models within the euphotic depth(0.03, 0.10, 0.30, 1.00 and 3.00 from the top to the bottom).

regional and global models are displayed at five Chl concentrations. $a_p^*(\lambda)$ shows a similar variability for the two models, though with some differences in the violet and the green domain at low Chl concentrations (**Fig. 5.35(a)**), where values are higher for the Mediterranean Sea. A similar shape for the absorption coefficients of particulate has been observed also in other coastal and offshore waters of the Western Mediterranean Sea (Duarte *et al.*, 1998; Allali *et al.*, 1995).

The two components, $a_{ph}^*(\lambda)$ and $a_{nap}^*(\lambda)$ have different patterns respect to [Chl] concentration. On average, $a_{nap}^*(\lambda)$ is higher in the Mediterranean at low [Chl] concentrations respect to the global ocean, and is lower in eutrophic conditions (**Fig. 5.35(c)**). The opposite pattern is found for $a_{ph}^*(\lambda)$ in the blue region. In the violet the $a_{ph}^*(\lambda)$ is always higher in the Mediterranean. In the green-orange, $a_{ph}^*(\lambda)$ is similar at high [Chl] concentration but higher in meso-oligotrophic conditions. Finally, in the red, $a_{ph}^*(\lambda)$ is similar in eutrophic conditions and more packaged at low [Chl] concentrations (**Fig. 5.35(b)**).

The relative maximum in the red absorption differs by only 1 nm (the peak is centered at 673 nm for the Mediterranean and at 674 nm for BR98) at all Chl concentrations. The blue maxima, instead, are close only at higher [Chl] and their distance increases, in the wavelength space, with decreasing [Chl] concentration. In fact the blue absorption peak for the Mediterranean is centered at 438-439 nm, whereas it shifts from 439 to 448 nm from 3.00 to 0.01 µg l^{-1} [Chl] concentration.

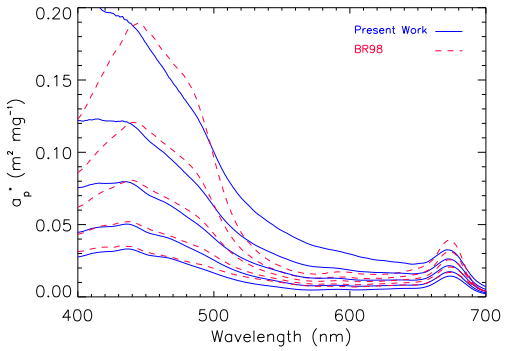

(a)

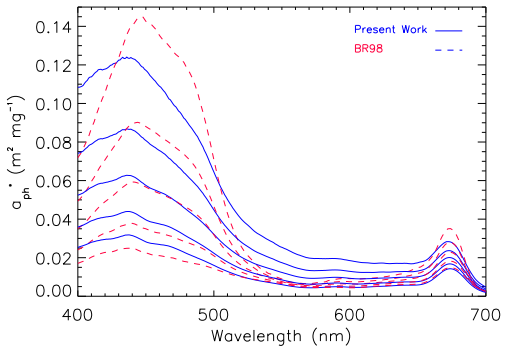

(b)

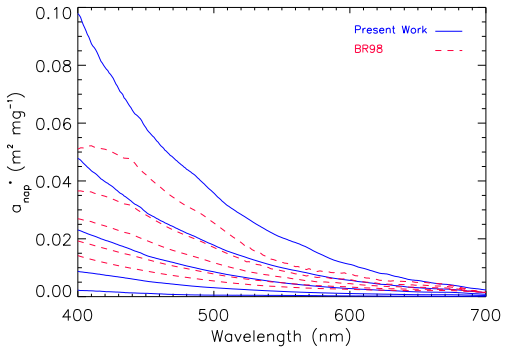

(c)

Figure 5.35: Specific absorption coefficients for (a) particulate, (b) phytoplankton and (c) for the regional (continuous line) and global (BR98 dashed line) models at five Chl concentrations (0.03, 0.10, 0.30, 1.00 and 3.00 from the top to the bottom).

5.2 Total Absorption without Water Contribution

Figure 5.36 shows the relationship established between Chl and $a_{pg}(\lambda)$. Data for case N1 are better predicted by the best fit line. Determination coefficient was 0.79 and 0.87 for the 440 and 555 nm bands, whereas it was less than 0.7 at 440 nm and less than 0.8 at 555 nm for the other two subsets. The spectral coefficients resulting from the least square fit analysis are reported in **Tab. 5.5**.

The cluster of data with the highest absorption at 440 nm derives from two stations sampled in the GoL. They are probably attributable to a plume from the Rhône river rich in CDOM, in fact these values decrease with increasing wavelength and the corresponding attenuation spectra show a higher slope and do not correspond to maxima in the $c_{pg}(\lambda)$ data set (cfr. **Fig. 2.15** and **Fig. 9.64**). Nonetheless they show a covariation with [Chl] and therefore they were not discarded from the study.

$a_{pg}(\lambda)$ for the subset N2 has been compared to the sum of global models for $a_p(\lambda)$ and $a_{ys}(\lambda)$. The relationship established between Chl and $a_{pg}(555)$(**Fig. 5.36(b)**) confirms a higher absorption in the green domain as observed for $a_p(\lambda)$ and $K_{bio}(\lambda)$. $a_{pg}(440)$ departs from the global model being higher toward low pigment concentrations (**Fig. 5.36**, **Tab. 5.5**).

Barnard *et al.* (1998) proposed global spectral relationships for IOPs measured with an ac9, and were used for a comparison with the regional models. **Fig. 5.37** shows a comparison of the relationship between $a_{pg}(440)$ and $a_{pg}(555)$ for the regional data set compared to Barnard *et al.* (1998) model. Note that coefficients for the global model are derived from relationships of the two variables with $a_{pg}(488)$. With the

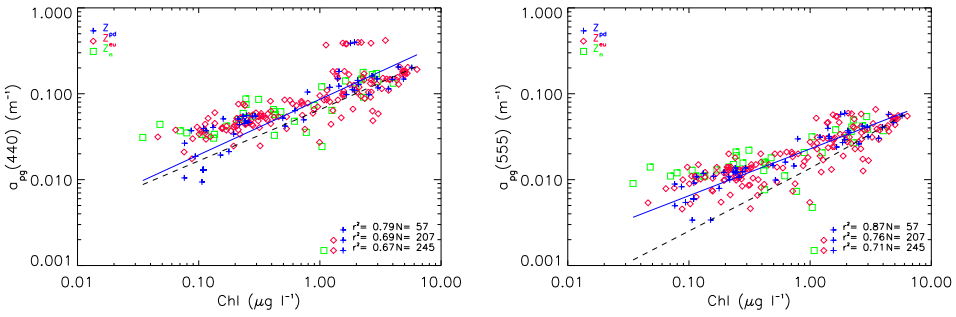

(a) (b)

Figure 5.36: Total absorption coefficient net of water contribution against Chl concentration at 440 nm **Fig. 5.36(a)** and 555 nm **Fig. 5.36(b)**. Symbols are the same of **Fig. 5.30**. The best fit line (continuous line) for the penetration depth and the sum of the global model for $a_p(\lambda)$ and $a_{ys}(\lambda)$ are also plotted.

		z_{pd}			z_{eu}			z_n	
λ	$\alpha(\lambda)$	$\beta(\lambda)$	r^2	$\alpha(\lambda)$	$\beta(\lambda)$	r^2	$\alpha(\lambda)$	$\beta(\lambda)$	r^2
412	0.110	0.463	0.724	0.111	0.379	0.545	0.111	0.357	0.525
440	0.086	0.647	0.799	0.087	0.512	0.695	0.087	0.487	0.678
488	0.057	0.661	0.835	0.056	0.558	0.773	0.056	0.538	0.763
510	0.042	0.649	0.824	0.040	0.556	0.765	0.040	0.534	0.748
532	0.031	0.601	0.845	0.030	0.537	0.778	0.030	0.513	0.756
555	0.022	0.545	0.876	0.021	0.482	0.761	0.022	0.454	0.715
650	0.010	0.454	0.683	0.009	0.431	0.655	0.009	0.426	0.637
676	0.019	0.706	0.822	0.019	0.697	0.831	0.019	0.679	0.810

Table 5.5: $\alpha(\lambda)$ and $\beta(\lambda)$ and coefficients for the total absorption net of water contribution for the three subset of data. The determination coefficients are also reported.

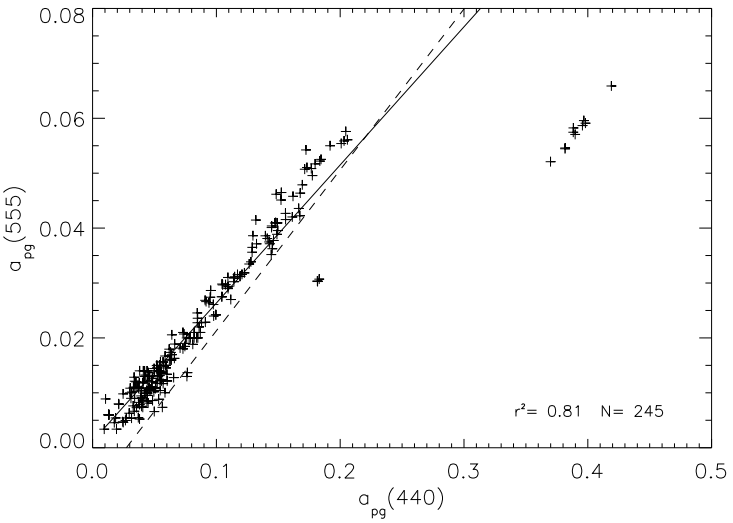

Figure 5.37: Scatter plot of $a_{pg}(555)$ versus $a_{pg}(440)$ The equation for the best line fit (continuous line) is: $a_{pg}(555) = 0.251a_{pg}(440)+0.001$, the global model from Barnard *et al.* (1998) (dashed line) is also plotted and its derived equation is $a_{pg}(555) = 0.293a_{pg}(440) - 0.008$.

exception of the high CDOM stations, the $a_{pg}(555)$ is constantly higher relative to $a_{pg}(555)$ respect to the global model over the entire range of measured values. By consequence the green to blue ratio for $a_{pg}(\lambda)$ is higher in the Mediterranean Sea.

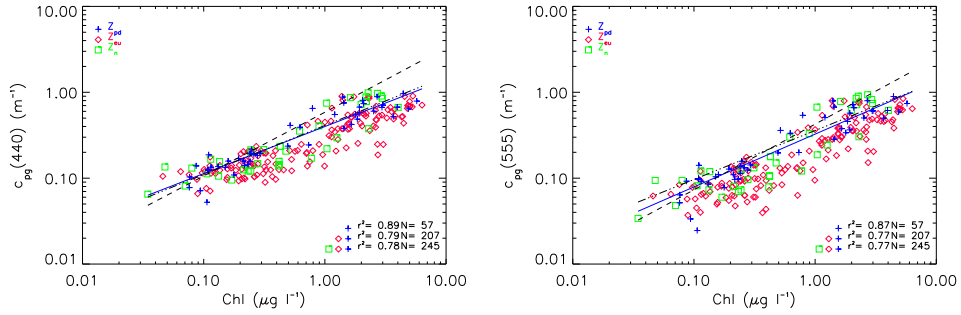

(a) (b)

Figure 5.38: Total attenuation coefficient net of water contribution against Chl concentration at 440 nm **Fig. 5.38(a)** and 555 nm **Fig. 5.38(b)**. Symbols are the same of **Fig. 5.30**. The best fit line (continuous line) for the penetration depth and the sum of the global model for $a_p(\lambda)$, $a_{ys}(\lambda)$ $b_p(\lambda)$ (dashed line) and the model of Voss (1992) are also plotted.

5.3 Total Attenuation without Water Contribution

Regression analysis on log-transformed Chl and $c_{pg}(\lambda)$ data has been performed too and the resulting spectral coefficients are reported in **Tab. 5.6**.

Similarly to $a_{pg}(\lambda)$, the determination coefficient for the surface layer is higher than for the other two subsets for both the blue and green bands considered. As observed by other authors Loisel and Morel (1998) the $c_{pg}(\lambda)$ is higher in the shallower layer.

The regional model has been compared to the sum of the $b_p(\lambda)$ model proposed by Loisel and Morel (1998) (that will be reminded in the next section) and that already described for $a_p(\lambda)$ and $a_{ys}(\lambda)$ and to that proposed by Voss (1992):

$$c_{pg}(\lambda) = 0.39\mathrm{Chl}^{0.57}(1.563 - 1.159 \cdot 10^{-3}\lambda). \tag{5.76}$$

The regional model is not significantly different from the two global models. Especially that of Voss (1992) is close to the regional model and they have similar slopes. The sum of the various IOPs has a greater slope, that causes a slight overestimation at higher pigment content at 440 nm (**Fig. 5.38**).

The relationship between $c_{pg}(440)$ and $c_{pg}(555)$ shows a similar slope respect the global model of (Barnard *et al.*, 1998) but a higher intercept (**Fig. 5.39**).

	z_{pd}			z_{eu}			z_n		
λ	$\alpha(\lambda)$	$\beta(\lambda)$	r^2	$\alpha(\lambda)$	$\beta(\lambda)$	r^2	$\alpha(\lambda)$	$\beta(\lambda)$	r^2
412	0.437	0.535	0.904	0.363	0.476	0.787	0.370	0.485	0.787
440	0.398	0.547	0.898	0.322	0.503	0.793	0.330	0.511	0.789
488	0.364	0.576	0.881	0.285	0.548	0.791	0.294	0.555	0.787
510	0.346	0.601	0.857	0.268	0.574	0.777	0.276	0.579	0.772
532	0.337	0.599	0.888	0.258	0.580	0.789	0.266	0.588	0.784
555	0.325	0.615	0.872	0.246	0.598	0.778	0.254	0.606	0.776
650	0.292	0.625	0.877	0.212	0.626	0.755	0.218	0.641	0.756
676	0.275	0.660	0.846	0.198	0.651	0.743	0.205	0.665	0.749

Table 5.6: $\alpha(\lambda)$ and $\beta(\lambda)$ and coefficients for the total attenuation net of water contribution for the three subset of data. The determination coefficients are also reported.

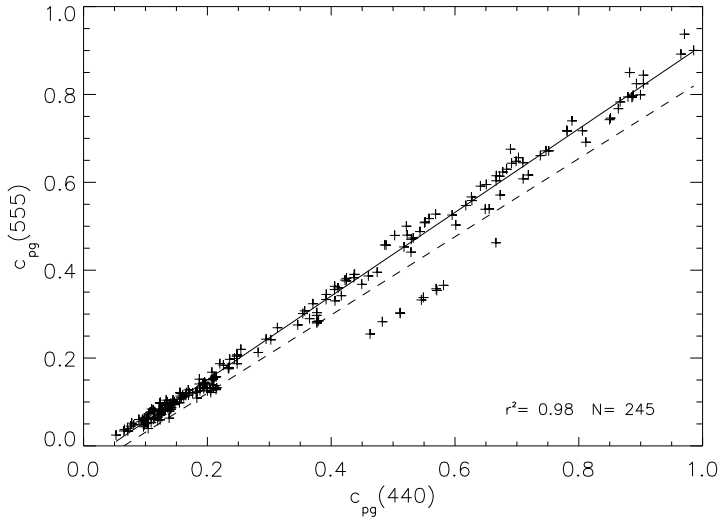

Figure 5.39: Scatter plot of $c_{pg}(555)$ versus $c_{pg}(440)$ The equation for the best line fit (continuous line) is: $c_{pg}(555) = 0.952c_{pg}(440) - 0.0397$, the global model from Barnard *et al.* (1998) (dashed line) is also plotted and its derived equation is $c_{pg}(555) = 0.890c_{pg}(440) - 0.058$.

5.4 Absorption of CDOM

Total absorption coefficient of CDOM has a functional form similar to that of $a_{nap}(\lambda)$ and the common model adopted for oceanic case I waters is that generated by combining the models of Bricaud *et al.* (1981) and Prieur and Sathyendranath (1981):

$$a_{ys}(\lambda) = 0.2 \left[a_w(440) + 0.06\mathrm{Chl}^{0.65} \right] e^{[-0.014(\lambda - 440)]}. \tag{5.77}$$

Here CDOM was not directly measured and I attempted to derive it by subtracting particulate absorption from total absorption (less water) on common wavelengths when concurrent measurements were available. It must be underlined that there are many uncertainties linked to this procedure since the two measurement protocols differ greatly. Moreover the difference between the two is in fact the absorption of particles and dissolved substances between 0.22 and 0.7 µm, *i.e.* the absorption of what passes through a filter used for the measure of $a_p(\lambda)$ but not passes through a filter used to determine $a_{ys}(\lambda)$.

179 matches between $a_{pg}(\lambda)$ and $a_p(\lambda)$ were found. The resulting $a_{ys}(\lambda)$ spectra were set to zero at 650 nm and then fitted with **Eq. 1.44** to derive the slope of the curve. The fitting was generally good, except for few spectra that were removed from the analysis using a threshold of $r = -0.95$ that reduced the data set to 129 spectra (**Fig. 5.40**). The mean determination coefficient for this data set was 0.99. The slope had a mean value of 0.013 ± 0.0032 nm^{-1} with a range of variation between 0.005 and 0.021 nm^{-1} that is close to that found by Bricaud *et al.* (1981) of 0.014 ± 0.0032 nm^{-1}, with data ranging between 0.010 and 0.010 nm^{-1}.

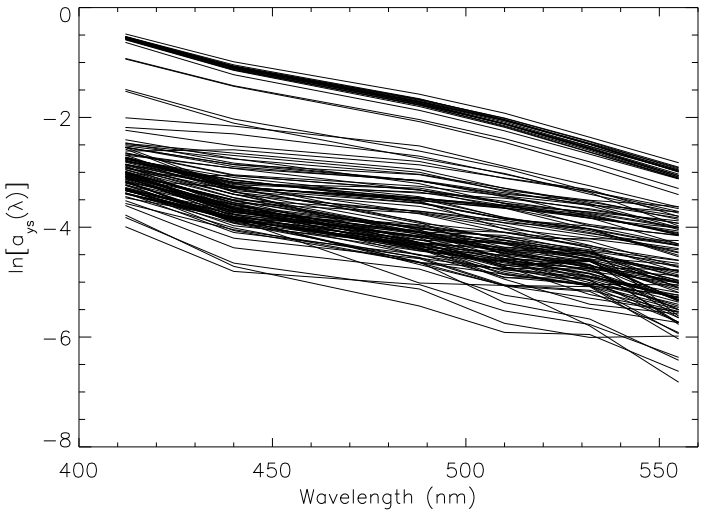

Figure 5.40: Natural logarithm of the 129 absorption spectra of CDOM used to retrieve the mean slope of the exponential function used to model the spectra.

Then the $a_{ys}(440)$ was compared to the sum of $a_p(440)$ and $a_w(440)$ to estimate its relative contribution to absorption (**Fig. 5.41**). The dispersion of data is very high, *i.e* there is a high variability in the ratio between absorption of CDOM and absorption of particulate (water is constant). The mean ratio for $a_{ys}(440)/[a_p(440) + a_w(440)]$ is 0.6 with minimum and maximum values of 0.02 and 2.2.

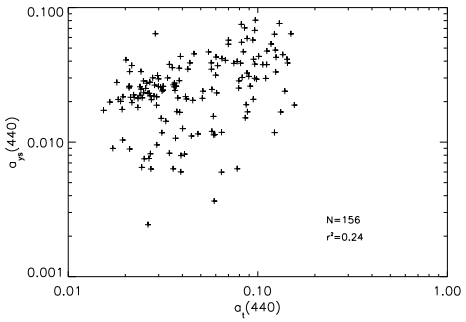

Figure 5.41: Scatter plot of the absorption coefficient of CDOM versus $a_p(\lambda)$ plus $a_w(\lambda)$ at 440 nm. Some outliers were excluded from the data set with less restrictive criteria respect to the estimate of the slope. The best fit line equation (not plotted) is $a_{ys}(440) = 0.218[a_p(440) + a_w(440)] + 0.0158$

This information, coupled with the estimates of the slope allow to tune a regional model for CDOM with same functional form of the global model:

$$a_{ys}(440) = 0.6 * [0.00635 + 0.0497\text{Chl}^{0.621} e^{[-0.013(\lambda - 440)]} \tag{5.78}$$

Figure 5.42 shows the application of the regional and global models at various Chl concentrations. For the Mediterranean Sea, $a_{ys}(\lambda)$ is higher at all the considered Chl concentration. At 0.10 µg l^{-1} the $a_{ys}(\lambda)$ is about 2.5-3.5 times higher over the whole spectrum (increasing from blue to green), whereas it is 2.4-3.2 times higher for 1.00 µg l^{-1}.

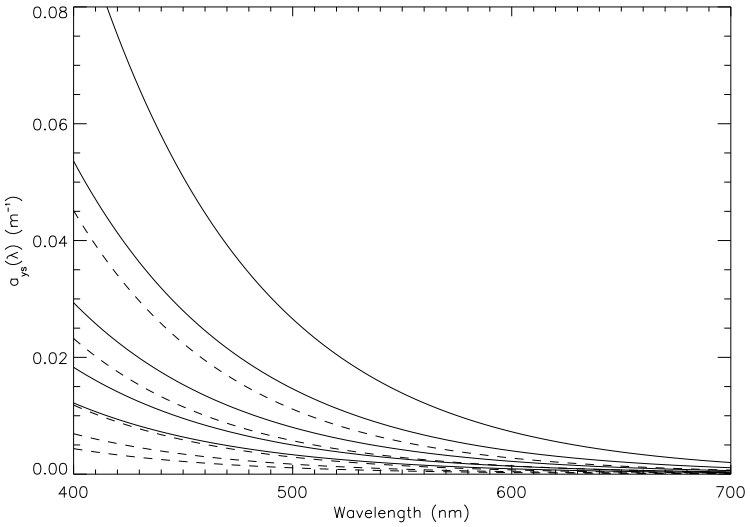

Figure 5.42: Absorption cofficients of CDOM obtained using the regional (continuous line) and global (dashed line) models at five Chl concentrations (0.03, 0.10, 0.30, 1.00 and 3.00 from the bottom to the top.

5.5 Total Scattering without Water Contribution

Total scattering coefficients without water contribution have been calculated as difference from the $c_{pg}(\lambda)$ and $a_{pg}(\lambda)$. The results for the regression analysis on log-transformed Chl and $b_p(\lambda)$ data are reported in **Tab. 5.7**. The determination coefficients for the relationships between $b_p(440)$ and $b_p(555)$ with Chl are 0.80 and 0.85 respectively for subset N1. They are higher than those for subsets N2 and N3, similarly to what observed by (Loisel and Morel, 1998).

The regional model for subset N1 has been compared to global model proposed by Loisel and Morel (1998) for the homogeneous surface layer:

$$b_p(\lambda) = 0.416[\text{Chl}]^{0.766}\left(\frac{550}{\lambda}\right). \tag{5.79}$$

For both 440 and 555 nm the two model are comparable at low [Chl] range, whereas the global models shows higher values for eutrophic regimes (**Fig. 5.43**).

The regional coefficients at 555 nmare almost identical to that found for the 550 nm band from Gordon and Morel (1983) (not shown), who reported $\alpha(550) = 0.30$ and $\beta(550) = 0.62$.

The spectral behavior of the regional model is close to that observed by Barnard *et al.* (1998) for the global ocean. In figure 5.44 the scatter plot between $b_p(440)$ and

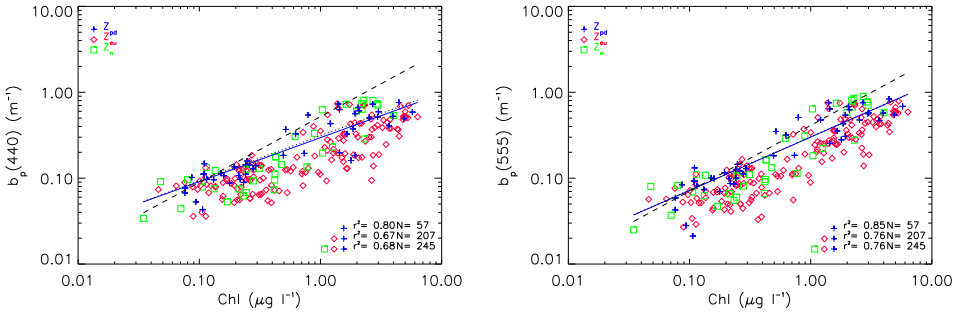

(a) (b)

Figure 5.43: Total scattering coefficient net of water contribution vs. Chl concentration at 440 nm **Fig. 5.43(a)** and 555 nm **Fig. 5.43(b)**. Symbols are the same of **Fig. 5.30**. The best fit line (continuous line) for the penetration depth and the model of Loisel and Morel (1998) are also plotted.

	z_{pd}			z_{eu}			z_n		
λ	$\alpha(\lambda)$	$\beta(\lambda)$	r^2	$\alpha(\lambda)$	$\beta(\lambda)$	r^2	$\alpha(\lambda)$	$\beta(\lambda)$	r^2
412	0.296	0.521	0.765	0.218	0.479	0.546	0.227	0.513	0.582
440	0.296	0.511	0.808	0.220	0.492	0.672	0.228	0.513	0.682
488	0.299	0.560	0.834	0.223	0.545	0.735	0.231	0.558	0.736
510	0.299	0.594	0.827	0.223	0.578	0.742	0.231	0.586	0.740
532	0.302	0.599	0.867	0.225	0.587	0.766	0.233	0.599	0.763
555	0.301	0.621	0.856	0.222	0.612	0.761	0.229	0.625	0.762
650	0.281	0.634	0.871	0.201	0.639	0.745	0.207	0.656	0.747
676	0.251	0.677	0.764	0.175	0.659	0.685	0.182	0.674	0.697

Table 5.7: $\alpha(\lambda)$ and $\beta(\lambda)$ and coefficients for the total scattering net of water contribution for the three subset of data. The determination coefficients are also reported.

$b_p(555)$ shows that the relationship is well constrained with the exclusion of the high CDOM stations in the GoL where the $b_p(555)$ is higher than $b_p(440)$.

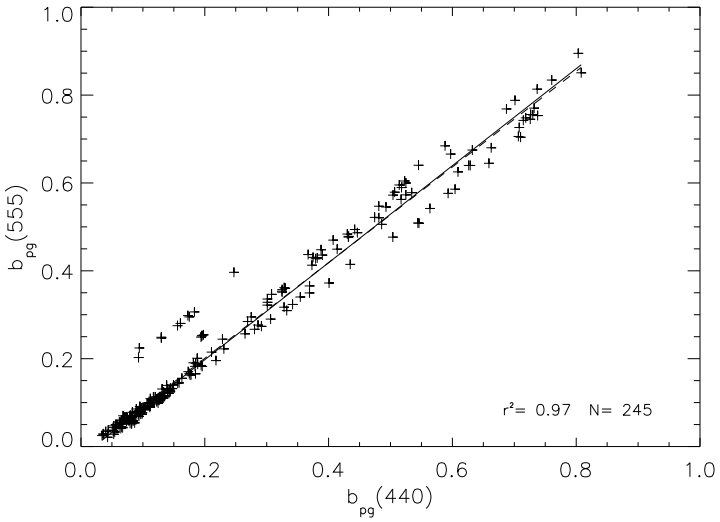

Figure 5.44: Scatter plot of $b_p(555)$ versus $b_p(440)$ The equation for the best line fit (continuous line) is: $b_p(555) = 1.104 b_p(440) - 0.023$, the global model from Barnard *et al.* (1998) (dashed line) is also plotted and its derived equation is $b_p(555) = 1.089 b_p(440) - 0.017$.

5.6 Particulate backscattering

Only in recent years specific sensors have become commercially available to measure the spectral backscattering coefficients *in situ* (Boss *et al.*, 2004). The inversion of reflectance models represents a valid alternative to estimate $b_{bt}(\lambda)$ and then $b_{bp}(\lambda)$ after subtracting the contribution of seawater. Here I derived $b_{bp}(\lambda)$ from the inversion of a simple model relating $R(\lambda)$ to $a_t(\lambda)$ and $b_{bt}(\lambda)$ (Gordon *et al.*, 1975; Prieur, 1976; Morel and Prieur, 1977):

$$R(\lambda) = f(\lambda)\frac{b_{bt}(\lambda)}{a_t(\lambda)}. \tag{5.80}$$

The input of **Eq. 5.80** are the $R(\lambda)$ measured *in situ* and $a_t(\lambda)$, modeled with measured mean $K_d(\lambda)$ in the penetration depth. The model for $a_t(\lambda)$ will be described in section 5.7. The proportionality factor between reflectance and the total backscattering/absorption ratio (f) is ≈ 0.33 at surface with the sun at the zenith. However, several studies demonstrated that the use of a variable f is preferable, since it depends on the light field structure, the particle concentration and wavelength (Kirk, 1984; Morel and Gentili, 1991; Sathyendranath and Platt, 1997; Morel *et al.*, 2002). In this work I used the values from Morel and Gentili (1991) for oceanic case I waters, which are calculated with Monte Carlo simulations and are available on the `www`.

The resulting relationships between Chl and $b_{bp}(\lambda)$ are compared to the model proposed by M88, as modified in MM01:

$$b_{bp}(\lambda) = \left[0.002 + 0.01\left(0.50 - 0.25\log_{10}\left([\mathrm{Chl}]\right)\left(\frac{\lambda}{550}\right)^{v}\right)\right] b_p(550); \qquad (5.81)$$

that is the product of $\tilde{b}_{bp}(\lambda)$ and $b_p(\lambda)\cdot\tilde{b}_{bp}(\lambda)$ is expressed as the sum of a constant background of 0.002 and of a second term that increases with decreasing Chl. This formulation for $\tilde{b}_{bp}(\lambda)$ implies that the maximal value is 1.2 % for a Chl concentration of 0.01 µg l^{-1}, based on the assumptions of a low refractive index (= 1.05) essentially due to biogenic matter, with a power (Jung) size distribution with exponent close to -4. $\tilde{b}_{bp}(\lambda)$ also has a spectral dependency that changes with Chl concentration as:

$$v = \frac{1}{2}(\log_{10}[\mathrm{Chl}] - 0.3),\ 0.02 < [\mathrm{Chl}] \leq 2\ \mu\mathrm{g\ l^{-1}};\quad v = 0,\ [\mathrm{Chl}] > 2\ \mu\mathrm{g\ l^{-1}}. \qquad (5.82)$$

The expression used for $b_p(550)$ is that of (Loisel and Morel, 1998) (**Eq. 5.79**).

Figure 5.45 shows the log-log relationships for the derived $b_{bp}(\lambda)$ and [Chl] at 443 and 555 nm. For both the blue and green wavelengths, the best line fit for the backscattering coefficient is higher for the Mediterranean at low [Chl] concentrations, and approaches the global model for higher [Chl] concentrations. The determination coefficients are low, 0.28 and 0.29 for 443 and 555 nm respectively. However, removing few outliers, they increase to more than 0.40 for both wavelengths. Since the outliers would change significantly the fitting line, a "robust" least absolute deviation has been used to fit the data and coefficients are reported in **Tab. 5.8** along with results of least square fit.

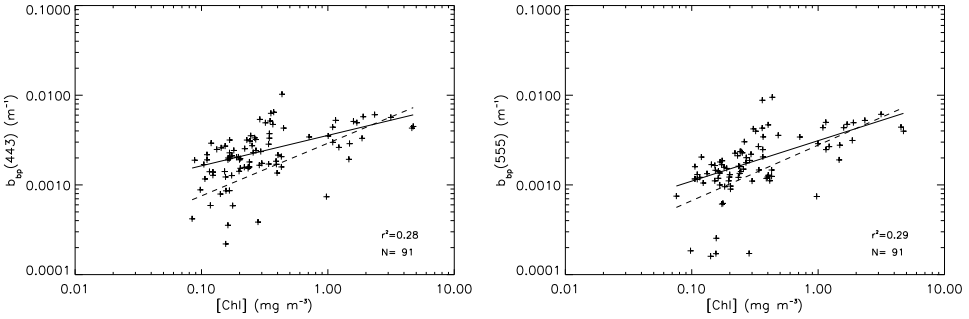

(a) (b)

Figure 5.45: Scatter plot of [Chl] concentration and total particulate backscattering coefficient at 443 nm (a) and 555 nm (b).

To increase the reliability of the model exercise, a set of new coefficients (that

λ	$\alpha(\lambda)$	$\beta(\lambda)$	r^2	$\alpha(\check{\lambda})$	$\beta(\check{\lambda})$
400	0.00342	0.48635	0.30	0.00363	0.44464
412	0.00384	0.47311	0.27	0.00412	0.41464
443	0.00342	0.39816	0.28	0.00356	0.33930
470	0.00366	0.45569	0.34	0.00374	0.41783
491	0.00340	0.51667	0.28	0.00340	0.48132
510	0.00366	0.51504	0.35	0.00389	0.46754
532	0.00318	0.57934	0.30	0.00312	0.44003
555	0.00315	0.64753	0.29	0.00311	0.45108

Table 5.8: $\alpha(\lambda)$, $beta(\lambda)$ and determination coefficients for the linear fit on log-transformed [Chl] and $b_{bp}(\lambda)$. The second set of coefficients ($\alpha(\check{\lambda})$ and $\beta(\check{\lambda})$) are obtained using a "robust" least absolute deviation method that removes outliers. The latter are used to display best fit lines in **Fig. 5.45** and **Fig. 9.67**.

	b_{bp}		b_p	
λ	$\alpha'(\lambda)$	$\beta'(\lambda)$	$\alpha'(\lambda)$	$\beta'(\lambda)$
400	0.00363	0.43468	-	-
412	0.00361	0.44460	0.30648	0.52558
443	0.00356	0.47128	0.30354	0.53863
470	0.00351	0.49600	-	-
491	0.00346	0.51643	0.29803	0.56221
510	0.00341	0.53603	0.29528	0.57361
532	0.00335	0.56035	0.29239	0.58544
555	0.00328	0.58811	0.28922	0.59833
650	-	-	0.27409	0.65888
676	-	-	0.26930	0.67824

Table 5.9: $\alpha'(\lambda)$ ¡nd $\beta'(\lambda)$ coefficients for $b_{bp}(\lambda)$ and $b_p(\lambda)$ after the. For $b_p(\lambda)$ the 443 and 491 nm bands correspond to the 440 and 488 nm bands measured with the ac9.

will be indicated as $\alpha'(\lambda)$ and $\beta'(\lambda)$ were derived using the following approach. $b_{bp}(\lambda)$ spectra were created from the original coefficients, for log-linearly distributed [Chl] concentrations from 0.10 to 5.00 µg l^{-1} (*i.e* $0.1-0.2-0.3\cdots1.\cdots1\cdots5.$, in the range of *in situ* data). The single spectra was linearly fitted with a least squares and a new set of $b_{bp}(\lambda)$ was created from the resulting coefficients. Using this artificial data set, $\alpha'(\lambda)$ and $\beta'(\lambda)$ were finally calculated and the results are reported in **Tab. 5.8**. The same mathematical processing has been applied to $b_p(\lambda)$ (**Tab. 5.9**).

Figure 5.46(a) shows the scattering and backscattering coefficients for the selected [Chl] concentrations, compared with the correspondent values from the MM01 model (**Fig. 5.46(b)**). $b_{bp}(\lambda)$ obtained with Mediterranean coefficients, are similar at high

pigment concentrations and become increasingly higher with decreasing [Chl]. For $b_p(\lambda)$, the Mediterranean shows comparable values in the lower [Chl] range, and but they are lower in mesotrophic and eutrophic conditions.

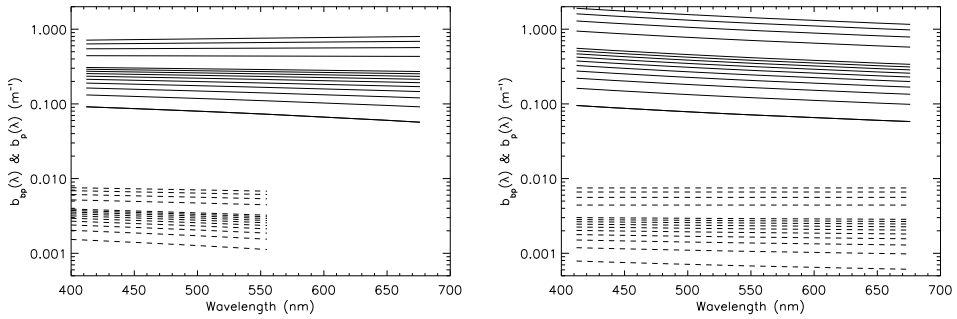

(a) (b)

Figure 5.46: Total particulate backscattering (dashed line) and scattering (continuous line) spectra at various [Chl] derived with coefficients in **Tab. 5.9**. Lines from bottom to top are for increasing [Chl] log-linearly distributed concentrations from 0.01 to 10.00. Extrapolation for values out of the range of values upon which the model has been built (*i.e* < 0.10 and > 5.00) gives realistic results.

Next the $\tilde{b}_{bp}(\lambda)$ has been estimated for the common wavelengths for $b_{bp}(\lambda)$ and $b_p(\lambda)$. $\tilde{b}_{bp}(\lambda)$ values are higher in the Mediterranean Sea at all [Chl] concentrations but with a similar dependence, *i.e* an higher efficiency at low pigment concentrations (**Fig. 5.47**). The $\tilde{b}_{bp}(\lambda)$ estimated for this set of [Chl], ranges between 0.009 and 0.020 (both at 412 nm) with a mean value of 0.012.

To adapt the global model for $b_{bp}(\lambda)$ to the Mediterranean Sea the background term is eliminated. The backscattering efficiency vary between the minimum and maximum values for the 491 nm band, that is ≈ 0.016 at 0.10 µg l^{-1} and ≈ 0.010 at 5.00 µg l^{-1}. The spectral dependency is let unchanged and the final expression is:

$$b_{bp}(\lambda) = \left[0.016 \left(0.77 - 0.23 \log_{10}\left([\mathrm{Chl}]\right) \left(\frac{\lambda}{555}\right)^{v}\right)\right] b_p(555). \tag{5.83}$$

The 491 nm wavelength has been chosen as the central point in the measured common wavelengths for scattering and backscattering (*i.e* 412 and 555 nm), and has been verified to be the best compromise to reproduce the observations. The regional parameterization for $b_p(555)$ substitutes the equation 5.79:

$$b_p(555) = 0.289[\mathrm{Chl}]^{0.598}; \tag{5.84}$$

which is closer to the value used in M88.

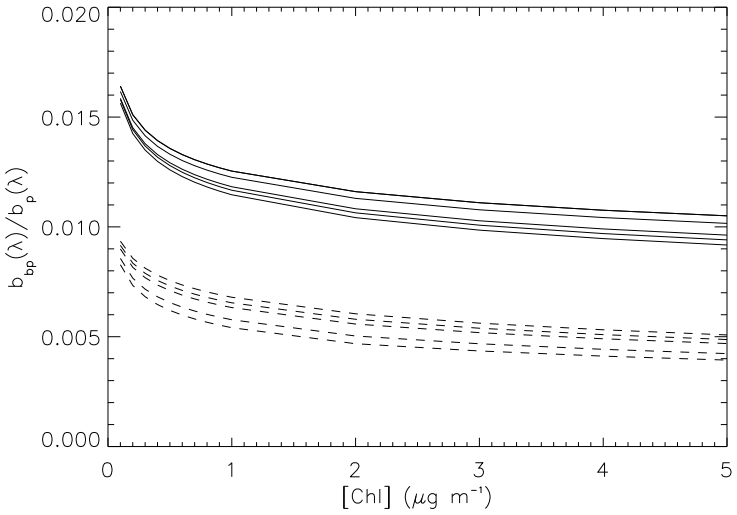

Figure 5.47: Particulate backscattering efficiency derived from regional (continuous line) and MM01 models (dashed line). Curves are for increasing wavelengths from the bottom to the top for the global model and from top to bottom for the regional model.

5.7 Summary and Preliminary Discussion

In this section the study has been focused on the regional parameterization of various IOPs, in the visible wavelengths, respect to Chl concentration. In general the results of the parameterizations were satisfactory, and the variability of each IOPs was well described by its model. Then the regional models were compared to homologous models used to describe the IOPs at global scale. There is not a unique global model for each of the IOPs and differences among global models may exists. However the choice that I made for each of the IOPs, though arbitrary, was aimed at using those widely used in optical modeling.

A critical aspect of such a comparison between regional and global relationship may reside in the methodological differences in Chl retrieving. It has to be taken into account that spectrofluorimetric analysis gives higher values in respect to HPLC analysis (Trees *et al.*, 2000). However the concurrent HPLC and optical available data was not large enough to allow a first preliminary assessment of basin scale optical properties over the Mediterranean. To give an estimate of this methodological difference, I derived a linear relationship with concurrent fluorimetric and HPLC measurements on a different data set from several Mediterranean cruises (**Fig. 5.7**). Results of linear fit on log transformed data are in the range of that found by Trees

et al. (2000).

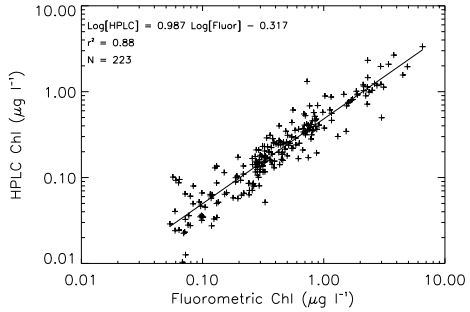

Figure 5.48: Log-Log relationship between Chl measured through spectrofluorimetric and HPLC techniques.

$a_p(\lambda)$, $a_{ph}(\lambda)$ and $a_{nap}(\lambda)$

$\alpha(\lambda)$ and $\beta(\lambda)$ coefficients have similar spectral shape between the three considered data set **Fig. 5.29**. However, their values increase from subset N3 to N1. This could be due to the package effect, since the data set from N3 to N1 were exposed to relatively higher irradiances.

Both $a_p(\lambda)$ and $a_{ph}(\lambda)$ at 443 nm show a similar dependence with Chl compared the BR98 model. At 555 nm, instead, they have higher values at low Chl concentrations (**Fig. 5.30** and **Fig. 5.31**. $a_{nap}(\lambda)$ is not correlated with [Chl] on the whole spectrum. In particular data collected in the Mediterranean Sea are lower than BR98 model especially at meso- eutrophic regimes (**Fig. 5.32**). This pattern seems to be a peculiarity of the Mediterranean, but it has to be understood whether it is attributable to methodological differences or to a different ecosystem functioning. In fact, the oxidation of samples with $NaClO$ probably provides lower values in respect to methanol extraction. This is evident from the convexity of $a_{nap}(\lambda)$ spectra in BR98, whereas our resulting spectra are concave (see **Fig. 5.35(c)**). This may probably be attributable to the bleaching of colored organic particles other than pigments, since the methanol extraction method removes effectively from cells only liposoluble pigments (Kishino *et al.*, 1985). However the pattern of $a^*_{nap}(\lambda)$ is reversed from low to high Chl concentrations, so it seems unlikely that the method itself could introduce a systematic bias. The mean slope of the $a_{nap}(\lambda)$ spectra is identical for regional and global models. Thus, on average, no significant contribution of non-algal particles larger than 0.7 µm, is able to modify the spectral shape of particulate Mediterranean surface waters.

The $a_p^*(\lambda)$ is higher in the violet and green domain respect BR98, with differences incresing with decreasing Chl (**Fig. 5.35**). The higher values are due to both $a_{ph}^*(\lambda)$ and $a_{nap}^*(\lambda)$, but the relative contribution of $a_{ph}^*(\lambda)$ increases with wavelength. $a_{ph}^*(\lambda)$ deviates more and more from BR98 model with decreasing Chl concentrations. For the Mediterranean it is higher in eutrophic regimes and lower in oligotrophic waters. Major differences can be seen in the spectral shape with decreasing Chl concentrations. These differences could be explained from a different size distribution of phytoplankton species for a given Chl concentrations. Global model have a variability in spectral shape for decreasing Chl concentrations similar to that shown from Ciotti *et al.* (2002) for decreasing cell size, with more peaked $a_{ph}^*(\lambda)$ in the blue and red absorption maxima for picoplankton. Mediterranean model instead seems to have a higher relative contribution of larger phytoplankton.

$a_{pg}(\lambda)$, $c_{pg}(\lambda)$ and $b_p(\lambda)$

Similarly to what observed for $a_p(\lambda)$, the regional model for $a_{pg}(\lambda)$ is close to the global model at 443 nm, and is higher at low Chl concentration at 555 nm (**Fig. 5.36**). The attenuation coefficient, instead, is similar to the global model at low Chl concentrations and is slightly lower at higher pigment content (**Fig. 5.38**). This patter could be linked to the low $a_{nap}(\lambda)$at the same Chl range, since non-algal particles are expected to be good contributors to scattering. In fact, the relationship for $b_p(\lambda)$ also shows lower values at high Chl concentrations (**Fig. 5.43**).

Barnard *et al.* (1998) proposed global spectral relationships for $a_{pg}(\lambda)$, $c_{pg}(\lambda)$, and $b_p(\lambda)$, underlining that more detailed model may be necessary to predict more accurately the IOPs spectral relationships on regional scales. This is the case of the Mediterranean Sea, where the ratio between $c_{pg}(555)/c_{pg}(443)$ is higher respect to the model of Barnard *et al.* (1998) (**Fig. 5.39**. The observed differences have to be attributed only to $a_{pg}(\lambda)$ (**Fig. 5.37**) since scattering has an identical behavior for the same spectral relationship (**Fig. 5.44**).

$a_{ys}(\lambda)$

The absorption of CDOM has been estimated subtracting particulate absorption from total absorption without water contribution where concurrent measurements were available. Though the two methods of measurements are quite different, the retrieved spectra were reasonably accurate to allow to build a regional model for $a_{ys}(\lambda)$. The mean slope of the $a_{ys}(\lambda)$ spectra is similar to that found from BR98. However the absorption of $a_{ys}(\lambda)$, was on average, 60 % of the sum of $a_p(\lambda)$ and $a_w(\lambda)$, repect to the often used value of 20 % or the global model.

The observed differences are quite high, especially at low [Chl] concentrations. In fact the Mediterranean is a basin with a high exposure to solar irradiance, then photobleaching is likely to occur, especially during summer when it is characterized from a general oligotrophy and water stratification. However the difference between the regional and global models (0.007 m^{-1} at 0.10 µg l^{-1}) is about half of that reported by Claustre *et al.* (2002) that used a similar approach to derive the absorption of what the authors called "other substances" than particulate during a summer cruise in the Mediterranean Sea (0.015 m^{-1} at the same Chl concentration) and that was attributed to lithogenic silica.

$b_{bp}(\lambda)$

The particulate backscattering has been estimated through the inversion of MM01 reflectance model initialized with mean measured $K_d(\lambda)$ within the z_{pd}. $b_{bp}(\lambda)$ was higher respect to the model of MM01 in olig- and meso-eutrophic regimes, and similar at higher pigment. These estimates are slightly lower than those estimated by Loisel *et al.* (2001) from satellite measurements over the basin using an optical model (derived from radiative transfer simulation) based on $K(\lambda)$ and $R(\lambda)$ (Loisel and Stramski, 2000).

From $b_{bp}(\lambda)$ and $b_p(\lambda)$ regional models, it was possible to estimate the backscattering efficiency of particulate. $\tilde{b}_{bp}(\lambda)$ was higher respect to the maximum value used from MM01 for modeling $b_{bp}(\lambda)$ in oceanic case I waters. Using this information, an *ad hoc* algorithm has been built to reproduce the estimated backscattering coefficients from [Chl] concentration. Using Mie theory, MM01 computed the $b_{bp}(\lambda)$ for varying refractive index and exponent of the Junge distribution for particles. The maximum value adopted in their model for $b_{bp}(\lambda)$ is 0.01 and falls within the domain of maximum ≈ 4.3 for the exponent and ≈ 1.10 for the refractive index. The maximum value estimated for the Mediterranean Seas should follow in the domain of ≈ 4.5 for the exponent and ≈ 1.16 for the refractive index. To the best of my knowledge, maximum estimated values for the refractive index of phytoplankton are less than 1.10. Thus the high $b_{bp}(\lambda)$ could be explained by the presence of particles with high refractive index such as mineral particles, or from a higher exponent of the Junge distribution, *i.e.* with relatively higher concentrations of small particles. In a recent study, Oubelkheir *et al.* (2005) reported values between 3.5 and 5.5 for the Junge exponent, in the 1.6–2.6 µm size range, for the Mediterranean surface waters, thus compatible with both possibilities.

6. Regionalization of the Reflectance Model

In this section some of the results obtained in the previous two sections are used to build a regional reflectance models on the scheme of that proposed from MM01. Both the MM01 and regional models are compared to *in situ* data. Two different simulations have been made for the regional model, changing one (Med1) or two (Med2) parameters of the MM01 model. A summary of the results with a preliminary discussion for this section are also given.

Run Med1

The reflectance model of MM01 is based upon an iterative scheme making use of the empirical relationships for $K(\lambda)$ and $b_b(\lambda)$ with Chl and will be briefly summarized. The model starts with a first computation of $R(\lambda)$ through **Eq. 5.80**. $b_b(\lambda)$ is introduced as the sum of $b_{bw}(\lambda)$ and $b_{bp}(\lambda)$ as derived from **Eq. 5.81** and f may be set to a mean value (0.33) or considered variable. $a_t(\lambda)$, instead, is initially approximated as $u_1 K(\lambda)$, with $u_1 = 0.75$ at all wavelengths.

Then a second set of $R(\lambda)$ is computed with the exact relationship derived from the divergence law for irradiance with no inelastic scatter and no internal sources (Gershun's law):

$$a_t(\lambda) = K(\lambda)\mu_d \left[1 + R(\lambda)\frac{\mu_d}{\mu_u}\right]^{-1} [1 - R(\lambda)], \text{ or } a_t(\lambda) = K(\lambda)u_2(\lambda); \qquad (6.85)$$

where $\mu_u = 0.40$ and μ_d values were computed in Morel *et al.* (2002) and are available on the `www`. The resulting $a_t(\lambda)$ is then reentered in **Eq. 5.80** and the whole iteration is repeated three times to obtain stable values of $R(\lambda)$.

Fig. 6.49(a) shows the comparison for *in situ* data and the model of MM01, wheres **Fig. 6.49(b)** the same model has been initialized with regional coefficients for $K_{bio}(\lambda)$. $b_b(\lambda)$, instead is let unchanged and a variable f from (Morel and Gentili, 1991) is used. In general both model do not perform particularly well at all considered wavelengths (see **Tab. 6.10**). The determination coefficient is 0.55 for MM01 and 0.48 for the Med1.

The global model has a slightly negative bias, whereas the introduction of the regional parameterization for $K_{bio}(\lambda)$ leads to a sensible bias respect to *in situ* measurements. This is expected however since the only effective change respect to MM01 is the parameterizazion of $a_t(\lambda)$ through $K_{bio}(\lambda)$, which has been shown to be higher at low pigment concentrations. In fact each band approaches 1:1 line when $R(\lambda)$ de-

	$R(\lambda)$	$\frac{R(443)}{R(555)}$	MBR	$R(\lambda)$	$\frac{R(443)}{R(555)}$	MBR	R	$\frac{R(443)}{R(555)}$	MBR
N	736	92	92	736	92	92	736	92	92
r^2	0.55	0.85	0.85	0.48	0.86	0.86	0.52	0.86	0.86
APD	26.94	25.13	22.58	30.87	22.79	20.36	26.08	19.37	16.87
RPD	-5.48	16.87	17.31	-21.02	13.82	13.45	-2.76	6.30	6.17
BIAS	-0.0028	0.55	0.56	-0.0084	0.34	0.35	-0.0030	0.062	0.067
RMS	0.011	1.02	1.02	0.014	0.79	0.79	0.011	0.68	0.67
		MM01			Med1			Med2	

Table 6.10: Stathistical parameters for the evaluation of the performances of global and regional reflectance models.

creases *i.e.* at relatively high pigment content. The spread of data is also higher for the regional model (0.01137 and 0.0111 respectively) and both absolute and especially relative error indicate a worst performance for this regional adaptation.

Though its utilization is not recommended, the Med1however shows slightly better performances in reproducing reflectance ratios repect to MM01. **Fig. 6.50** shows a comparison of modeled and *in situ* reflectance ratios for the 443 and 555 nm bands. The spread of data is similar for the two models but for the regional model they are better distributed around the 1:1 line. APD, RPD, BIAS and RMS are all lower for the Med1 respect to MM01 (**Tab. 6.10**). The MBR (that is different to that introduced in chapter 2.5 only in the use of $R(\lambda)$ instead of $R_{rs}(\lambda)$), is better reproduced by both models respect to a fixed band ratio (**Fig. 6.51**), but a similar argument can be made if we make a comparison among the two models **Tab. 6.10**.

A comparison between the total absorption derived from the reflectance model initialized with *in situ* measured $K_{pd}(\lambda)$, and that derived from MM01 and regional coefficients (**Eq. 6.85**) is also reported in the appendix (section 6.1).

Run Med2

After evaluating the effect of the introduction of new coefficients for $K_{bio}(\lambda)$ in the reflectance model of MM01, a tuning of the model is made by introducing also the regional parameterization for $b_{bp}(\lambda)$ (**Eq. 5.83**). This modification significantly improves the overall performances of the model. Though having still a low covariation ($r^2 = 0.52$), data are now better distributed around the 1:1 line at all wavelengths (**Fig. 6.52**). The APD of the Med2is slightly lower respect to the MM01model. The RPD is halved, whereas the BIAS and the RMS are similar.

More significant, instead, is the improvement of the model for what concerns its spectral behavior. For the reflectance ratios the APD is less than 20 % and the RPD is around 6 % and BIAS and spread of the data are also reduced respect the global

model (**Tab. 6.10** and **Fig. 6.53**).

The variations of the Med2 and MM01 reflectance models at various [Chl] concentrations are compared in **Fig. 6.54** and also displayed with a higher resolution for [Chl] concentrations in **Fig. 6.55**.

For the Mediterranean, $R(\lambda)$ has a narrower range of variation in the blue. In this region it shows higher values at higher pigment concentrations, and lower values in oligotrophic regimes. In the green, the regional model has a higher range of variation. In this region of the spectrum, the Med2 has similar values at the highest [Chl] concentrations, and higher values at low [Chl].

The spectral shapes are almost similar at high [Chl], but becomes more evident with decreasing [Chl] concentration. In particular, the global model show more marked peaks at lowest [Chl] concentrations, and the maximum shifts from 400 to 412 nm wavelenght. The Med2, instead, has a more flat spectrum, and it starts to peak at 412 nm earlier with decreasing [Chl] concentration respect to the global model. Moreover, this peak is less pronounced respect to the 443 nm if compared to MM01. Finally a small peak is also visible at 530 nm at meso- and moderately eutrophic conditions.

The variations in terms of $R(\lambda)$ ratios are better evidenced in **Fig. 6.56**, where at each [Chl] concentration the spectral reflectance is normalized at 555 nm. Overall, the Mediterranean ratios are constrained in a narrower range of variation for the considered [Chl] concentrations.

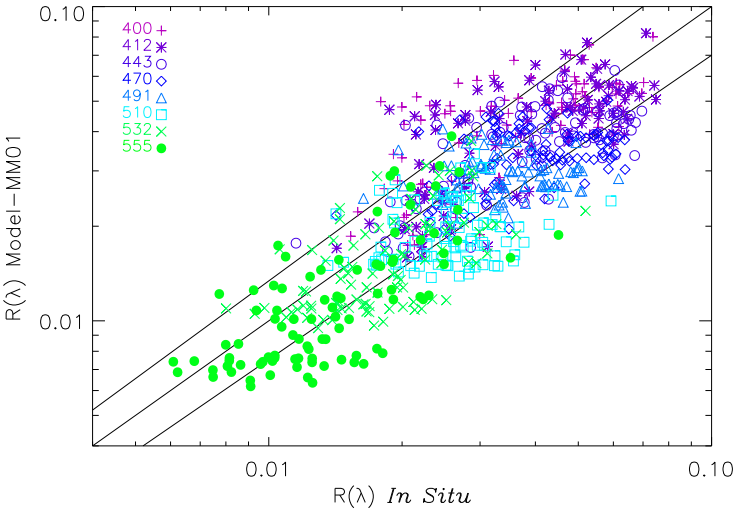

(a)

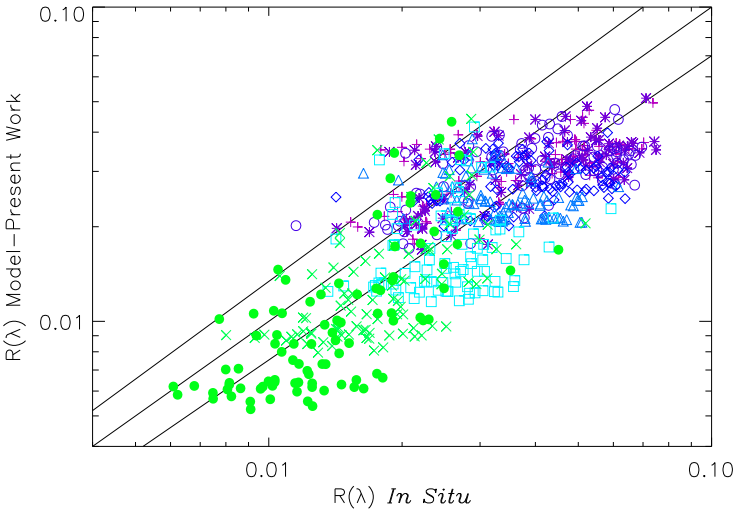

(b)

Figure 6.49: (a) Scatter plot of *in situ* vs. MM01 modeled $R(\lambda)$ for all considered wavelength. (b) the same comparison but for Med1. The 1:1 and ± 30 % are also plotted.

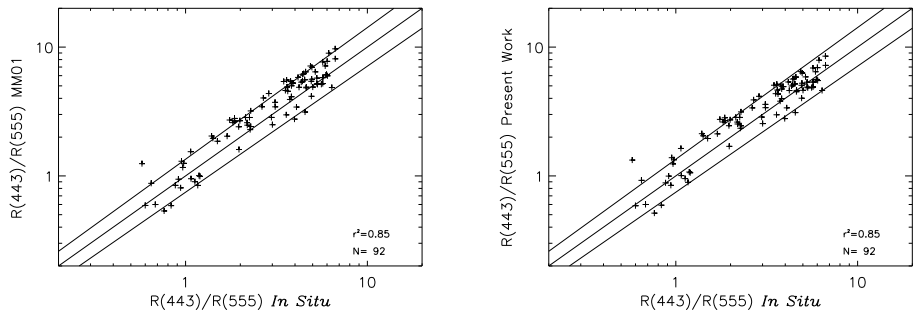

(a) (b)

Figure 6.50: Blu (555 nm) to green (555 nm) reflectance ratio for MM01 (a) and Med2 (a) models against *in situ* data. The 1:1 and ±30 % are also plotted.

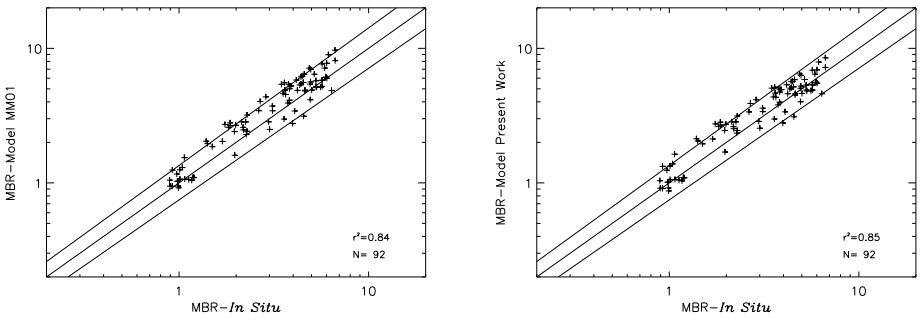

(a) (b)

Figure 6.51: The same plot of **Fig. 6.50** but for MBR.

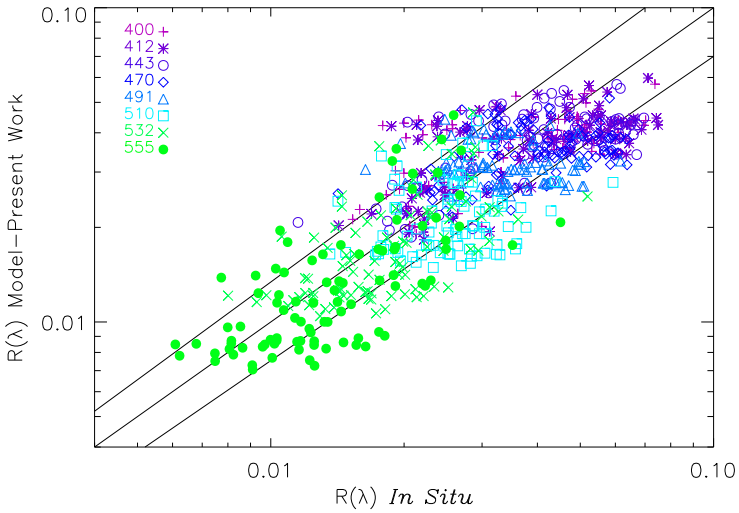

Figure 6.52: Scatter plot of *in situ* vs. Med2 modeled $R(\lambda)$ for all considered wavelength

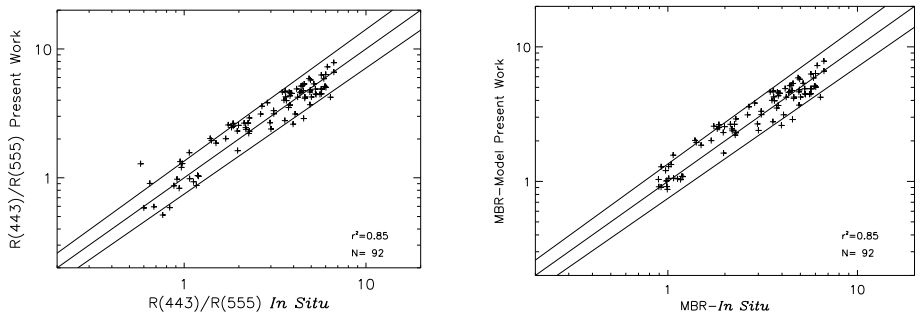

(a) (b)

Figure 6.53: Blu (555 nm) to green (555 nm) reflectance ratio (a) and MBR (b) modeled with Med2, against *in situ* data. The 1:1 and ±30 % are also plotted.

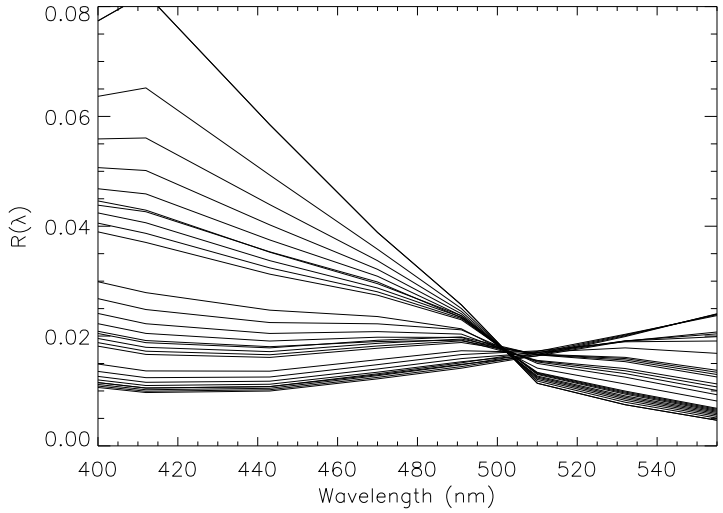

(a)

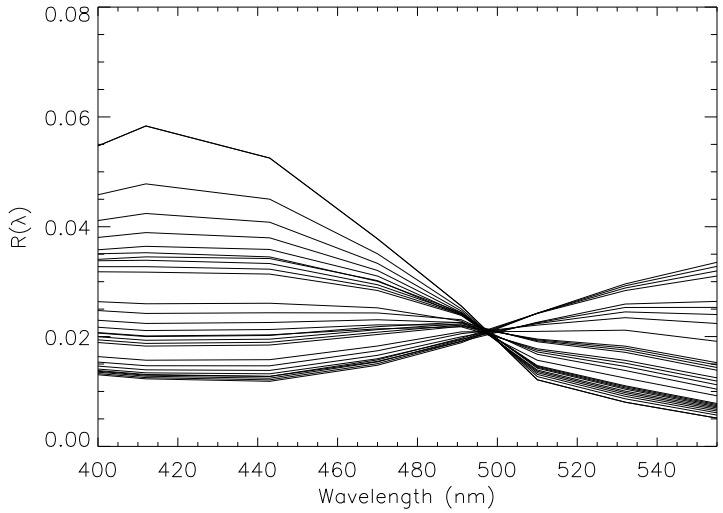

(b)

Figure 6.54: Reflectance spectra derived with MM01 (a) and Med2 (b) at various [Chl] concentrations, with and sun at the zenith. The [Chl] values used to initialize the model are the same of that used for **Fig. 5.46**.

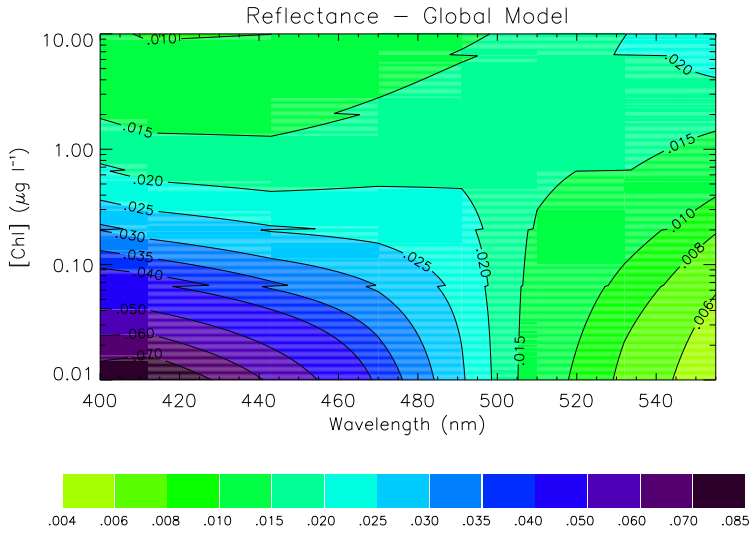

(a)

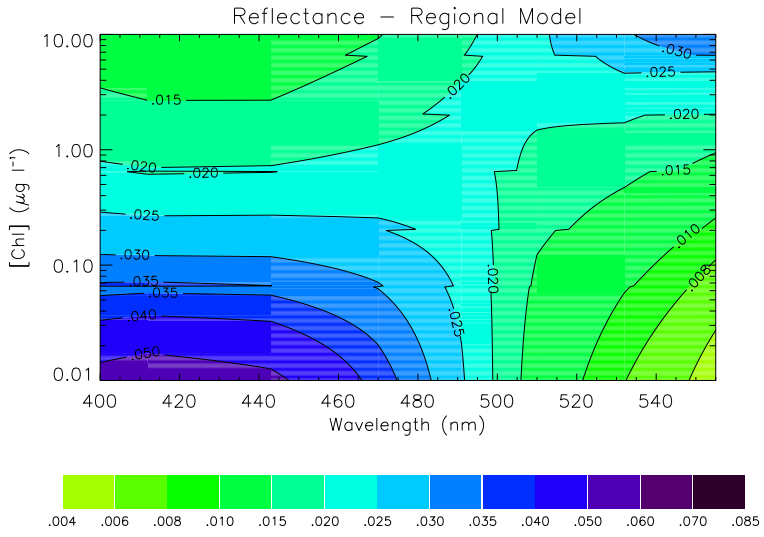

(b)

Figure 6.55: Contour map of $R(\lambda)$ derived with MM01 (a) and Med2 ((b)) model with sun at the zenith.

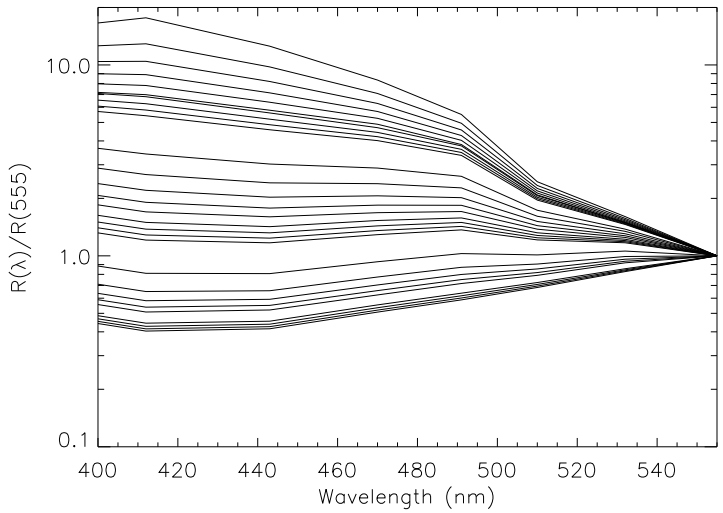

(a)

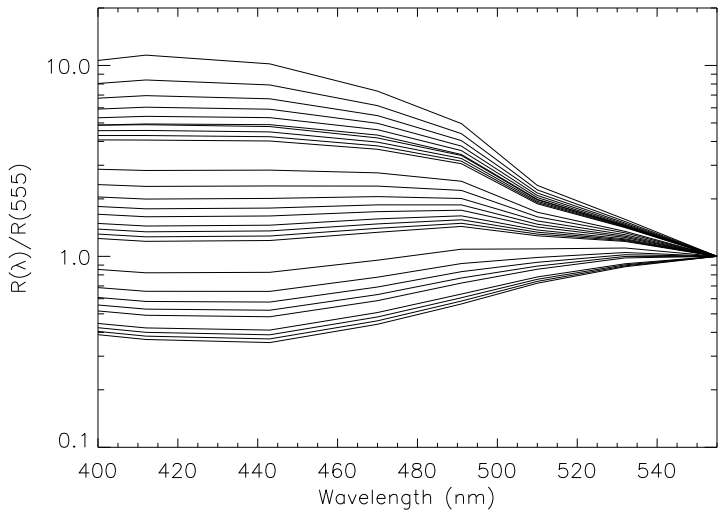

(b)

Figure 6.56: 0.01-10.00

6.1 Summary and preliminary discussion

In this section the MM01 reflectance model have been tuned for the Mediterranean making use of some of the results of the previous chapters. For Med1 simulation the results of the simulation are low compared to *in situ* $R(\lambda)$, but the spectral response of the model is improved respect to the global model. The introduction of the regional parameterization for $b_{bp}(\lambda)$ improves the performances of regional model. The determination coefficient for alla wavelengths is low for all the three models. However the proportion of variability that they are able to represent is not far from that obtained by introducing measured $K_d(\lambda)$ ($r^2 = 0.58$).

The pattern of the $R(\lambda)$ spectra, modeled with the Med2, are coherent with what observed for the IOPs. In the blue region in fact the higher absorption of particulate and dissolved matter is likely to cause the flattening of the reflectance spectra, and, in particular the lower $R(440)$. In the green instead at low high [Chl], where the backscattering and absorption are similar the $R(\lambda)$ display similar values, whereas the higher backscattering is not compensated from the high absorption of particulate and the resulting $R(\lambda)$ is higher.

Reflectance ratios have similar values than the Remote sensing reflectance ratio (the difference consisting in the ratio of the $Q(\lambda)$ factor at the same wavelengths and is close to 1), and they can be roughly compared to what observed for the Chl$-a$ retrieving algorithms. In accord to observation of chapter 2.5 at low pigment content the blue to green ratio is lower for the Mediterranean model, however the differences with the global model are less pronounced respect to that seen for global and regional Chl$-a$ retrieving algorithms.

7. Discussion

The color of the ocean is determined by the interactions occurring between sunlight and the dissolved and particulate optically active constituents within a certain, variable, surface layer (e.g. the penetration depth). This natural phenomenon is synthesized in the relationship linking $R(\lambda)$ to the absorption and backscattering coefficients (**Eq. 5.80**).

The variability of $R(\lambda)$ in relation to the Chl$-a$ content, for ocean color purposes, is usually expressed in terms of B/G. The green band is often set to 555 nm whereas the blue band is usually chosen as the maximum between 443, 490 and 510 nm.

The Mediterranean Sea is characterized by an anomalous B/G ratio respect to the global ocean, for the same Chl$-a$ concentrations. In particular the B/G is lower at low Chl$-a$ concentration. Volpe *et al.* (2007) showed that the low B/G derives from both a lower blue and a higher green reflectance. The next step is to understand which of the optically significant constituents of the Mediterranean waters is responsible for the low B/G.

Equation 5.80 can be rewritten in the following form:

$$\frac{R(B)}{R(G)} = \frac{f(B)}{f(G)} \frac{b_{bt}(B)}{b_{bt}(G)} \frac{a_t(G)}{a_t(B)}; \tag{7.86}$$

or, simplifying the notation:

$$\rho_G^B = f_G^B b_{btG}^{\ B} a_{tB}^{\ G}. \tag{7.87}$$

f_G^B depends on the sun position, wavelength and water content. Though its value may significantly change, f_G^B has a low variability, and the presence (or absence) of optical components in a water body is not expected to change significantly f_G^B. Thus a low ρ_G^B can be due to a low $b_{btG}^{\ B}$ and/or to a low $a_{tB}^{\ G}$.

Table 7.11 reports $b_{btG}^{\ B}$ and $a_{tB}^{\ G}$ calculated with regional and global models. The regional model is calculated as the sum of $a_{pg}(\lambda)+a_w(\lambda)$ and as the sum of $a_p(\lambda)+a_{ys}(\lambda)+a_w(\lambda)$. The global model for $a_t(\lambda)$ is the sum of $a_w(\lambda)$, BR98 model for $a_p(\lambda)$ and Bricaud *et al.* (1981) for $a_{ys}(\lambda)$. The two estimates for the Mediterranean are in good agreement. Both estimates are lower than $a_{tB}^{\ G}$for the global model. The gap between the regional and global models decreases with increasing wavelength and Chl concentration. Also $b_{btG}^{\ B}$ is almost always lower for the Mediterranean Sea, but with minor differences at 1.0 and 3.0 µg l^{-1} of Chl. So from my estimates it seems that the low B/G is due to both $a_t(\lambda)$ and $b_{bt}(\lambda)$.

Table 7.11 also reports ρ_G^B calculated with regional and global models for the total

absorption and scattering, and the corresponding values derived using the Med2 and MM01 reflectance models. The regional IOPs models shows lower estimates for ρ_G^B respect to the globalIOPs model. The two estimates for the regional models are in good agreement for the 443 nm at 0.1 µg l^{-1}, the 490 nm at 1.0 µg l^{-1} and 510 nm at 1.0 and 3.0 µg l^{-1}. More in general, the regional and global ρ_G^B calculated frome IOPs models have similar differences respect to the corresponding ρ_G^B from the reflectance model.

To make explicit each optical component, and how they can modify the B/G, **Eq. 5.80** can be also written as:

$$\rho_G^B = f_G^B \frac{b_t(B)^{GO} + \Delta b_{bp}(B)}{b_t(G) + \Delta b_{bp}(G)} \frac{a_t(G)^{GO} + \sum_j \Delta a_j(G)}{a_t(B)^{GO} + \sum_j \Delta a_j(B)}. \tag{7.88}$$

The suffix j indicates either ph, nap or ys, and absorption and backscattering are written as the sum of the global model and the difference between the regional model and global models (Δb_{bp} and Δa_j).

$\Delta_{b_{bp}}$ is slightly higher in the blue than in the green (**Tab. 7.12**). The overall effect of $b_{bp}(\lambda)$ is to lowering the b_{btG}^B, since the %Δ is higher in the green than in the blu (see **Tab. 7.13**). AT higher pigment content, the %Δ is similar for green and blue bands.

$\Delta_{a_{nap}}$ is negligible at low Chl concentrations, but it is negative at higher Chl, being lower in the blue than in the green. Its relative contribute decreases the B/G with increasing [Chl].

At 0.1 µg l^{-1}, $\Delta_{a_{ph}}$ is negative in the first two blue band and positive for the 555 nm band, whereas it is higher in the blue than in the green for higher Chl content. At low Chl, the absorption of phytoplankton populations in the Mediterranean Sea would increase, rather than decrease, the B/G ratio, but its effect is somewhat negligible, with %Δ accounting for few percent. At higher Chl, the $a_{ph}(\lambda)$ decreases the B/G, mainly for the 443 nm.

Finally, $\Delta_{a_{ys}}$ is always higher for the Mediterranean. The difference between regional and global model is higher in the blue bands that for the green one. This have a significative impact on the B/G, especially at low Chl where %Δ is 30.9 % at 443 nm and only 2.66 % at 555 nm.

Thus the low B/G observed in the Mediterranean oligotrophic waters seems to be due to concurrent factors. Both $b_{bp}(\lambda)$ and $a_{ys}(\lambda)$ contribute to lower the B/G at very low Chl concentrations. With increasing Chl concentrations also $a_{nap}(\lambda)$ and $a_{ph}(\lambda)$ are expected to give a contribution to the low B/G.

It has to be reminded that $b_{bt}(\lambda)$ and $a_{ys}(\lambda)$ were not directly measured, and their modeling was obtained from derived quantities. The first was obtained through

the inversion of the reflectance model of MM01 (initialized with *in situ* measured $K_d(\lambda)$) and the second was obtained from differences between $a_{pg}(\lambda)$ measured with ac9 and absorpion spectra on filters.

It seems unlikely that Saharan dust is the responsible for the higher $b_{bp}(\lambda)$ observed in my dataset. High $b_p(\lambda)$ such that reported from Claustre *et al.* (2002) seem to be linked to events that are not observed so frequently. (cfr. section 2.5). Iluz *et al.* (2003) reported anomalous B/G ratios in the Red Sea, which is, as the Mediterranean, a semi-enclosed basin near to Sahara desert. However in this case the B/G was higher respect to global ocean at the same Chl$-a$ concentration. This factors let me exclude Saharan dust as a ordinary optical component present in the Mediterranean surface water. Among other factors, a size spectra shifted toward small cells could explain a higher $b_{bp}(\lambda)$.

For what $a_{ys}(\lambda)$ concerns, the estimates are rather high and it is difficult to explain them. First because the DOC estimates are not high in the Mediterranean Seritti *et al.* (2000). Second it is linked to biological activity, and Primary Production estimates over the basin indicate a low activity for this basin Bosc *et al.* (2004), enough to be compared to a *Marine Desert* (Azov, 1991). Third, the Mediterranean Sea has a high solar irradiance, at least higher if compared to similar latitudes, and photobleaching is likely to occur in its surface layer, especially during summer stratification.

What is a peculiarity for the basin is to have a very low surface to coast length ratio. So, it is possible that small colored particles, coming from rivers, land and atmospheric inputs enrich the Mediterranean Surface waters. This could be at the origin also of a higher $b_{bp}(\lambda)$. Unfortunately there is not enough information to go deeper into the understanding of this aspect.

Oligotrophic nutrient poor waters are dominated by picophytoplankton biomass and production, whereas in eutrophic nutrient rich waters they represent only a small fraction of autotrophic biomass (Agawin *et al.*, 2000). Bacterial variability instead closely mirrors that of phytoplankton, and they standing stocks are remarkably similar throughout the world ocean (Ducklow, 1999). Picoplankton and bacteria are efficient backscatterers. Picoplankton are also efficient absorber. The interest in these fractions of microscopic organism has increased a lot since their discovering. The introduction of cytofluorometry also made their counting easier and ther is knowledge enough to make a fist comparison between distribution of these organisms.

With the aim to understand if the distribution of picoplankton and bacteria may explain some of the optical characteristics observed in the Mediterranean Sea, I gathered two data set (one for the Mediterranean Sea and one for Global Ocean) for surface picoplankton concentration. In particular I assempled data for HBAC, *Synechococcuss spp.*, *Prochlorococcus spp.* and picoeukariots whith concurrent measurement of

Chl$-a$ concentration (sometimes derive from carbon estimates). The references for papers and data base used for these data set are given in the appendix (section 6.1, **Tab. 9.23**), along with the station location for each group, for both the Mediterranean and Global Ocean (**Fig. 9.70** to 9.74).

Heterotrophic bacteria (**Fig. 7.57**), show a similar pattern to that observed for data from the global ocean. Their relative concentration respect to Chl concentration is negatively correlated with Chl concentration, with low variability at various Chl concentrations. The distribution of *Synechococcus spp.* for Mediterranean data (**Fig. 7.58**) falls within the upper limit of that for the global ocean. The two distributions have significantly different means. On the contrary, *Prochlorococcus spp.*, show significantly lower concentration, especially at low Chl concentrations, where it reaches a minimum value not observed in the global data set. Finally, picoeukariots show a similar distribution to that of the global ocean, but the slope of the fitting line is lower, with cell concentrations that tend to be on average lower at low Chl and higher at high Chl.

The low concentration of picoeukaryots and *Prochlorococcus spp.* at low Chl concentrations, seems to confirm what observed for the low $a_{ph}(\lambda)$. Instead it seems unlikely that the higher relative number of *Synechococcus spp.* could be the cause of the high $b_{bp}(\lambda)$, because it should also compensate the low concentrations observed for the other two groups. The build up of this data set, will allow to obtain more quantitative estimate on the contribution to the bulk absorption and backscattering coefficents for each group, on the basis of literature data on their respective efficiency factors.

λ_B	a_{tB}^G			b_{btG}^B			ρ_G^B				Chl
	2.56	2.22	2.77	1.75	1.94		4.36	3.78	5.22	4.02	4.57	0.1
443	0.89	0.89	1.02	1.31	1.35		1.13	1.13	1.34	3.05	3.35	1.0
	0.55	0.57	0.67	1.18	1.19		0.63	0.66	0.78	1.88	1.95	3.0
	2.44	2.29	2.47	1.33	1.41		3.26	3.06	3.50	1.21	1.17	0.1
490	1.14	1.23	1.30	1.13	1.15		1.30	1.41	1.50	1.43	1.36	1.0
	0.75	0.87	0.95	1.07	1.08		0.81	0.94	1.03	1.28	1.21	3.0
	1.57	1.53	1.60	1.20	1.24		1.74	1.70	1.84	0.65	0.65	0.1
510	1.10	1.16	1.20	1.08	1.09		1.09	1.16	1.21	0.91	0.87	1.0
	0.84	0.95	0.99	1.04	1.04		0.81	0.92	0.96	0.98	0.90	3.0
	Med		GO	Med	GO		Med		GO	Med2	GO	

Table 7.11: G/B ratios of $a_t(\lambda)$ and B/G ratios of $b_{bt}(\lambda)$ and ρ_G^B, calculated with regional (Med) and global (GO) models. $a_t(\lambda)$ coefficients are calculated both as $a_{pg}(\lambda)+a_w(\lambda)$ (left column) and $a_p(\lambda)+a_{ys}(\lambda)+a_w(\lambda)$ (right column). The first three column for ρ_G^B are calculated with **Eq. 7.87**, combining a_{tB}^G and b_{btG}^B for the two regional and the global models. The last two column for ρ_G^B are computed with Med2 and MM01 reflectance models. For each components, three different ratios are given for the 443, 490 and 510 nm bands respect to the 555 nm, at three different Chl concentrations (0.1, 1.0 and 3.0 µgl).

λ	$\Delta_{a_{ph}}$	$\Delta_{a_{nap}}$	$\Delta_{a_{ys}}$	$\Delta_{b_{bp}}$	Chl
	-0.00031	$4.09 \cdot 10^{-5}$	0.0069	0.00059	0.1
443	0.0032	-0.0085	0.019	0.00070	1.0
	0.011	-0.025	0.032	0.00029	3.0
	-0.00070	$-3.87 \cdot 10^{-6}$	0.0038	0.00054	0.1
490	0.00054	-0.0057	0.010	0.00068	1.0
	0.0044	-0.017	0.018	0.00029	3.0
	0.00050	$1.28 \cdot 10^{-5}$	0.0029	0.00052	0.1
510	0.00083	-0.0044	0.0078	0.00067	1.0
	0.00010	-0.013	0.01	0.00029	3.0
	0.00094	$5.37 \cdot 10^{-5}$	0.0016	0.00048	0.1
555	0.0012	-0.0030	0.0045	0.00065	1.0
	-0.0022	-0.0086	0.0078	0.00029	3.0

Table 7.12: Regional less global (Δ) absorption and backscattering coefficients for some optical components for the 443, 490, 510, and 555 nm bands at three Chl concentrations (0.1, 1.0 and 3.0 µgl).

λ	$\Delta_{a_{ph}}/a_t$	$\Delta_{a_{nap}}/a_t$	$\Delta_{a_{ys}}/a_t$	$\Delta_{b_{bp}}/b_{b_t}$	Chl
	-1.40	-0.39	30.95	21.86	0.1
443	4.53	43.34	25.96	14.28	1.0
	8.20	79.18	23.56	3.87	3.0
	-2.81	0.023	15.22	27.66	0.1
490	0.96	26.82	18.34	16.20	1.0
	4.62	59.93	18.63	4.26	3.0
	1.29	-0.03	7.51	30.24	0.1
510	1.38	11.79	12.93	16.89	1.0
	0.11	31.07	14.76	4.40	3.0
	1.52	-0.08	2.66	35.16	0.1
555	1.71	4.86	6.15	17.95	1.0
	-2.38	13.24	8.51	4.61	3.0

Table 7.13: Ratio between regional less global model $a_t(\lambda)$(backscattering) coefficients (*e.g.* values in **Tab. 7.12**) and total for the same optical components of. In the text I will refer to this quantity as %Δ

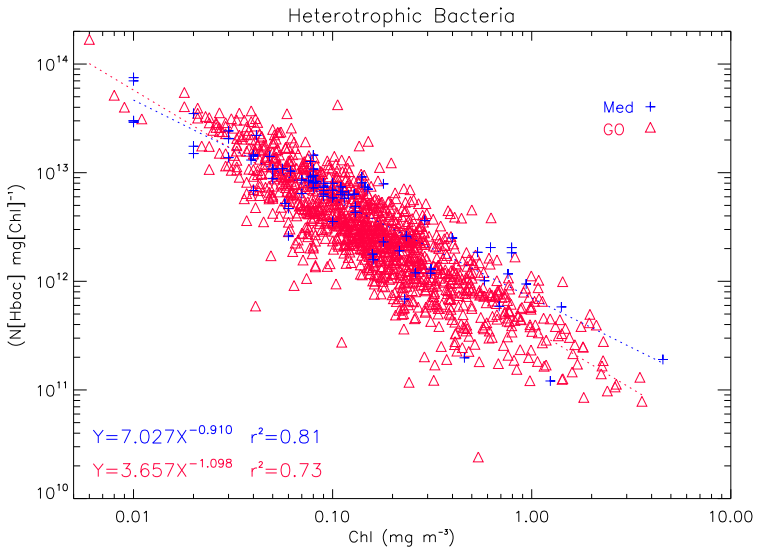

Figure 7.57: Heterotrophic bacteria per Chl−*a*unit, against Chl−*a* concentration.

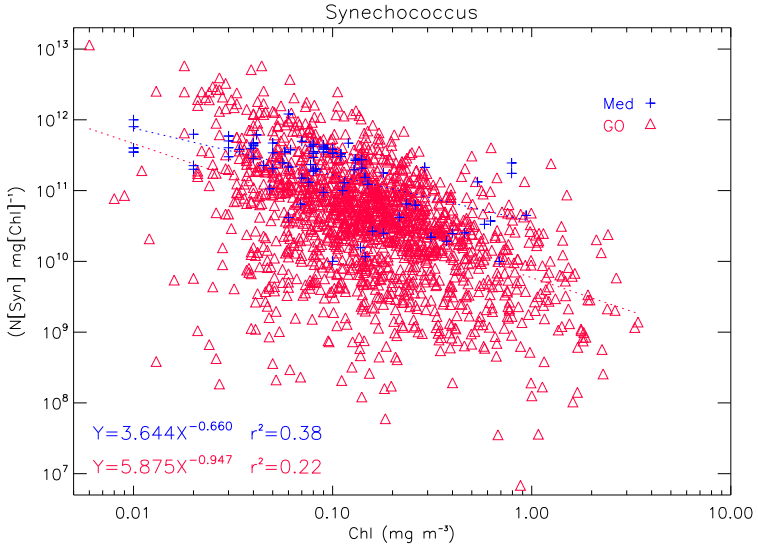

Figure 7.58: *Synechococcus spp.* per Chl unit, against Chl concentration.

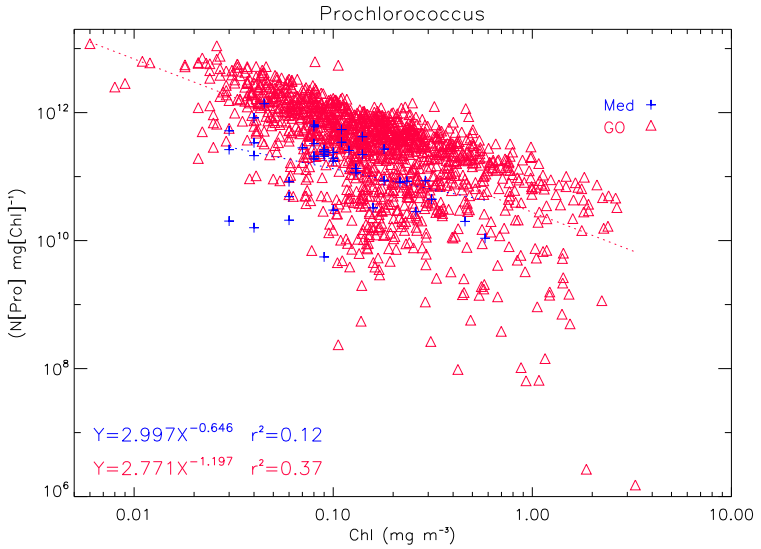

Figure 7.59: *Prochlorococcus spp.* per Chl unit, against Chl concentration.

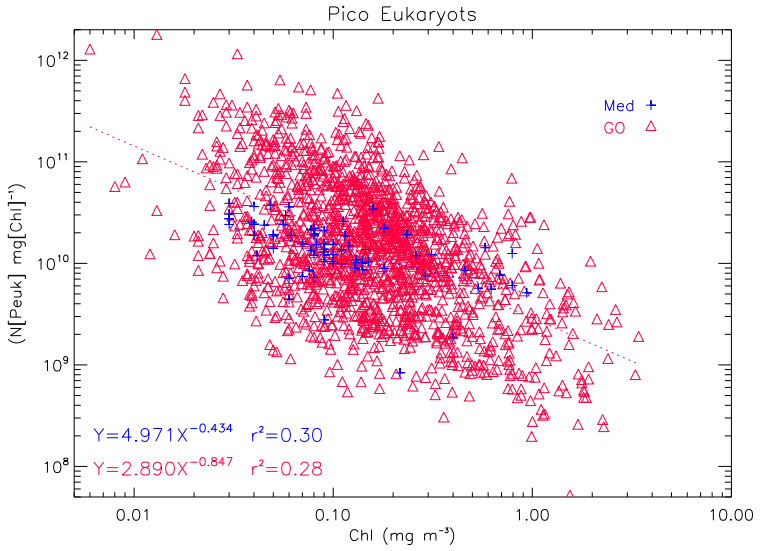

Figure 7.60: Picoeukariots per Chl unit, against Chl concentration.

8. Conclusions

The Mediterranean Sea shows a lower blue to green reflectance ratio respect to the global ocean, for a given Chl$-a$ concentration. This leads to an overestimation of the Chl$-a$ concentration when retrieved through standard ocean color algorithms. Some regional algorithms have been proposed to improve the accuracy of satellite Chl$-a$ estimates over the basin. At the same time, some hypotheses that may explain the observed behavior have been analyzed, but there is still not a definitive answer. Though some published work reports some Mediterranean IOPs and AOPs, a comprehensive study on them at basin scale is missing.

In this work, a data set of Mediterranean IOPs and AOPs have been built, along with Chl concentrations. Data covered almost all trophic regimes generally found in the basin, and cover all seasons. This allowed for the first time the development of preliminary regional Chl based models for the major optical properties suited for the Mediterranean Sea. These models were used as input for a simple reflectance model, improving its performances.

Though a validation of these models is still needed, and their improvement is certainly required, it was possible to carry out a comparative analysis on regional and standard global models. Results show that a high $a_{ys}(\lambda)$ and a high $b_{bp}(\lambda)$ seem to be the main responsible for the high $K_d(\lambda)$ and the low B/G in the Mediterranean Sea.

This study also points out some peculiarities in some of the optical components in the Mediterranean. The results show a low and high Chl specific absorption coefficients in the blue and green, respectively, in oligotrophic conditions. The mean absorption spectra of phytoplankton is also shifted toward shorter wavelengths at low Chl concentration. The absorption coefficient of "non algal particles", instead, is uncorrelated with Chl showing unexpectedly low values in eutrophic waters.

The distribution of picophytoplanktonic groups seems to be different in the Mediterranean Sea. This could explain some of the features observed for the IOPs but it seems unlikely that they can be responsible for the *green shift*.

9. Appendix

Attenuation Coefficients

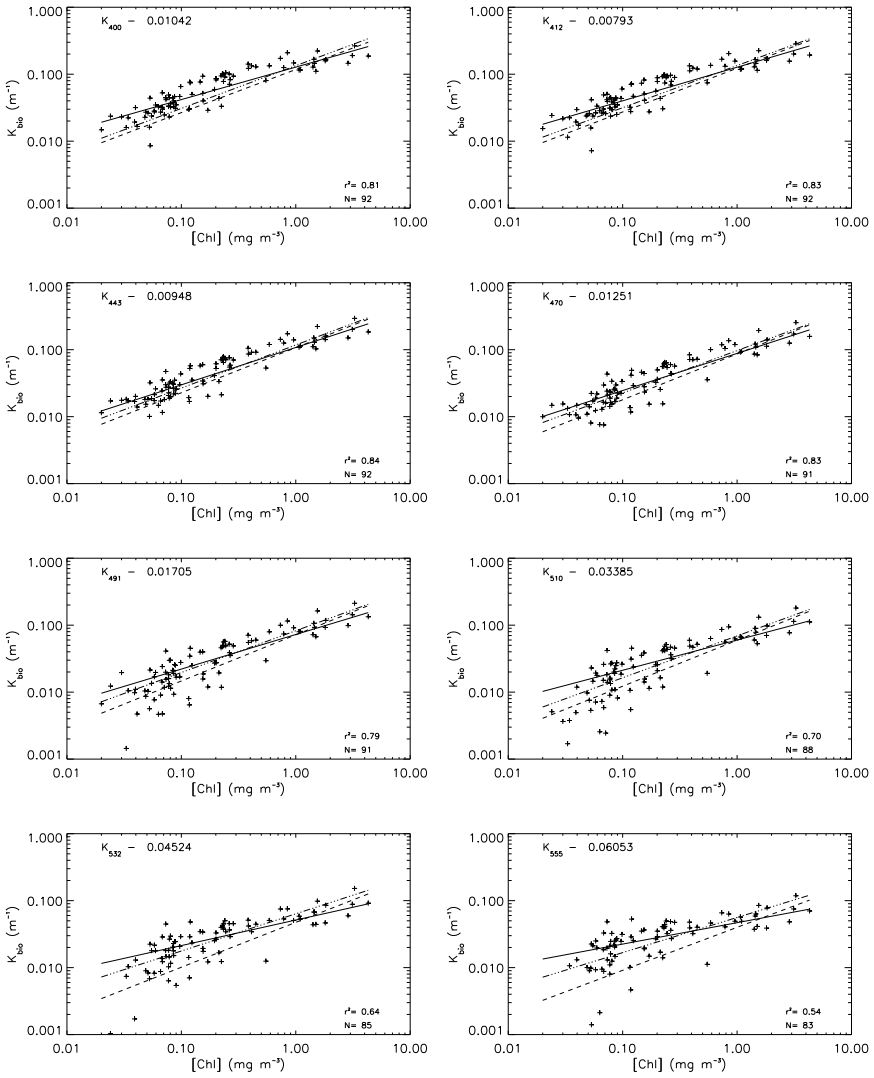

Figure 9.61: $K_{bio}(\lambda)$ versus [Chl] concentration for subset N1.

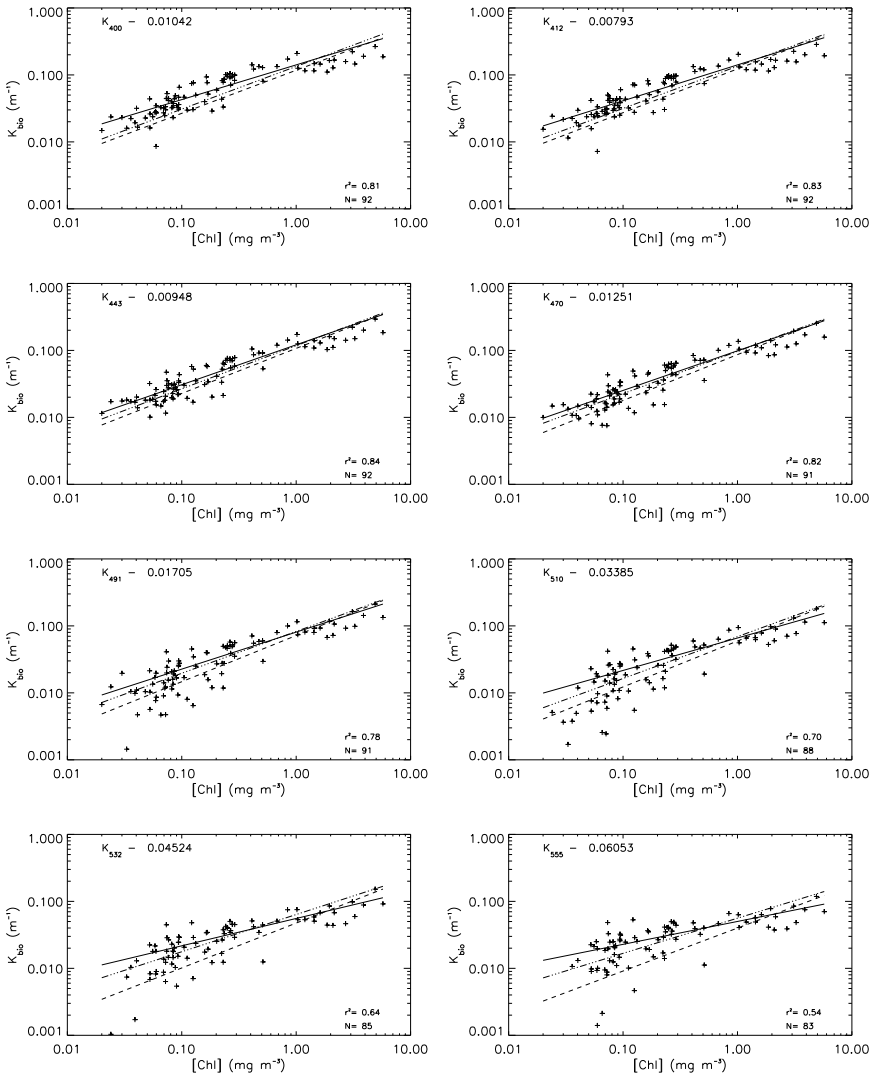

Figure 9.62: $K_{bio}(\lambda)$ versus [Chl] concentration for subset N2.

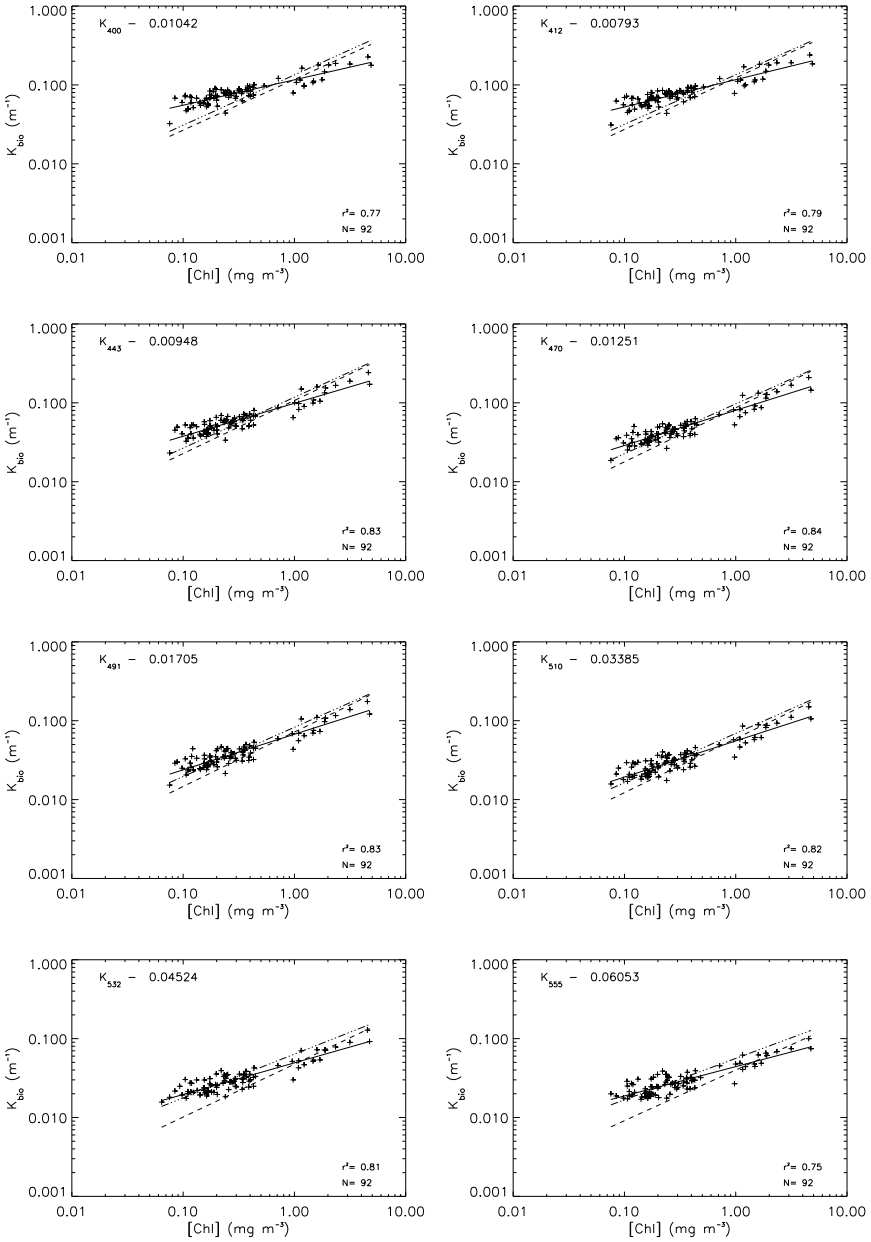

Figure 9.63: $K_{bio}(\lambda)$ versus [Chl] concentration for subset N3.

Absorption Coefficients of Particulate Phytoplankton and Non-algal Particles

λ	α_{a_p}	β_{a_p}	r^2	λ	α_{a_p}	β_{a_p}	r^2	λ	α_{a_p}	β_{a_p}	r^2
400	0.04461	0.56335	0.83	500	0.02542	0.60856	0.85	600	0.00755	0.61035	0.87
402	0.04494	0.56693	0.83	502	0.02437	0.60871	0.85	602	0.00744	0.61079	0.87
404	0.04536	0.57213	0.84	504	0.02334	0.60852	0.85	604	0.00737	0.61373	0.87
406	0.04598	0.57612	0.84	506	0.02236	0.60821	0.85	606	0.00733	0.61835	0.87
408	0.04663	0.58048	0.84	508	0.02144	0.60777	0.85	608	0.00733	0.62284	0.88
410	0.04726	0.58682	0.84	510	0.02057	0.60689	0.85	610	0.00737	0.62769	0.88
412	0.04759	0.58839	0.85	512	0.01974	0.60540	0.85	612	0.00742	0.63312	0.88
414	0.04799	0.59128	0.85	514	0.01894	0.60395	0.85	614	0.00748	0.63954	0.88
416	0.04823	0.59426	0.85	516	0.01817	0.60200	0.85	616	0.00753	0.64629	0.89
418	0.04834	0.59773	0.85	518	0.01745	0.60041	0.85	618	0.00759	0.65284	0.89
420	0.04846	0.59993	0.85	520	0.01679	0.59857	0.85	620	0.00764	0.65737	0.89
422	0.04854	0.60094	0.85	522	0.01617	0.59652	0.85	622	0.00770	0.66147	0.89
424	0.04862	0.60147	0.85	524	0.01558	0.59409	0.85	624	0.00773	0.66408	0.90
426	0.04875	0.60311	0.85	526	0.01504	0.59229	0.84	626	0.00776	0.66746	0.90
428	0.04905	0.60747	0.86	528	0.01452	0.59137	0.84	628	0.00781	0.67198	0.90
430	0.04946	0.60975	0.86	530	0.01405	0.59084	0.84	630	0.00787	0.67794	0.90
432	0.04989	0.61302	0.86	532	0.01362	0.58966	0.84	632	0.00795	0.68328	0.90
434	0.05019	0.61733	0.86	534	0.01321	0.58760	0.84	634	0.00802	0.68774	0.90
436	0.05034	0.61883	0.86	536	0.01282	0.58621	0.84	636	0.00808	0.69156	0.90
438	0.05018	0.62126	0.86	538	0.01245	0.58550	0.84	638	0.00811	0.69575	0.90
440	0.04968	0.62071	0.86	540	0.01209	0.58427	0.84	640	0.00814	0.69879	0.91
442	0.04895	0.61932	0.86	542	0.01173	0.58287	0.84	642	0.00813	0.70222	0.91
444	0.04803	0.61703	0.86	544	0.01136	0.58076	0.84	644	0.00812	0.70606	0.91
446	0.04702	0.61512	0.86	546	0.01100	0.57966	0.84	646	0.00810	0.70796	0.91
448	0.04601	0.61329	0.86	548	0.01063	0.57770	0.84	648	0.00813	0.70707	0.91
450	0.04501	0.61171	0.85	550	0.01026	0.57370	0.83	650	0.00823	0.70799	0.91
452	0.04422	0.61156	0.85	552	0.00990	0.56966	0.83	652	0.00844	0.71157	0.91
454	0.04363	0.61244	0.85	554	0.00955	0.56543	0.83	654	0.00877	0.72156	0.91
456	0.04319	0.61383	0.85	556	0.00920	0.56208	0.83	656	0.00929	0.73279	0.91
458	0.04275	0.61601	0.85	558	0.00887	0.55921	0.83	658	0.01003	0.74327	0.91
460	0.04232	0.61770	0.85	560	0.00858	0.55566	0.82	660	0.01097	0.75538	0.92
462	0.04189	0.61912	0.85	562	0.00832	0.55366	0.82	662	0.01211	0.76956	0.92
464	0.04143	0.62104	0.86	564	0.00810	0.55228	0.82	664	0.01336	0.78297	0.92
466	0.04088	0.62302	0.86	566	0.00793	0.55290	0.83	666	0.01463	0.79594	0.92
468	0.04018	0.62304	0.86	568	0.00781	0.55510	0.83	668	0.01580	0.80578	0.92
470	0.03942	0.62295	0.86	570	0.00772	0.55737	0.83	670	0.01674	0.81365	0.92
472	0.03858	0.62138	0.86	572	0.00767	0.56084	0.83	672	0.01730	0.82036	0.92
474	0.03769	0.62069	0.86	574	0.00766	0.56549	0.84	674	0.01741	0.82462	0.92
476	0.03678	0.61836	0.86	576	0.00768	0.56966	0.84	676	0.01706	0.82726	0.92
478	0.03581	0.61705	0.86	578	0.00772	0.57479	0.85	678	0.01627	0.82756	0.92
480	0.03488	0.61461	0.85	580	0.00777	0.58095	0.85	680	0.01509	0.82770	0.92
482	0.03397	0.61283	0.85	582	0.00785	0.58756	0.86	682	0.01358	0.82682	0.92
484	0.03311	0.61097	0.85	584	0.00792	0.59355	0.86	684	0.01188	0.82388	0.92
486	0.03224	0.60952	0.85	586	0.00798	0.59892	0.87	686	0.01012	0.81936	0.92
488	0.03133	0.60801	0.85	588	0.00802	0.60353	0.87	688	0.00845	0.81105	0.91
490	0.03042	0.60803	0.85	590	0.00802	0.60663	0.87	690	0.00696	0.80054	0.91
492	0.02949	0.60750	0.84	592	0.00798	0.60904	0.87	692	0.00570	0.78983	0.90
494	0.02850	0.60778	0.84	594	0.00791	0.60987	0.87	694	0.00469	0.77433	0.90
496	0.02749	0.60807	0.85	596	0.00780	0.61102	0.87	696	0.00391	0.76079	0.89
498	0.02647	0.60839	0.85	598	0.00767	0.61056	0.87	698	0.00330	0.74857	0.88
								700	0.00282	0.73719	0.87

Table 9.14: $\alpha(\lambda)$ and $\beta(\lambda)$ coefficients for $a_p(\lambda)$ with determination coefficients. Subset N2.

λ	$\alpha_{a_{ph}}$	$\beta_{a_{ph}}$	r^2	λ	$\alpha_{a_{ph}}$	$\beta_{a_{ph}}$	r^2	λ	$\alpha_{a_{ph}}$	$\beta_{a_{ph}}$	r^2
400	0.03585	0.68449	0.89	500	0.02234	0.69770	0.88	600	0.00649	0.70198	0.90
402	0.03638	0.68810	0.89	502	0.02136	0.69946	0.88	602	0.00640	0.70171	0.90
404	0.03690	0.69009	0.89	504	0.02039	0.70128	0.88	604	0.00635	0.70352	0.90
406	0.03762	0.69053	0.89	506	0.01947	0.70232	0.88	606	0.00633	0.70625	0.90
408	0.03842	0.69185	0.89	508	0.01860	0.70375	0.89	608	0.00634	0.71035	0.90
410	0.03913	0.69558	0.90	510	0.01780	0.70434	0.89	610	0.00639	0.71443	0.90
412	0.03960	0.69497	0.89	512	0.01702	0.70495	0.89	612	0.00646	0.71843	0.90
414	0.04014	0.69594	0.89	514	0.01629	0.70569	0.89	614	0.00654	0.72337	0.90
416	0.04048	0.69573	0.89	516	0.01556	0.70529	0.89	616	0.00660	0.72891	0.91
418	0.04075	0.69840	0.89	518	0.01489	0.70526	0.89	618	0.00668	0.73355	0.91
420	0.04103	0.69920	0.89	520	0.01429	0.70510	0.89	620	0.00676	0.73570	0.91
422	0.04121	0.69877	0.90	522	0.01371	0.70408	0.89	622	0.00683	0.73708	0.91
424	0.04142	0.69716	0.89	524	0.01318	0.70228	0.89	624	0.00688	0.73896	0.92
426	0.04170	0.69721	0.89	526	0.01270	0.70116	0.89	626	0.00692	0.74290	0.91
428	0.04214	0.69970	0.89	528	0.01223	0.70134	0.88	628	0.00698	0.74735	0.92
430	0.04266	0.69927	0.89	530	0.01180	0.70181	0.88	630	0.00706	0.75119	0.92
432	0.04323	0.70101	0.89	532	0.01141	0.70102	0.88	632	0.00716	0.75382	0.92
434	0.04365	0.70387	0.89	534	0.01106	0.69906	0.88	634	0.00725	0.75628	0.92
436	0.04394	0.70403	0.89	536	0.01072	0.69772	0.88	636	0.00732	0.75925	0.92
438	0.04394	0.70553	0.89	538	0.01040	0.69758	0.88	638	0.00737	0.76164	0.92
440	0.04359	0.70335	0.89	540	0.01009	0.69630	0.88	640	0.00742	0.76206	0.92
442	0.04301	0.70071	0.89	542	0.00977	0.69505	0.88	642	0.00743	0.76323	0.92
444	0.04223	0.69854	0.89	544	0.00945	0.69271	0.88	644	0.00743	0.76599	0.92
446	0.04135	0.69662	0.89	546	0.00912	0.69242	0.88	646	0.00742	0.76645	0.92
448	0.04051	0.69336	0.89	548	0.00879	0.69118	0.88	648	0.00747	0.76388	0.92
450	0.03965	0.69093	0.88	550	0.00847	0.68725	0.88	650	0.00758	0.76398	0.92
452	0.03901	0.69013	0.88	552	0.00816	0.68377	0.88	652	0.00780	0.76498	0.92
454	0.03851	0.69102	0.88	554	0.00784	0.67959	0.87	654	0.00814	0.77241	0.92
456	0.03819	0.69266	0.88	556	0.00754	0.67692	0.87	656	0.00866	0.78155	0.92
458	0.03786	0.69452	0.88	558	0.00724	0.67467	0.87	658	0.00939	0.78886	0.92
460	0.03752	0.69600	0.88	560	0.00698	0.67193	0.87	660	0.01034	0.79629	0.92
462	0.03717	0.69711	0.88	562	0.00676	0.67039	0.86	662	0.01147	0.80721	0.93
464	0.03682	0.69887	0.88	564	0.00658	0.66880	0.86	664	0.01271	0.81806	0.93
466	0.03637	0.70171	0.88	566	0.00644	0.66956	0.86	666	0.01398	0.82765	0.93
468	0.03578	0.70150	0.89	568	0.00635	0.67233	0.86	668	0.01516	0.83621	0.93
470	0.03509	0.70209	0.88	570	0.00629	0.67306	0.86	670	0.01609	0.84273	0.93
472	0.03437	0.70028	0.88	572	0.00627	0.67432	0.87	672	0.01665	0.84872	0.93
474	0.03357	0.69998	0.88	574	0.00628	0.67678	0.87	674	0.01677	0.85239	0.93
476	0.03276	0.69754	0.88	576	0.00633	0.67857	0.88	676	0.01643	0.85504	0.93
478	0.03189	0.69681	0.88	578	0.00640	0.68226	0.88	678	0.01566	0.85537	0.92
480	0.03105	0.69431	0.88	580	0.00648	0.68677	0.88	680	0.01449	0.85650	0.92
482	0.03024	0.69329	0.88	582	0.00658	0.69115	0.89	682	0.01300	0.85724	0.92
484	0.02947	0.69172	0.88	584	0.00668	0.69493	0.89	684	0.01132	0.85681	0.92
486	0.02868	0.69094	0.88	586	0.00677	0.69764	0.89	686	0.00958	0.85511	0.92
488	0.02784	0.68918	0.88	588	0.00682	0.70000	0.90	688	0.00794	0.85052	0.92
490	0.02702	0.69022	0.87	590	0.00686	0.70177	0.90	690	0.00647	0.84530	0.92
492	0.02616	0.69049	0.87	592	0.00684	0.70294	0.90	692	0.00524	0.84113	0.92
494	0.02524	0.69194	0.87	594	0.00679	0.70298	0.90	694	0.00425	0.83160	0.91
496	0.02429	0.69341	0.88	596	0.00670	0.70370	0.90	696	0.00348	0.82268	0.90
498	0.02334	0.69587	0.88	598	0.00659	0.70239	0.90	698	0.00290	0.81450	0.89
								700	0.00244	0.80941	0.88

Table 9.15: $\alpha(\lambda)$ and $\beta(\lambda)$ coefficients for $a_{ph}(\lambda)$ with determination coefficients. Subset N2.

λ	α_{anap}	β_{anap}	r^2	λ	α_{anap}	β_{anap}	r^2	λ	α_{anap}	β_{anap}	r^2
400	0.00556	-0.0243	0.00	500	0.00191	-0.0589	0.01	600	0.00062	-0.0619	0.01
402	0.00552	-0.0226	0.00	502	0.00186	-0.0562	0.01	602	0.00060	-0.0691	0.01
404	0.00547	-0.0176	0.00	504	0.00182	-0.0581	0.01	604	0.00059	-0.0690	0.01
406	0.00538	-0.0166	0.00	506	0.00178	-0.0546	0.01	606	0.00058	-0.0577	0.01
408	0.00527	-0.0174	0.00	508	0.00174	-0.0558	0.01	608	0.00057	-0.0610	0.01
410	0.00520	-0.0145	0.00	510	0.00170	-0.0530	0.01	610	0.00055	-0.0671	0.01
412	0.00510	-0.0138	0.00	512	0.00167	-0.0549	0.01	612	0.00057	-0.0221	0.00
414	0.00503	-0.0095	0.00	514	0.00163	-0.0575	0.01	614	0.00050	-0.1024	0.02
416	0.00498	-0.0043	0.00	516	0.00159	-0.0608	0.01	616	0.00050	-0.0861	0.02
418	0.00489	-0.0050	0.00	518	0.00156	-0.0573	0.01	618	0.00051	-0.0628	0.01
420	0.00484	-0.0008	0.00	520	0.00154	-0.0430	0.00	620	0.00050	-0.0582	0.01
422	0.00477	-0.0019	0.00	522	0.00152	-0.0186	0.00	622	0.00049	-0.0477	0.00
424	0.00470	-0.0006	0.00	524	0.00148	-0.0404	0.00	624	0.00048	-0.0410	0.00
426	0.00461	-0.0002	0.00	526	0.00144	-0.0452	0.00	626	0.00047	-0.0435	0.00
428	0.00453	0.00504	0.00	528	0.00141	-0.0451	0.00	628	0.00048	-0.0288	0.00
430	0.00445	0.00976	0.00	530	0.00137	-0.0794	0.02	630	0.00047	-0.0242	0.00
432	0.00437	0.00754	0.00	532	0.00134	-0.0791	0.02	632	0.00045	-0.0278	0.00
434	0.00426	0.00436	0.00	534	0.00131	-0.0772	0.02	634	0.00045	-0.0055	0.00
436	0.00419	0.00532	0.00	536	0.00128	-0.0752	0.02	636	0.00042	-0.0298	0.00
438	0.00407	0.00428	0.00	538	0.00125	-0.0759	0.02	638	0.00042	0.02407	0.00
440	0.00399	0.01154	0.00	540	0.00122	-0.0740	0.02	640	0.00042	0.01033	0.00
442	0.00389	0.01019	0.00	542	0.00120	-0.0726	0.02	642	0.00040	0.01727	0.00
444	0.00381	0.00718	0.00	544	0.00118	-0.0704	0.02	644	0.00040	0.03053	0.00
446	0.00372	0.00396	0.00	546	0.00115	-0.0713	0.02	646	0.00038	0.02074	0.00
448	0.00362	0.00337	0.00	548	0.00113	-0.0694	0.02	648	0.00038	0.03327	0.00
450	0.00354	0.00311	0.00	550	0.00111	-0.0656	0.01	650	0.00037	0.01690	0.00
452	0.00344	0.00239	0.00	552	0.00108	-0.0652	0.01	652	0.00037	0.04339	0.00
454	0.00337	0.00330	0.00	554	0.00106	-0.0641	0.01	654	0.00038	0.09983	0.03
456	0.00327	-0.0035	0.00	556	0.00103	-0.0624	0.01	656	0.00036	0.08213	0.02
458	0.00319	0.00940	0.00	558	0.00101	-0.0633	0.01	658	0.00035	0.05998	0.01
460	0.00310	-0.0038	0.00	560	0.00099	-0.0645	0.01	660	0.00032	-0.0038	0.00
462	0.00305	-0.0101	0.00	562	0.00097	-0.0629	0.01	662	0.00036	0.05111	0.00
464	0.00298	-0.0117	0.00	564	0.00094	-0.0630	0.01	664	0.00034	-0.0028	0.00
466	0.00288	-0.0217	0.00	566	0.00092	-0.0658	0.01	666	0.00035	0.04308	0.00
468	0.00281	-0.0255	0.00	568	0.00089	-0.0672	0.01	668	0.00035	0.04530	0.00
470	0.00274	-0.0320	0.00	570	0.00087	-0.0652	0.01	670	0.00035	0.04942	0.00
472	0.00266	-0.0338	0.00	572	0.00085	-0.0622	0.01	672	0.00036	0.06284	0.01
474	0.00259	-0.0353	0.00	574	0.00083	-0.0637	0.01	674	0.00035	0.07143	0.01
476	0.00254	-0.0370	0.00	576	0.00080	-0.0676	0.01	676	0.00035	0.08392	0.01
478	0.00248	-0.0399	0.00	578	0.00078	-0.0727	0.02	678	0.00035	0.08602	0.02
480	0.00242	-0.0413	0.00	580	0.00076	-0.0712	0.01	680	0.00034	0.10097	0.02
482	0.00235	-0.0501	0.01	582	0.00075	-0.0698	0.01	682	0.00032	0.11133	0.02
484	0.00229	-0.0511	0.01	584	0.00072	-0.0746	0.02	684	0.00032	0.11881	0.03
486	0.00224	-0.0532	0.01	586	0.00071	-0.0733	0.02	686	0.00031	0.12245	0.03
488	0.00220	-0.0446	0.00	588	0.00070	-0.0684	0.01	688	0.00029	0.12068	0.03
490	0.00214	-0.0446	0.00	590	0.00069	-0.0636	0.01	690	0.00028	0.14020	0.05
492	0.00209	-0.0476	0.00	592	0.00067	-0.0612	0.01	692	0.00026	0.13364	0.03
494	0.00204	-0.0543	0.01	594	0.00066	-0.0590	0.01	694	0.00025	0.11589	0.03
496	0.00199	-0.0592	0.01	596	0.00064	-0.0647	0.01	696	0.00023	0.15927	0.05
498	0.00194	-0.0613	0.01	598	0.00063	-0.0629	0.01	698	0.00025	0.18701	0.09
								700	0.00023	0.14758	0.06

Table 9.16: $\alpha(\lambda)$ and $\beta(\lambda)$ coefficients for $a_{nap}(\lambda)$ with determination coefficients. Subset N2.

λ	α_{a_p}	β_{a_p}	r^2	λ	α_{a_p}	β_{a_p}	r^2	λ	α_{a_p}	β_{a_p}	r^2
400	0.04773	0.57002	0.76	500	0.02697	0.61880	0.77	600	0.00755	0.60241	0.81
402	0.04834	0.57564	0.76	502	0.02580	0.61695	0.77	602	0.00743	0.60439	0.82
404	0.04887	0.58072	0.76	504	0.02467	0.61565	0.77	604	0.00735	0.60632	0.82
406	0.04958	0.58333	0.77	506	0.02355	0.61361	0.77	606	0.00731	0.61150	0.82
408	0.05017	0.58595	0.77	508	0.02252	0.61112	0.77	608	0.00731	0.61600	0.82
410	0.05088	0.59529	0.78	510	0.02153	0.60715	0.77	610	0.00734	0.62046	0.82
412	0.05126	0.59732	0.78	512	0.02060	0.60446	0.77	612	0.00740	0.62665	0.83
414	0.05176	0.60139	0.78	514	0.01972	0.60102	0.77	614	0.00746	0.63326	0.83
416	0.05208	0.60454	0.78	516	0.01887	0.59763	0.77	616	0.00751	0.64141	0.84
418	0.05221	0.60903	0.78	518	0.01809	0.59463	0.76	618	0.00757	0.64694	0.84
420	0.05228	0.61214	0.79	520	0.01736	0.59076	0.76	620	0.00761	0.65117	0.85
422	0.05243	0.61543	0.79	522	0.01669	0.58742	0.76	622	0.00768	0.65537	0.85
424	0.05246	0.61512	0.79	524	0.01605	0.58320	0.75	624	0.00774	0.66036	0.85
426	0.05261	0.61748	0.79	526	0.01547	0.58055	0.75	626	0.00777	0.66568	0.85
428	0.05296	0.62197	0.80	528	0.01491	0.57823	0.75	628	0.00780	0.67068	0.86
430	0.05334	0.62510	0.80	530	0.01440	0.57612	0.75	630	0.00784	0.67608	0.86
432	0.05381	0.63088	0.81	532	0.01393	0.57341	0.75	632	0.00791	0.68171	0.86
434	0.05411	0.63483	0.81	534	0.01348	0.57104	0.75	634	0.00798	0.68787	0.87
436	0.05421	0.63609	0.81	536	0.01307	0.57012	0.75	636	0.00804	0.69313	0.87
438	0.05393	0.63829	0.81	538	0.01269	0.56944	0.75	638	0.00806	0.69810	0.87
440	0.05341	0.63923	0.81	540	0.01233	0.56791	0.75	640	0.00808	0.70274	0.87
442	0.05262	0.63836	0.81	542	0.01195	0.56601	0.75	642	0.00807	0.70898	0.87
444	0.05162	0.63698	0.80	544	0.01156	0.56301	0.75	644	0.00804	0.71317	0.87
446	0.05055	0.63597	0.80	546	0.01118	0.56225	0.75	646	0.00801	0.71715	0.88
448	0.04955	0.63401	0.80	548	0.01081	0.56050	0.75	648	0.00802	0.71565	0.88
450	0.04852	0.63230	0.80	550	0.01044	0.55642	0.75	650	0.00812	0.71736	0.88
452	0.04762	0.63148	0.80	552	0.01007	0.55177	0.74	652	0.00832	0.72093	0.88
454	0.04696	0.63266	0.79	554	0.00971	0.54664	0.74	654	0.00866	0.73417	0.88
456	0.04649	0.63441	0.79	556	0.00937	0.54378	0.74	656	0.00920	0.74652	0.89
458	0.04599	0.63573	0.79	558	0.00905	0.54154	0.74	658	0.00997	0.75909	0.89
460	0.04548	0.63740	0.79	560	0.00875	0.53892	0.73	660	0.01095	0.77446	0.90
462	0.04492	0.63850	0.80	562	0.00849	0.53816	0.73	662	0.01213	0.79018	0.90
464	0.04432	0.64027	0.80	564	0.00827	0.53694	0.74	664	0.01342	0.80560	0.90
466	0.04361	0.64123	0.80	566	0.00809	0.53699	0.74	666	0.01474	0.82076	0.90
468	0.04282	0.64237	0.80	568	0.00797	0.53953	0.74	668	0.01594	0.83382	0.90
470	0.04196	0.64263	0.80	570	0.00788	0.54305	0.75	670	0.01692	0.84346	0.90
472	0.04104	0.64041	0.80	572	0.00781	0.54598	0.75	672	0.01749	0.85144	0.90
474	0.04003	0.63942	0.80	574	0.00778	0.54990	0.76	674	0.01761	0.85641	0.90
476	0.03900	0.63544	0.80	576	0.00779	0.55443	0.77	676	0.01725	0.86031	0.90
478	0.03792	0.63465	0.79	578	0.00782	0.56146	0.77	678	0.01644	0.86005	0.90
480	0.03693	0.63276	0.79	580	0.00787	0.56914	0.78	680	0.01522	0.85801	0.90
482	0.03603	0.63116	0.79	582	0.00793	0.57699	0.79	682	0.01367	0.85460	0.89
484	0.03515	0.62962	0.78	584	0.00799	0.58361	0.80	684	0.01193	0.85042	0.89
486	0.03426	0.62624	0.78	586	0.00804	0.58978	0.80	686	0.01013	0.84318	0.89
488	0.03332	0.62464	0.78	588	0.00807	0.59455	0.81	688	0.00841	0.83238	0.89
490	0.03237	0.62380	0.77	590	0.00806	0.59840	0.81	690	0.00689	0.81695	0.88
492	0.03136	0.62248	0.77	592	0.00801	0.60094	0.81	692	0.00562	0.80216	0.88
494	0.03032	0.62312	0.77	594	0.00792	0.60363	0.81	694	0.00460	0.78274	0.87
496	0.02925	0.62281	0.77	596	0.00780	0.60414	0.81	696	0.00382	0.76677	0.86
498	0.02812	0.62047	0.77	598	0.00766	0.60285	0.81	698	0.00322	0.74849	0.85
								700	0.00274	0.73509	0.84

Table 9.17: $\alpha(\lambda)$ and $\beta(\lambda)$ coefficients for $a_p(\lambda)$ with determination coefficients. Subset N1.

λ	$\alpha_{a_{ph}}$	$\beta_{a_{ph}}$	r^2	λ	$\alpha_{a_{ph}}$	$\beta_{a_{ph}}$	r^2	λ	$\alpha_{a_{ph}}$	$\beta_{a_{ph}}$	r^2
400	0.03761	0.69726	0.85	500	0.02356	0.71984	0.83	600	0.00637	0.70559	0.87
402	0.03840	0.70337	0.86	502	0.02247	0.72010	0.83	602	0.00629	0.70793	0.87
404	0.03913	0.70444	0.85	504	0.02140	0.72188	0.83	604	0.00623	0.70949	0.87
406	0.03997	0.70308	0.85	506	0.02036	0.72239	0.83	606	0.00621	0.71238	0.87
408	0.04066	0.70239	0.86	508	0.01939	0.72062	0.83	608	0.00622	0.71648	0.87
410	0.04151	0.70988	0.86	510	0.01847	0.71760	0.83	610	0.00627	0.72020	0.87
412	0.04203	0.70935	0.86	512	0.01760	0.71698	0.84	612	0.00634	0.72463	0.88
414	0.04269	0.71236	0.86	514	0.01679	0.71521	0.84	614	0.00642	0.72951	0.88
416	0.04315	0.71222	0.86	516	0.01598	0.71255	0.83	616	0.00650	0.73666	0.88
418	0.04347	0.71621	0.85	518	0.01527	0.71102	0.83	618	0.00657	0.73974	0.88
420	0.04373	0.71819	0.85	520	0.01460	0.70909	0.83	620	0.00663	0.74167	0.89
422	0.04403	0.72136	0.86	522	0.01399	0.70694	0.83	622	0.00671	0.74422	0.89
424	0.04423	0.71816	0.86	524	0.01341	0.70301	0.82	624	0.00679	0.74909	0.89
426	0.04456	0.71874	0.86	526	0.01289	0.70037	0.82	626	0.00685	0.75416	0.89
428	0.04505	0.72105	0.86	528	0.01239	0.69912	0.82	628	0.00689	0.75768	0.90
430	0.04559	0.72147	0.86	530	0.01192	0.69807	0.82	630	0.00695	0.76091	0.90
432	0.04627	0.72554	0.86	532	0.01150	0.69560	0.82	632	0.00704	0.76412	0.90
434	0.04676	0.72915	0.86	534	0.01112	0.69325	0.82	634	0.00713	0.76886	0.90
436	0.04700	0.72900	0.86	536	0.01076	0.69278	0.83	636	0.00720	0.77288	0.90
438	0.04692	0.73179	0.86	538	0.01042	0.69279	0.83	638	0.00724	0.77479	0.90
440	0.04657	0.73119	0.86	540	0.01011	0.69116	0.83	640	0.00727	0.77749	0.91
442	0.04594	0.72925	0.86	542	0.00979	0.68877	0.83	642	0.00729	0.78204	0.91
444	0.04511	0.72758	0.85	544	0.00944	0.68487	0.83	644	0.00728	0.78448	0.91
446	0.04422	0.72759	0.85	546	0.00910	0.68482	0.83	646	0.00727	0.78815	0.91
448	0.04340	0.72430	0.85	548	0.00877	0.68419	0.83	648	0.00728	0.78585	0.91
450	0.04254	0.72230	0.85	550	0.00845	0.68089	0.82	650	0.00740	0.78503	0.91
452	0.04179	0.71921	0.84	552	0.00813	0.67667	0.82	652	0.00760	0.78479	0.91
454	0.04124	0.72059	0.84	554	0.00782	0.67126	0.82	654	0.00796	0.79546	0.91
456	0.04092	0.72217	0.84	556	0.00752	0.66899	0.82	656	0.00850	0.80613	0.91
458	0.04055	0.72424	0.84	558	0.00724	0.66811	0.82	658	0.00927	0.81534	0.92
460	0.04014	0.72605	0.84	560	0.00699	0.66576	0.81	660	0.01025	0.82486	0.92
462	0.03969	0.72744	0.84	562	0.00677	0.66571	0.81	662	0.01141	0.83551	0.92
464	0.03919	0.72948	0.84	564	0.00659	0.66346	0.81	664	0.01271	0.84757	0.92
466	0.03862	0.73182	0.84	566	0.00645	0.66362	0.81	666	0.01401	0.85911	0.92
468	0.03795	0.73311	0.84	568	0.00635	0.66562	0.82	668	0.01521	0.87052	0.92
470	0.03720	0.73414	0.84	570	0.00629	0.66789	0.82	670	0.01619	0.87871	0.91
472	0.03639	0.73107	0.84	572	0.00626	0.66975	0.82	672	0.01676	0.88518	0.91
474	0.03549	0.73143	0.84	574	0.00627	0.67219	0.83	674	0.01689	0.88925	0.91
476	0.03457	0.72696	0.84	576	0.00630	0.67429	0.83	676	0.01654	0.89313	0.91
478	0.03358	0.72665	0.84	578	0.00636	0.68016	0.84	678	0.01574	0.89327	0.91
480	0.03268	0.72521	0.83	580	0.00645	0.68608	0.85	680	0.01453	0.89288	0.91
482	0.03188	0.72501	0.83	582	0.00654	0.69165	0.85	682	0.01301	0.89224	0.90
484	0.03110	0.72452	0.83	584	0.00662	0.69582	0.86	684	0.01130	0.89045	0.90
486	0.03030	0.72096	0.83	586	0.00669	0.70058	0.86	686	0.00952	0.88636	0.90
488	0.02946	0.71921	0.83	588	0.00675	0.70366	0.86	688	0.00783	0.87856	0.90
490	0.02859	0.71892	0.82	590	0.00677	0.70566	0.87	690	0.00635	0.86896	0.91
492	0.02767	0.71870	0.82	592	0.00674	0.70662	0.87	692	0.00510	0.86132	0.90
494	0.02671	0.72069	0.82	594	0.00668	0.70911	0.87	694	0.00411	0.84982	0.90
496	0.02571	0.72149	0.83	596	0.00658	0.70941	0.87	696	0.00335	0.83977	0.89
498	0.02464	0.72052	0.83	598	0.00647	0.70703	0.87	698	0.00278	0.82786	0.89
								700	0.00232	0.82282	0.87

Table 9.18: $\alpha(\lambda)$ and $\beta(\lambda)$ coefficients for $a_{ph}(\lambda)$ with determination coefficients. Subset N1.

λ	α_{anap}	β_{anap}	r^2	λ	α_{anap}	β_{anap}	r^2	λ	α_{anap}	β_{anap}	r^2
400	0.00695	0.02673	0.00	500	0.00232	-0.0255	0.00	600	0.00077	-0.0272	0.00
402	0.00684	0.02507	0.00	502	0.00228	-0.0243	0.00	602	0.00075	-0.0286	0.00
404	0.00670	0.02917	0.00	504	0.00222	-0.0282	0.00	604	0.00073	-0.0353	0.00
406	0.00656	0.02458	0.00	506	0.00215	-0.0345	0.00	606	0.00071	-0.0297	0.00
408	0.00645	0.02466	0.00	508	0.00211	-0.0319	0.00	608	0.00070	-0.0312	0.00
410	0.00638	0.02953	0.00	510	0.00206	-0.0329	0.00	610	0.00068	-0.0313	0.00
412	0.00630	0.03251	0.00	512	0.00202	-0.0321	0.00	612	0.00066	-0.0249	0.00
414	0.00618	0.03041	0.00	514	0.00198	-0.0322	0.00	614	0.00066	-0.0244	0.00
416	0.00613	0.03819	0.00	516	0.00194	-0.0312	0.00	616	0.00064	-0.0333	0.00
418	0.00601	0.03867	0.00	518	0.00189	-0.0328	0.00	618	0.00063	-0.0321	0.00
420	0.00592	0.04240	0.00	520	0.00186	-0.0290	0.00	620	0.00061	-0.0229	0.00
422	0.00585	0.04329	0.00	522	0.00182	-0.0284	0.00	622	0.00061	-0.0178	0.00
424	0.00576	0.04671	0.00	524	0.00179	-0.0266	0.00	624	0.00060	-0.0054	0.00
426	0.00565	0.04689	0.00	526	0.00175	-0.0251	0.00	626	0.00058	0.00056	0.00
428	0.00555	0.05181	0.00	528	0.00171	-0.0229	0.00	628	0.00055	-0.0339	0.00
430	0.00546	0.05640	0.01	530	0.00165	-0.0533	0.01	630	0.00053	-0.0427	0.00
432	0.00530	0.05444	0.01	532	0.00161	-0.0553	0.01	632	0.00052	-0.0398	0.00
434	0.00513	0.04519	0.00	534	0.00158	-0.0550	0.01	634	0.00049	-0.0522	0.00
436	0.00504	0.04587	0.00	536	0.00154	-0.0542	0.01	636	0.00049	-0.0305	0.00
438	0.00491	0.04179	0.00	538	0.00152	-0.0480	0.00	638	0.00041	-0.0720	0.02
440	0.00479	0.04360	0.00	540	0.00148	-0.0465	0.00	640	0.00047	-0.0558	0.00
442	0.00469	0.04524	0.00	542	0.00144	-0.0464	0.00	642	0.00044	-0.0613	0.00
444	0.00460	0.04626	0.00	544	0.00142	-0.0475	0.00	644	0.00044	-0.0413	0.00
446	0.00448	0.04251	0.00	546	0.00140	-0.0443	0.00	646	0.00042	-0.0391	0.00
448	0.00434	0.03867	0.00	548	0.00137	-0.0400	0.00	648	0.00043	-0.0267	0.00
450	0.00423	0.03517	0.00	550	0.00134	-0.0394	0.00	650	0.00039	-0.0546	0.00
452	0.00412	0.03795	0.00	552	0.00130	-0.0435	0.00	652	0.00041	-0.0381	0.00
454	0.00403	0.03379	0.00	554	0.00127	-0.0467	0.00	654	0.00038	0.01460	0.00
456	0.00392	0.02948	0.00	556	0.00125	-0.0428	0.00	656	0.00035	-0.0147	0.00
458	0.00382	0.02575	0.00	558	0.00122	-0.0426	0.00	658	0.00032	-0.1087	0.02
460	0.00374	0.02714	0.00	560	0.00119	-0.0428	0.00	660	0.00042	0.09038	0.01
462	0.00366	0.02501	0.00	562	0.00116	-0.0432	0.00	662	0.00042	0.02558	0.00
464	0.00358	0.02284	0.00	564	0.00114	-0.0393	0.00	664	0.00043	0.03607	0.00
466	0.00347	0.01278	0.00	566	0.00111	-0.0399	0.00	666	0.00043	0.06494	0.01
468	0.00338	0.00910	0.00	568	0.00109	-0.0383	0.00	668	0.00043	0.03062	0.00
470	0.00328	0.00148	0.00	570	0.00107	-0.0373	0.00	670	0.00043	0.03110	0.00
472	0.00320	0.00093	0.00	572	0.00104	-0.0338	0.00	672	0.00044	0.09224	0.02
474	0.00311	-0.0060	0.00	574	0.00102	-0.0320	0.00	674	0.00043	0.10063	0.02
476	0.00306	-0.0056	0.00	576	0.00100	-0.0302	0.00	676	0.00042	0.12883	0.02
478	0.00300	-0.0040	0.00	578	0.00096	-0.0385	0.00	678	0.00041	0.06401	0.01
480	0.00294	-0.0034	0.00	580	0.00093	-0.0395	0.00	680	0.00041	0.11276	0.03
482	0.00286	-0.0121	0.00	582	0.00091	-0.0434	0.00	682	0.00040	0.14706	0.04
484	0.00279	-0.0167	0.00	584	0.00089	-0.0395	0.00	684	0.00037	0.08676	0.01
486	0.00272	-0.0222	0.00	586	0.00088	-0.0377	0.00	686	0.00036	0.08690	0.01
488	0.00265	-0.0218	0.00	588	0.00085	-0.0368	0.00	688	0.00034	0.08874	0.01
490	0.00259	-0.0224	0.00	590	0.00084	-0.0388	0.00	690	0.00033	0.14224	0.05
492	0.00253	-0.0254	0.00	592	0.00082	-0.0357	0.00	692	0.00031	0.06252	0.01
494	0.00247	-0.0250	0.00	594	0.00081	-0.0335	0.00	694	0.00023	-0.0099	0.00
496	0.00242	-0.0273	0.00	596	0.00079	-0.0346	0.00	696	0.00021	-0.0131	0.00
498	0.00237	-0.0282	0.00	598	0.00077	-0.0319	0.00	698	0.00025	0.19164	0.10
								700	0.00021	0.22766	0.10

Table 9.19: $\alpha(\lambda)$ and $\beta(\lambda)$ coefficients for $a_{nap}(\lambda)$ with determination coefficients. Subset N1.

λ	α_{ap}	β_{ap}	r^2	λ	α_{ap}	β_{ap}	r^2	λ	α_{ap}	β_{ap}	r^2
400	0.04195	0.54596	0.81	500	0.02408	0.58590	0.83	600	0.00737	0.58659	0.85
402	0.04230	0.54949	0.81	502	0.02310	0.58659	0.83	602	0.00727	0.58701	0.85
404	0.04270	0.55474	0.81	504	0.02215	0.58686	0.83	604	0.00721	0.58969	0.85
406	0.04325	0.55869	0.82	506	0.02125	0.58726	0.83	606	0.00718	0.59401	0.86
408	0.04380	0.56266	0.82	508	0.02040	0.58749	0.83	608	0.00718	0.59882	0.86
410	0.04440	0.56887	0.82	510	0.01959	0.58700	0.83	610	0.00723	0.60418	0.86
412	0.04475	0.57022	0.82	512	0.01882	0.58636	0.83	612	0.00728	0.60986	0.86
414	0.04514	0.57310	0.82	514	0.01808	0.58537	0.83	614	0.00734	0.61639	0.87
416	0.04538	0.57542	0.82	516	0.01737	0.58418	0.83	616	0.00740	0.62341	0.87
418	0.04545	0.57775	0.83	518	0.01671	0.58310	0.83	618	0.00746	0.63001	0.87
420	0.04555	0.57915	0.83	520	0.01610	0.58191	0.83	620	0.00751	0.63448	0.88
422	0.04561	0.57964	0.83	522	0.01552	0.58095	0.83	622	0.00757	0.63876	0.88
424	0.04571	0.58063	0.83	524	0.01498	0.57944	0.83	624	0.00760	0.64181	0.88
426	0.04585	0.58258	0.83	526	0.01447	0.57850	0.83	626	0.00762	0.64523	0.88
428	0.04611	0.58667	0.83	528	0.01399	0.57794	0.83	628	0.00767	0.64940	0.88
430	0.04649	0.58854	0.83	530	0.01355	0.57745	0.83	630	0.00774	0.65498	0.88
432	0.04692	0.59157	0.83	532	0.01314	0.57669	0.83	632	0.00782	0.65980	0.88
434	0.04720	0.59536	0.83	534	0.01275	0.57541	0.83	634	0.00789	0.66357	0.88
436	0.04732	0.59724	0.83	536	0.01238	0.57433	0.83	636	0.00795	0.66670	0.89
438	0.04717	0.59877	0.84	538	0.01203	0.57370	0.82	638	0.00799	0.66940	0.89
440	0.04676	0.59866	0.84	540	0.01169	0.57240	0.82	640	0.00801	0.67092	0.89
442	0.04609	0.59653	0.83	542	0.01135	0.57086	0.82	642	0.00801	0.67302	0.89
444	0.04525	0.59381	0.83	544	0.01100	0.56877	0.82	644	0.00801	0.67528	0.88
446	0.04431	0.59150	0.83	546	0.01065	0.56746	0.82	646	0.00800	0.67604	0.88
448	0.04336	0.58910	0.83	548	0.01030	0.56510	0.82	648	0.00804	0.67450	0.88
450	0.04241	0.58700	0.83	550	0.00994	0.56109	0.82	650	0.00815	0.67462	0.88
452	0.04165	0.58692	0.83	552	0.00959	0.55688	0.82	652	0.00837	0.67811	0.88
454	0.04109	0.58754	0.83	554	0.00925	0.55272	0.82	654	0.00870	0.68766	0.88
456	0.04066	0.58881	0.83	556	0.00892	0.54904	0.82	656	0.00922	0.69896	0.88
458	0.04024	0.59074	0.83	558	0.00861	0.54599	0.81	658	0.00994	0.71075	0.89
460	0.03985	0.59284	0.83	560	0.00832	0.54234	0.81	660	0.01086	0.72411	0.89
462	0.03945	0.59409	0.83	562	0.00807	0.53989	0.81	662	0.01197	0.73927	0.90
464	0.03904	0.59571	0.83	564	0.00786	0.53819	0.81	664	0.01317	0.75383	0.90
466	0.03854	0.59713	0.83	566	0.00770	0.53854	0.81	666	0.01440	0.76742	0.90
468	0.03792	0.59654	0.83	568	0.00758	0.54010	0.81	668	0.01553	0.77822	0.91
470	0.03722	0.59614	0.83	570	0.00750	0.54198	0.82	670	0.01643	0.78692	0.91
472	0.03645	0.59406	0.83	572	0.00745	0.54451	0.82	672	0.01696	0.79423	0.91
474	0.03563	0.59286	0.83	574	0.00744	0.54839	0.82	674	0.01706	0.79932	0.91
476	0.03478	0.59013	0.83	576	0.00746	0.55243	0.83	676	0.01671	0.80257	0.91
478	0.03389	0.58815	0.83	578	0.00750	0.55682	0.83	678	0.01595	0.80344	0.90
480	0.03302	0.58604	0.82	580	0.00756	0.56235	0.84	680	0.01481	0.80361	0.90
482	0.03216	0.58437	0.82	582	0.00763	0.56834	0.84	682	0.01336	0.80269	0.90
484	0.03135	0.58307	0.82	584	0.00770	0.57401	0.85	684	0.01171	0.79959	0.90
486	0.03052	0.58234	0.82	586	0.00776	0.57861	0.85	686	0.01001	0.79476	0.90
488	0.02966	0.58157	0.82	588	0.00780	0.58242	0.85	688	0.00838	0.78574	0.90
490	0.02879	0.58227	0.82	590	0.00781	0.58491	0.85	690	0.00692	0.77382	0.89
492	0.02790	0.58235	0.82	592	0.00777	0.58651	0.85	692	0.00569	0.76121	0.89
494	0.02697	0.58321	0.82	594	0.00770	0.58690	0.85	694	0.00469	0.74476	0.88
496	0.02603	0.58413	0.82	596	0.00760	0.58759	0.85	696	0.00392	0.72877	0.86
498	0.02507	0.58497	0.82	598	0.00748	0.58707	0.85	698	0.00331	0.71470	0.85
								700	0.00285	0.70145	0.84

Table 9.20: $\alpha(\lambda)$ and $\beta(\lambda)$ coefficients for $a_p(\lambda)$ with determination coefficients. Subset N3.

λ	$\alpha_{a_{ph}}$	$\beta_{a_{ph}}$	r^2	λ	$\alpha_{a_{ph}}$	$\beta_{a_{ph}}$	r^2	λ	$\alpha_{a_{ph}}$	$\beta_{a_{ph}}$	r^2
400	0.03388	0.65940	0.86	500	0.02123	0.66913	0.86	600	0.00637	0.66926	0.87
402	0.03439	0.66237	0.86	502	0.02031	0.67142	0.86	602	0.00629	0.66916	0.87
404	0.03490	0.66503	0.87	504	0.01942	0.67323	0.86	604	0.00625	0.67099	0.87
406	0.03556	0.66625	0.87	506	0.01856	0.67508	0.86	606	0.00624	0.67359	0.87
408	0.03621	0.66760	0.87	508	0.01776	0.67719	0.87	608	0.00625	0.67807	0.88
410	0.03688	0.67193	0.87	510	0.01701	0.67800	0.87	610	0.00631	0.68265	0.88
412	0.03736	0.67134	0.87	512	0.01629	0.67905	0.87	612	0.00637	0.68695	0.88
414	0.03786	0.67239	0.87	514	0.01560	0.67979	0.87	614	0.00645	0.69218	0.88
416	0.03820	0.67191	0.87	516	0.01494	0.68024	0.87	616	0.00652	0.69844	0.88
418	0.03841	0.67318	0.87	518	0.01432	0.68070	0.87	618	0.00660	0.70366	0.89
420	0.03865	0.67315	0.87	520	0.01376	0.68114	0.87	620	0.00667	0.70614	0.89
422	0.03880	0.67227	0.87	522	0.01322	0.68112	0.87	622	0.00674	0.70815	0.89
424	0.03903	0.67172	0.87	524	0.01273	0.68029	0.87	624	0.00679	0.71036	0.89
426	0.03929	0.67246	0.87	526	0.01227	0.68006	0.87	626	0.00683	0.71405	0.89
428	0.03968	0.67494	0.87	528	0.01184	0.68049	0.87	628	0.00689	0.71817	0.89
430	0.04017	0.67412	0.87	530	0.01144	0.68076	0.87	630	0.00697	0.72221	0.90
432	0.04072	0.67558	0.87	532	0.01107	0.68069	0.87	632	0.00708	0.72453	0.90
434	0.04112	0.67814	0.87	534	0.01073	0.67982	0.87	634	0.00716	0.72643	0.90
436	0.04136	0.67883	0.86	536	0.01041	0.67880	0.87	636	0.00723	0.72852	0.90
438	0.04135	0.67947	0.86	538	0.01010	0.67847	0.87	638	0.00729	0.72951	0.90
440	0.04107	0.67796	0.86	540	0.00981	0.67700	0.86	640	0.00733	0.72847	0.90
442	0.04054	0.67456	0.86	542	0.00951	0.67557	0.86	642	0.00735	0.72850	0.90
444	0.03983	0.67196	0.86	544	0.00920	0.67343	0.86	644	0.00736	0.72956	0.89
446	0.03903	0.66909	0.86	546	0.00888	0.67279	0.86	646	0.00736	0.72895	0.89
448	0.03823	0.66533	0.86	548	0.00857	0.67089	0.86	648	0.00742	0.72602	0.89
450	0.03742	0.66233	0.86	550	0.00825	0.66688	0.86	650	0.00754	0.72506	0.89
452	0.03679	0.66166	0.85	552	0.00795	0.66271	0.86	652	0.00776	0.72612	0.89
454	0.03632	0.66226	0.85	554	0.00764	0.65859	0.86	654	0.00810	0.73344	0.89
456	0.03600	0.66383	0.85	556	0.00735	0.65515	0.85	656	0.00862	0.74282	0.89
458	0.03569	0.66563	0.85	558	0.00707	0.65245	0.85	658	0.00934	0.75219	0.90
460	0.03539	0.66773	0.85	560	0.00681	0.64904	0.85	660	0.01026	0.76196	0.90
462	0.03507	0.66833	0.85	562	0.00660	0.64675	0.85	662	0.01136	0.77426	0.90
464	0.03476	0.66937	0.85	564	0.00643	0.64480	0.85	664	0.01256	0.78631	0.91
466	0.03435	0.67103	0.86	566	0.00630	0.64524	0.85	666	0.01379	0.79718	0.91
468	0.03383	0.66996	0.86	568	0.00621	0.64710	0.85	668	0.01492	0.80698	0.91
470	0.03322	0.66988	0.85	570	0.00615	0.64739	0.85	670	0.01581	0.81465	0.91
472	0.03255	0.66743	0.85	572	0.00613	0.64778	0.85	672	0.01634	0.82123	0.91
474	0.03181	0.66672	0.85	574	0.00615	0.64955	0.85	674	0.01645	0.82582	0.91
476	0.03107	0.66381	0.85	576	0.00620	0.65157	0.86	676	0.01611	0.82921	0.91
478	0.03026	0.66208	0.85	578	0.00626	0.65446	0.86	678	0.01537	0.83053	0.91
480	0.02948	0.65974	0.85	580	0.00634	0.65854	0.86	680	0.01423	0.83172	0.91
482	0.02870	0.65881	0.85	582	0.00644	0.66242	0.87	682	0.01280	0.83219	0.91
484	0.02798	0.65794	0.85	584	0.00653	0.66609	0.87	684	0.01117	0.83151	0.91
486	0.02723	0.65802	0.85	586	0.00662	0.66811	0.87	686	0.00949	0.82934	0.91
488	0.02643	0.65718	0.85	588	0.00668	0.66988	0.88	688	0.00788	0.82395	0.90
490	0.02565	0.65882	0.85	590	0.00671	0.67126	0.88	690	0.00646	0.81695	0.90
492	0.02483	0.65963	0.85	592	0.00670	0.67174	0.88	692	0.00524	0.81024	0.90
494	0.02396	0.66171	0.85	594	0.00665	0.67138	0.88	694	0.00426	0.79910	0.89
496	0.02307	0.66376	0.85	596	0.00657	0.67152	0.88	696	0.00351	0.78742	0.87
498	0.02217	0.66656	0.85	598	0.00647	0.67026	0.88	698	0.00292	0.77692	0.86
								700	0.00247	0.76854	0.85

Table 9.21: $\alpha(\lambda)$ and $\beta(\lambda)$ coefficients for $a_{ph}(\lambda)$ with determination coefficients. Subset N3.

λ	α_{anap}	β_{anap}	r^2	λ	α_{anap}	β_{anap}	r^2	λ	α_{anap}	β_{anap}	r^2
400	0.00525	-0.0098	0.00	500	0.00182	-0.0412	0.00	600	0.00061	-0.0223	0.00
402	0.00521	-0.0063	0.00	502	0.00178	-0.0397	0.00	602	0.00060	-0.0283	0.00
404	0.00515	-0.0006	2.24	504	0.00174	-0.0400	0.00	604	0.00058	-0.0276	0.00
406	0.00507	-0.0003	5.63	506	0.00170	-0.0366	0.00	606	0.00058	-0.0167	0.00
408	0.00499	-0.0005	1.40	508	0.00166	-0.0384	0.00	608	0.00056	-0.0191	0.00
410	0.00492	0.00140	8.82	510	0.00163	-0.0346	0.00	610	0.00055	-0.0229	0.00
412	0.00485	0.00185	1.54	512	0.00160	-0.0340	0.00	612	0.00056	0.00430	7.58
414	0.00479	0.00627	0.00	514	0.00157	-0.0358	0.00	614	0.00050	-0.0442	0.00
416	0.00473	0.00926	0.00	516	0.00153	-0.0388	0.00	616	0.00051	-0.0337	0.00
418	0.00464	0.00821	0.00	518	0.00150	-0.0366	0.00	618	0.00051	-0.0169	0.00
420	0.00459	0.01166	0.00	520	0.00147	-0.0263	0.00	620	0.00050	-0.0133	0.00
422	0.00454	0.01243	0.00	522	0.00145	-0.0080	0.00	622	0.00049	-0.0050	9.01
424	0.00448	0.01355	0.00	524	0.00142	-0.0237	0.00	624	0.00048	-0.0020	1.46
426	0.00439	0.01339	0.00	526	0.00138	-0.0265	0.00	626	0.00047	-0.0048	8.36
428	0.00432	0.01826	0.00	528	0.00135	-0.0270	0.00	628	0.00047	0.00110	4.43
430	0.00425	0.02292	0.00	530	0.00132	-0.0509	0.01	630	0.00046	0.00603	0.00
432	0.00417	0.02105	0.00	532	0.00129	-0.0517	0.01	632	0.00044	0.00576	0.00
434	0.00407	0.01712	0.00	534	0.00126	-0.0494	0.01	634	0.00044	0.01174	0.00
436	0.00400	0.01738	0.00	536	0.00124	-0.0472	0.01	636	0.00042	0.00025	2.07
438	0.00390	0.01618	0.00	538	0.00121	-0.0460	0.00	638	0.00042	0.00964	0.00
440	0.00382	0.02197	0.00	540	0.00118	-0.0440	0.00	640	0.00041	0.01669	0.00
442	0.00372	0.02009	0.00	542	0.00116	-0.0427	0.00	642	0.00039	0.01971	0.00
444	0.00365	0.01782	0.00	544	0.00114	-0.0413	0.00	644	0.00038	0.02255	0.00
446	0.00357	0.01743	0.00	546	0.00111	-0.0406	0.00	646	0.00037	0.03386	0.00
448	0.00346	0.01491	0.00	548	0.00109	-0.0376	0.00	648	0.00037	0.01857	0.00
450	0.00338	0.01455	0.00	550	0.00108	-0.0331	0.00	650	0.00036	0.02898	0.00
452	0.00330	0.01426	0.00	552	0.00105	-0.0320	0.00	652	0.00036	0.03582	0.00
454	0.00323	0.01465	0.00	554	0.00103	-0.0321	0.00	654	0.00036	0.04585	0.00
456	0.00314	0.00834	0.00	556	0.00100	-0.0305	0.00	656	0.00036	0.05613	0.00
458	0.00306	0.01604	0.00	558	0.00098	-0.0317	0.00	658	0.00035	0.05853	0.01
460	0.00297	0.00470	9.88	560	0.00096	-0.0313	0.00	660	0.00033	0.03550	0.00
462	0.00291	3.46584	5.64	562	0.00094	-0.0300	0.00	662	0.00035	0.07980	0.01
464	0.00285	0.00047	1.07	564	0.00092	-0.0300	0.00	664	0.00034	0.04139	0.00
466	0.00276	-0.0061	0.00	566	0.00089	-0.0327	0.00	666	0.00035	0.09927	0.02
468	0.00268	-0.0106	0.00	568	0.00087	-0.0342	0.00	668	0.00035	0.07420	0.01
470	0.00262	-0.0149	0.00	570	0.00085	-0.0313	0.00	670	0.00036	0.08076	0.02
472	0.00255	-0.0165	0.00	572	0.00083	-0.0281	0.00	672	0.00036	0.11140	0.03
474	0.00248	-0.0195	0.00	574	0.00081	-0.0283	0.00	674	0.00035	0.11171	0.03
476	0.00243	-0.0219	0.00	576	0.00079	-0.0308	0.00	676	0.00035	0.15616	0.04
478	0.00237	-0.0250	0.00	578	0.00076	-0.0345	0.00	678	0.00035	0.11675	0.04
480	0.00231	-0.0259	0.00	580	0.00075	-0.0343	0.00	680	0.00034	0.13387	0.04
482	0.00225	-0.0330	0.00	582	0.00073	-0.0318	0.00	682	0.00032	0.16324	0.05
484	0.00219	-0.0340	0.00	584	0.00071	-0.0347	0.00	684	0.00032	0.12425	0.04
486	0.00214	-0.0368	0.00	586	0.00070	-0.0322	0.00	686	0.00031	0.12835	0.04
488	0.00210	-0.0314	0.00	588	0.00068	-0.0279	0.00	688	0.00029	0.12965	0.04
490	0.00204	-0.0306	0.00	590	0.00067	-0.0255	0.00	690	0.00028	0.13303	0.04
492	0.00199	-0.0324	0.00	592	0.00066	-0.0240	0.00	692	0.00026	0.14025	0.04
494	0.00195	-0.0377	0.00	594	0.00065	-0.0232	0.00	694	0.00025	0.09403	0.02
496	0.00190	-0.0411	0.00	596	0.00063	-0.0274	0.00	696	0.00024	0.12630	0.03
498	0.00186	-0.0421	0.00	598	0.00062	-0.0256	0.00	698	0.00024	0.12321	0.04
								700	0.00022	0.11917	0.03

Table 9.22: $\alpha(\lambda)$ and $\beta(\lambda)$ coefficients for $a_{nap}(\lambda)$ with determination coefficients. Subset N3.

Ac9 Data

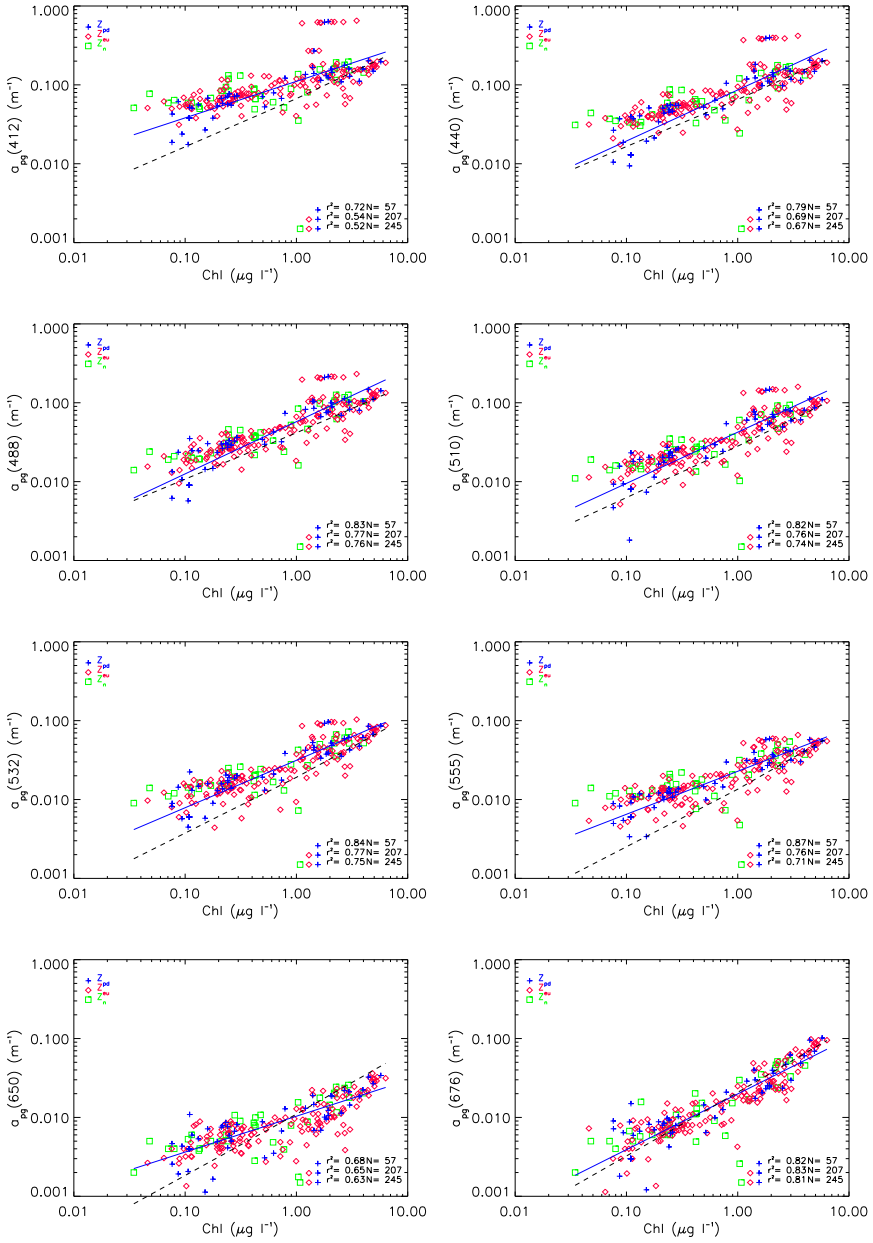

Figure 9.64: Total absorption coefficient without water contribution versus Chl concentration.

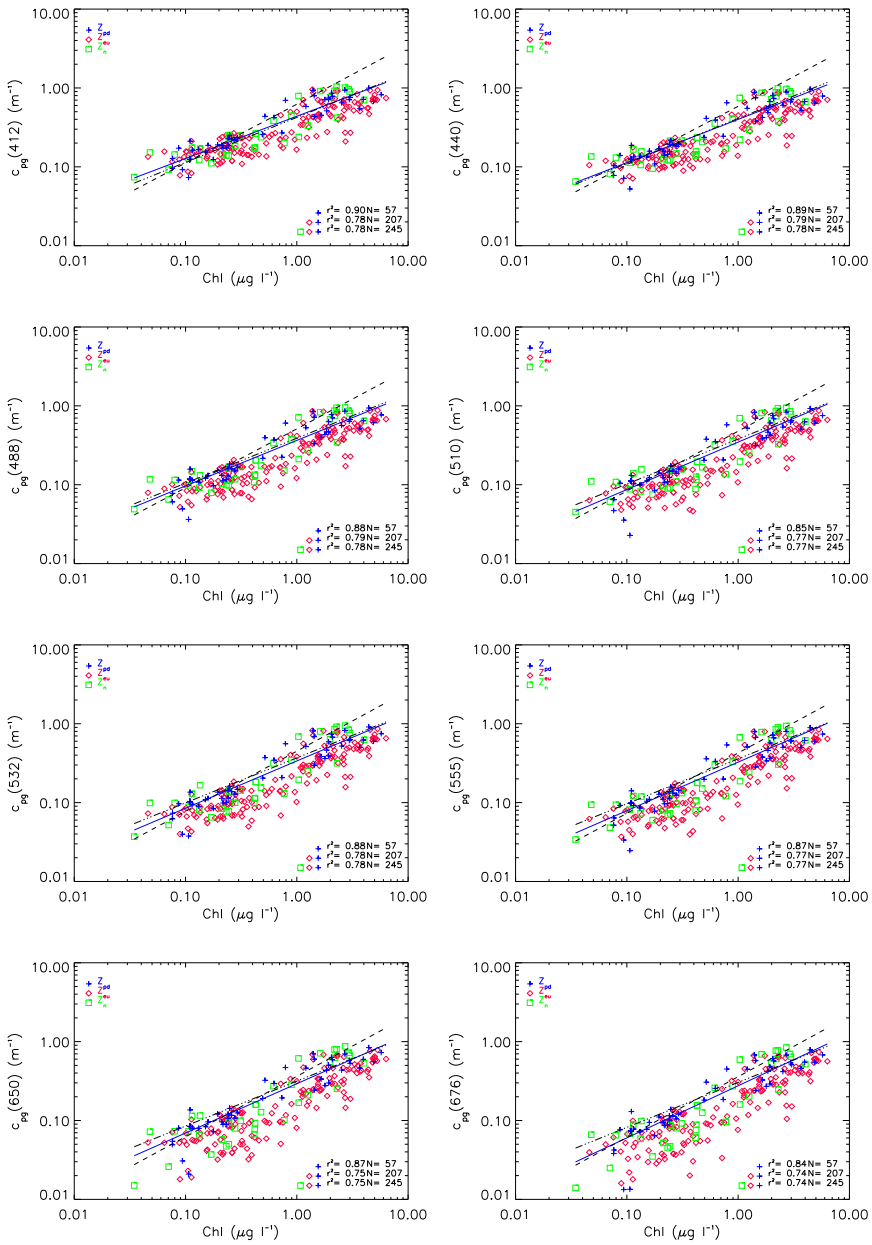

Figure 9.65: Total attenuation coefficient without water contribution versus Chl concentration.

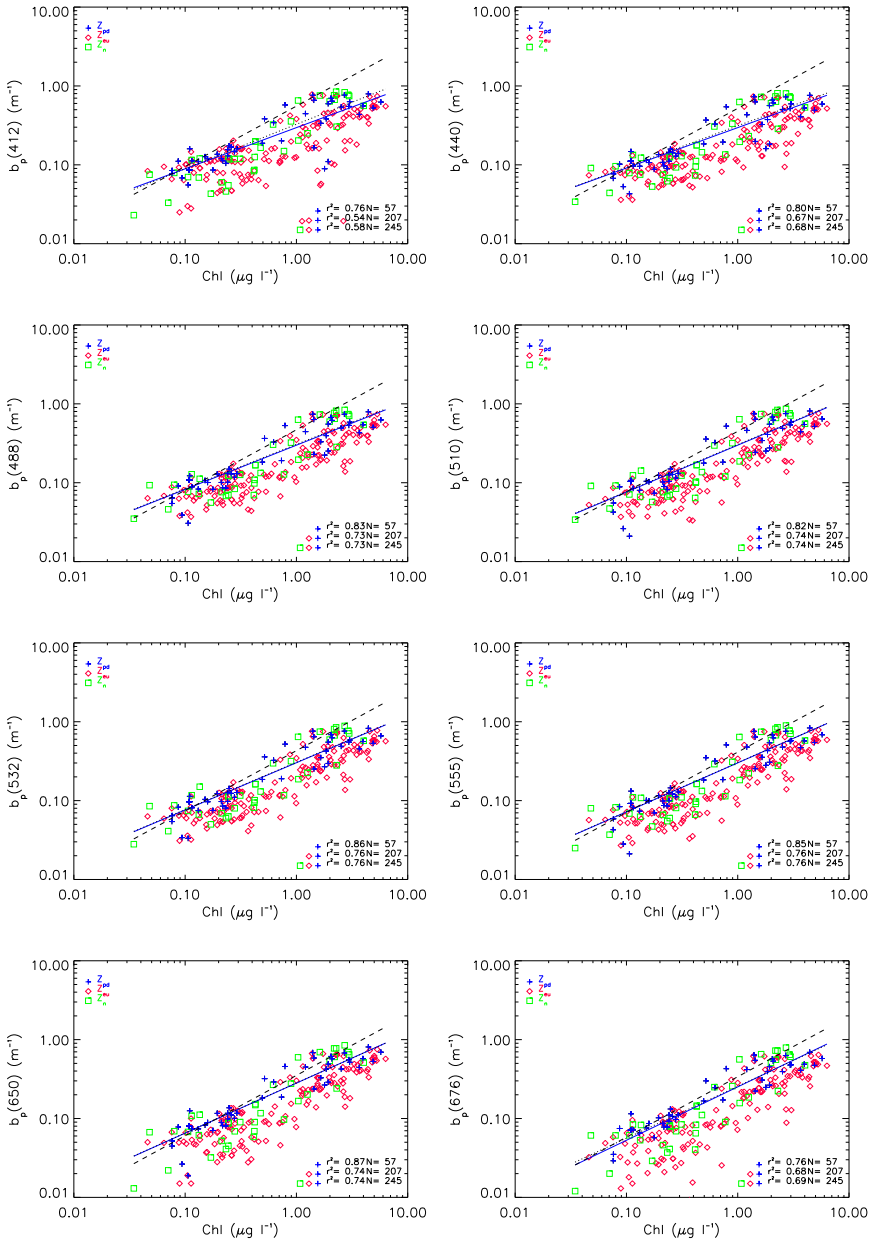

Figure 9.66: Total scattering coefficient without water contribution versus Chl concentration.

Particulate Backscattering

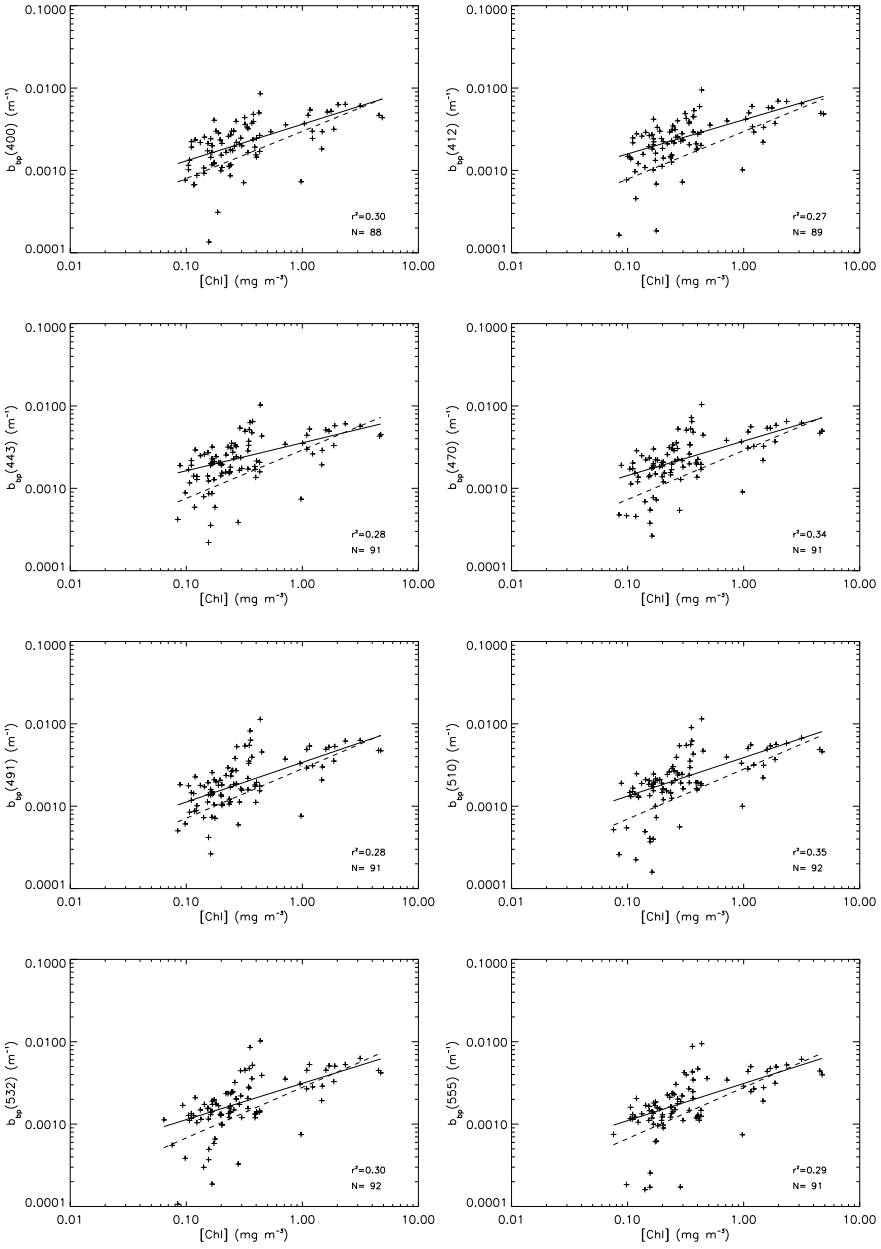

Figure 9.67: Scatter plots of $b_{bp}(\lambda)$versus [Chl] concentration.

Comparison AC9 SPMR

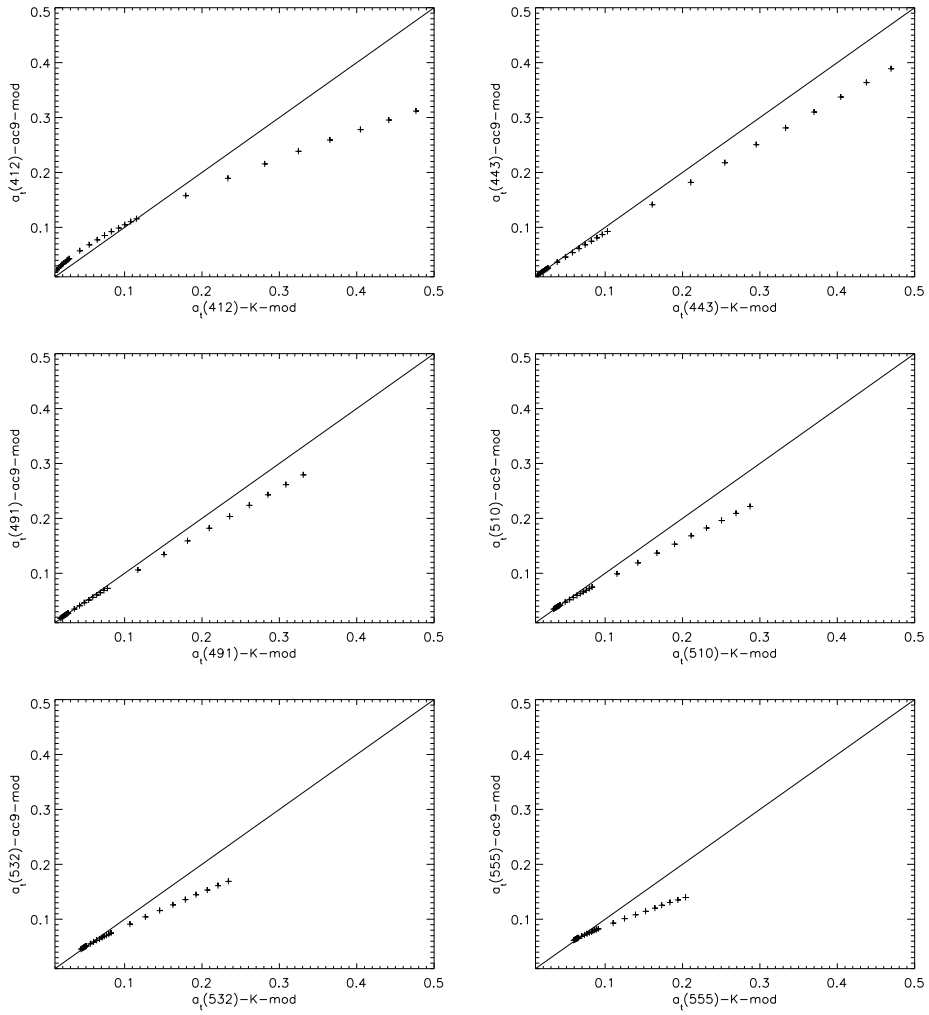

Figure 9.68: Scatter plot of $a_t(\lambda)$ derived from the MM01 reflectance model (abscissa) and from coefficients of **Tab. 5.5** within the z_{pd} (subset N1, ordinates).

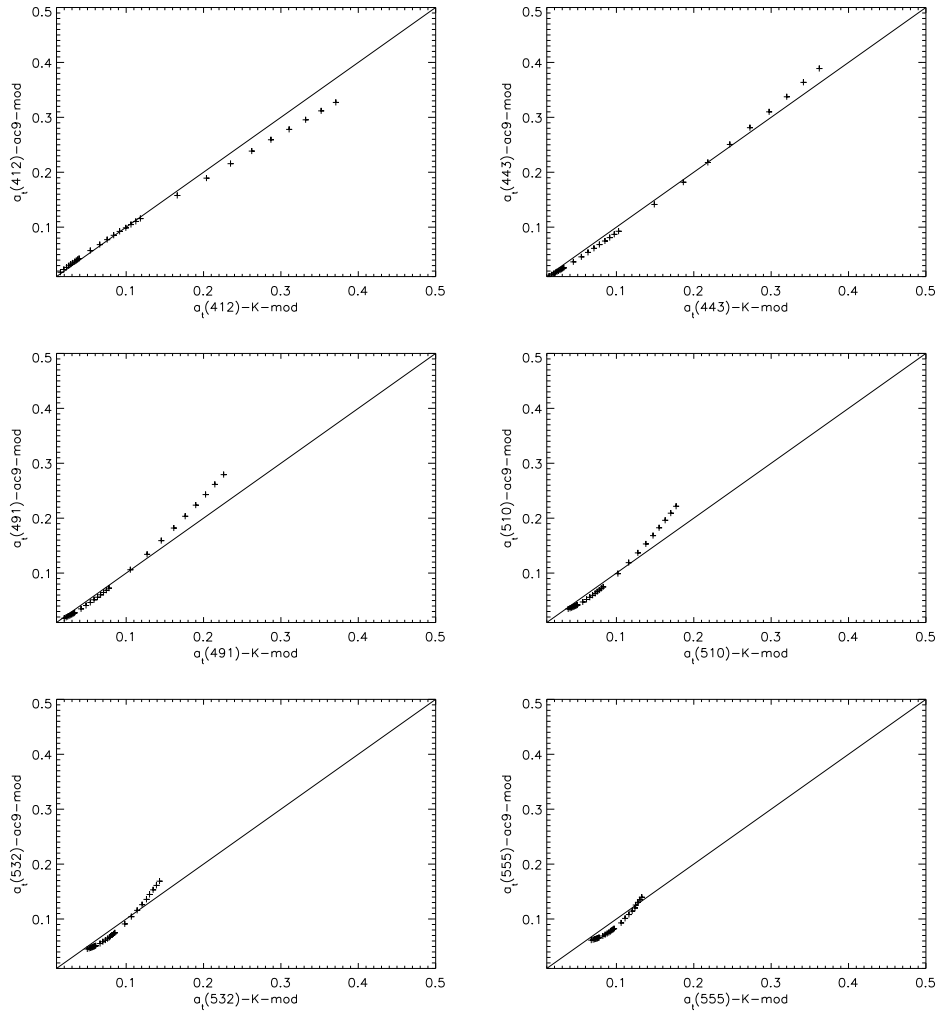

Figure 9.69: Scatter plot of $a_t(\lambda)$ derived from the Med2 reflectance model (abscissa) and from coefficients of **Tab. 5.5** within the z_{pd} (subset N1, ordinates).

Picoplankton Location Maps

	Reference	HBAC	SYN	PRO	PEUK
Mediterranean Sea	Agawin and Agusti (1997)	-	x	-	-
	Brunet *et al.* (2006)	-	x	x	x
	Casotti *et al.* (2003)	x	x	x	x
	Christaki *et al.* (2001)	x	x	-	-
	Li *et al.* (1993)	-	x	x	x
	Moutin *et al.* (2002)	x	x	-	x
	Pedros-Alio *et al.* (1999)	x	-	-	-
	Robarts *et al.* (1996)	x	-	-	-
	Zohary and Robarts (1998)	x	x	x	x
	Prosope	x	x	x	x
Global Ocean	Andre *et al.* (1999)	-	x	x	x
	Binder *et al.* (1996)	x	x	x	x
	Blanchot *et al.* (2001)	-	x	x	x
	Brown *et al.* (1999)	-	x	x	x
	Brown *et al.* (2003)	x	x	x	x
	Buck *et al.* (1996)	x	x	x	x
	Cai *et al.* (2007)	x	x	x	x
	Calvo-Díaz *et al.* (2004)	x	x	x	x
	Campbell *et al.* (1997)	x	x	x	x
	Caron *et al.* (1995)	x	x	-	-
	Cavender-Bares *et al.* (1999)	-	x	x	x
	Fiala *et al.* (2003)	x	-	x	x
	Fuhrman *et al.* (1989)	x	-	-	-
	Grob *et al.* (2007)	x	x	x	x
	Heinänen *et al.* (1997)	x	-	-	-
	Jiao and Ni (1997)	x	x	-	-
	Li and Harrison (2001)	x	-	-	-
	Li (1995)	-	x	x	x
	Li *et al.* (1992)	x	x	x	x
	Li (1994)	-	x	x	x
	Moran *et al.* (2002)	x	x	x	-
	Morel (1997)	-	x	-	-
	Selph *et al.* (2005)	x	x	x	x
	Worden and Binder (2003)	-	x	x	-
	GEP&CO	x	x	x	x
	HOT Time series	x	x	x	x

Table 9.23: References for the picoplankton and heterotrophic bacteria data.

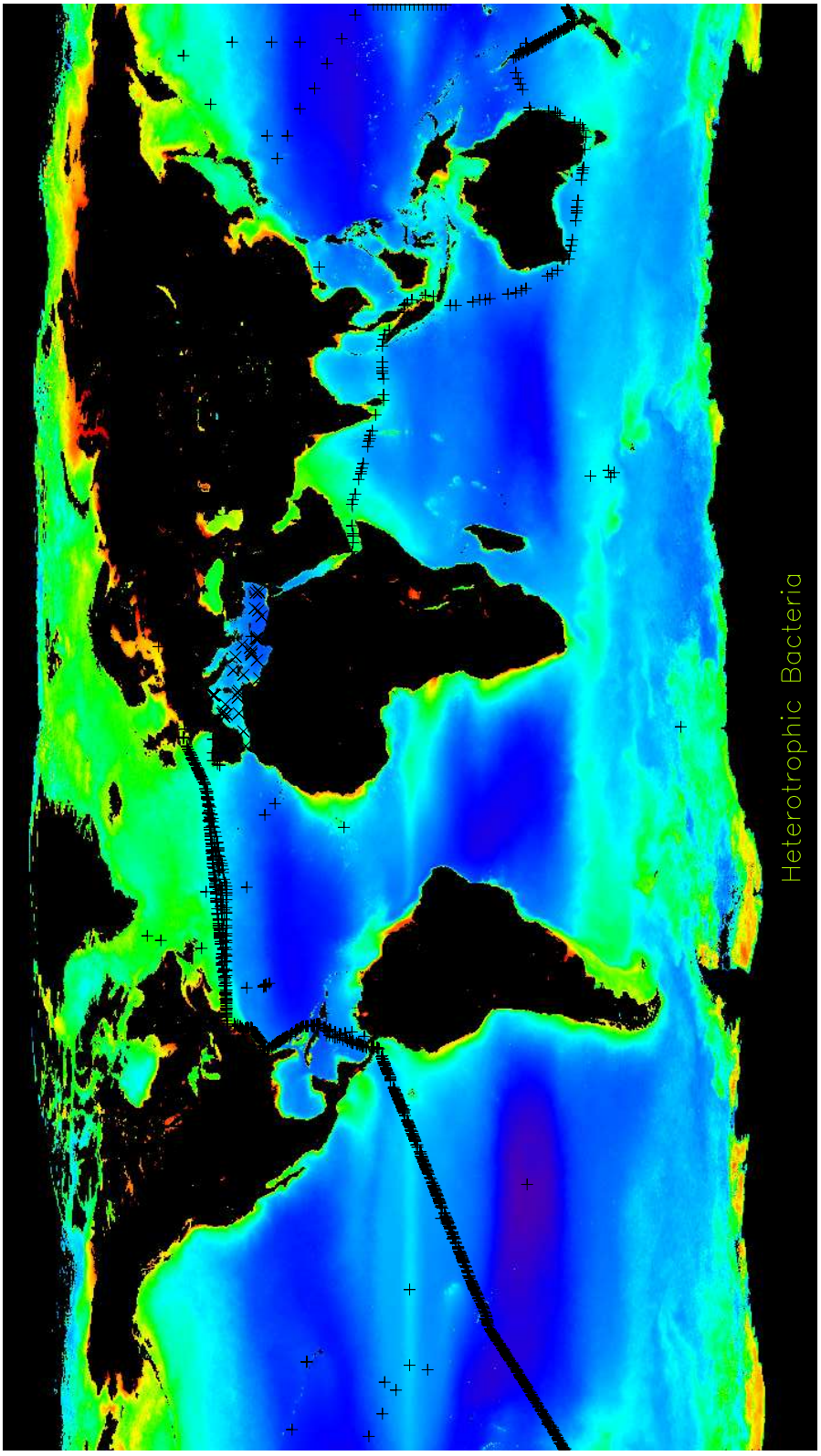

Figure 9.70: Station location for heterotrophic bacteria global data.

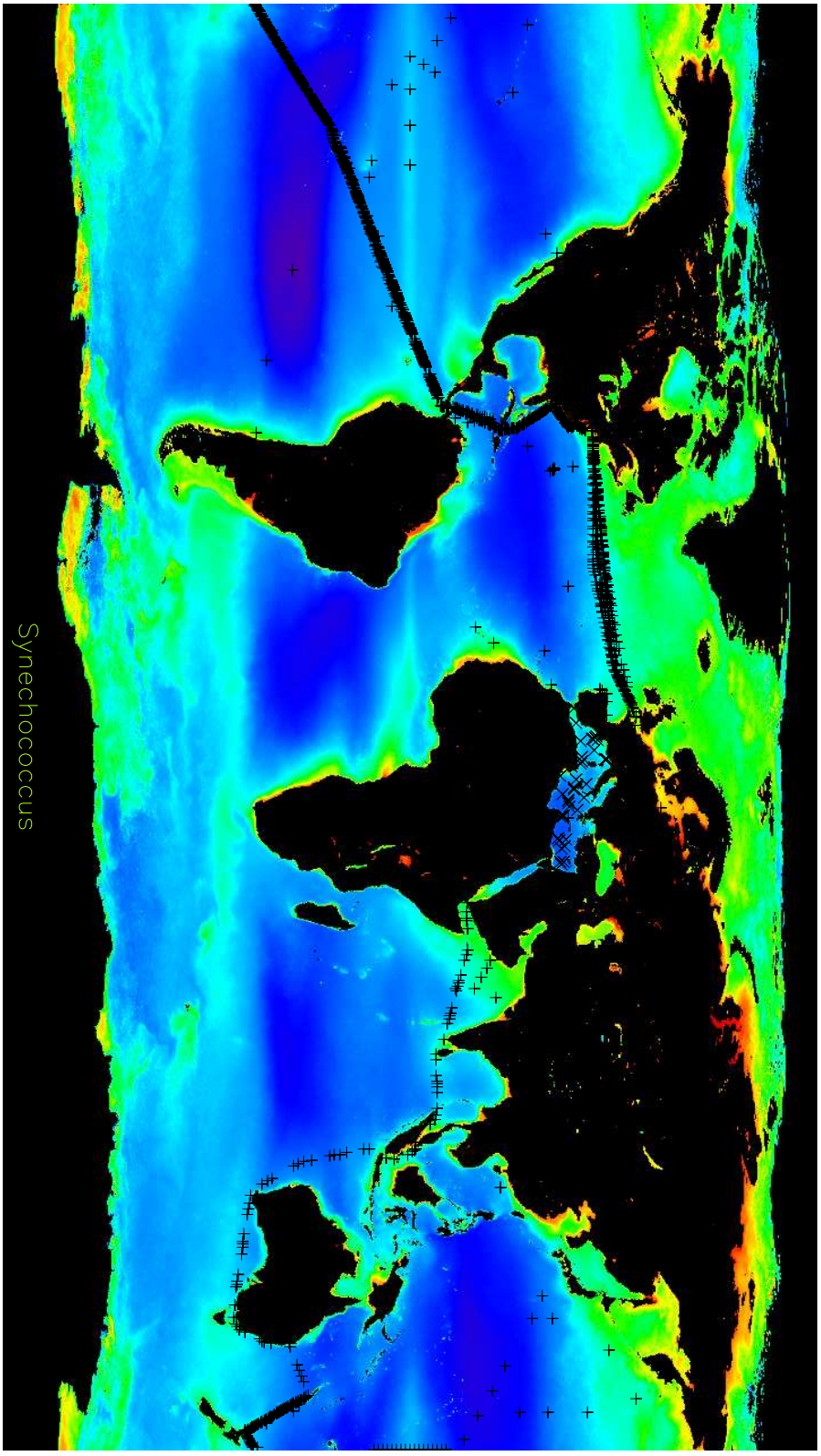

Figure 9.71: Station location for *Synechococcus spp.* global data.

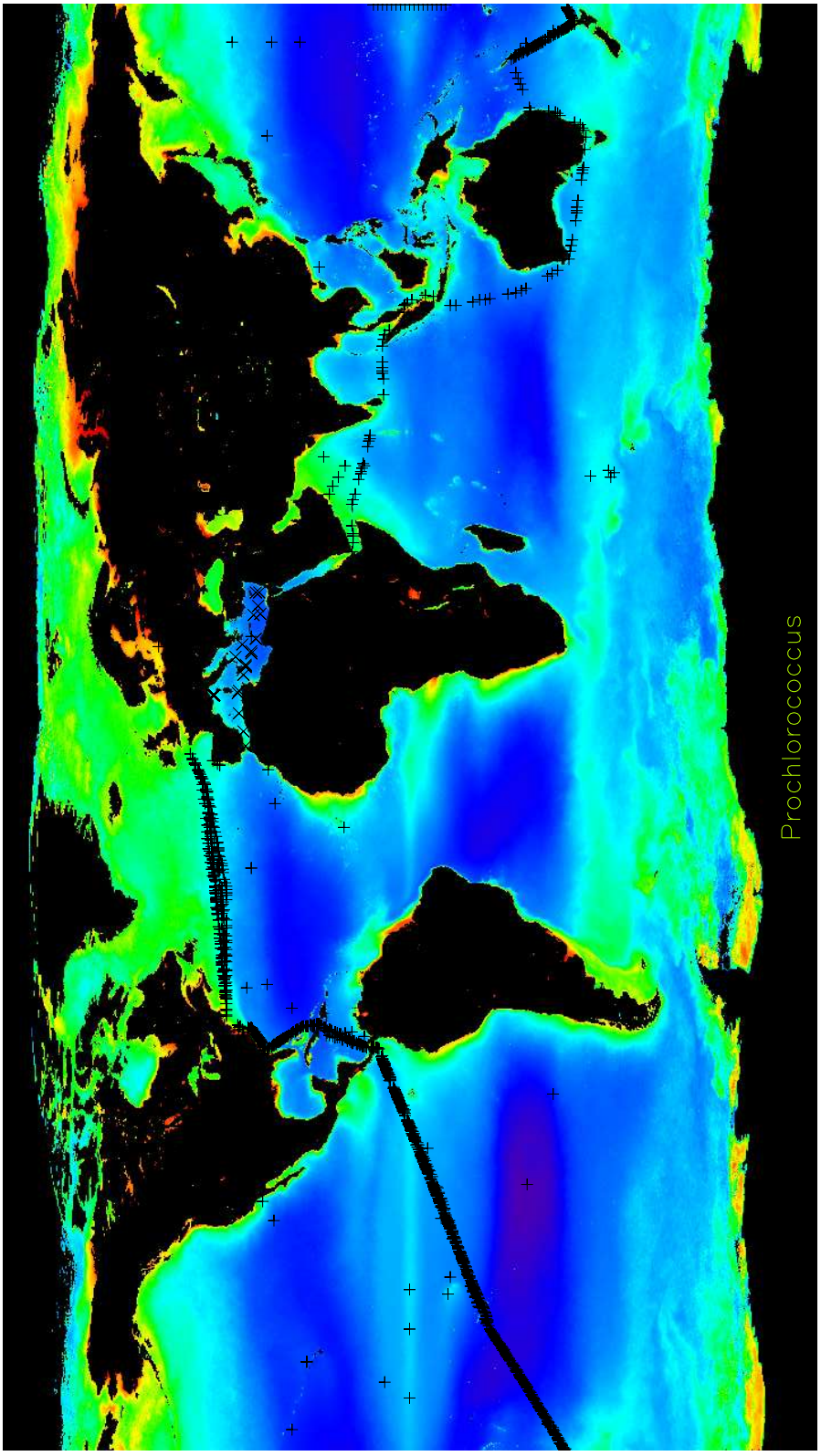

Figure 9.72: Station location for *Prochlorococcus spp.* global data.

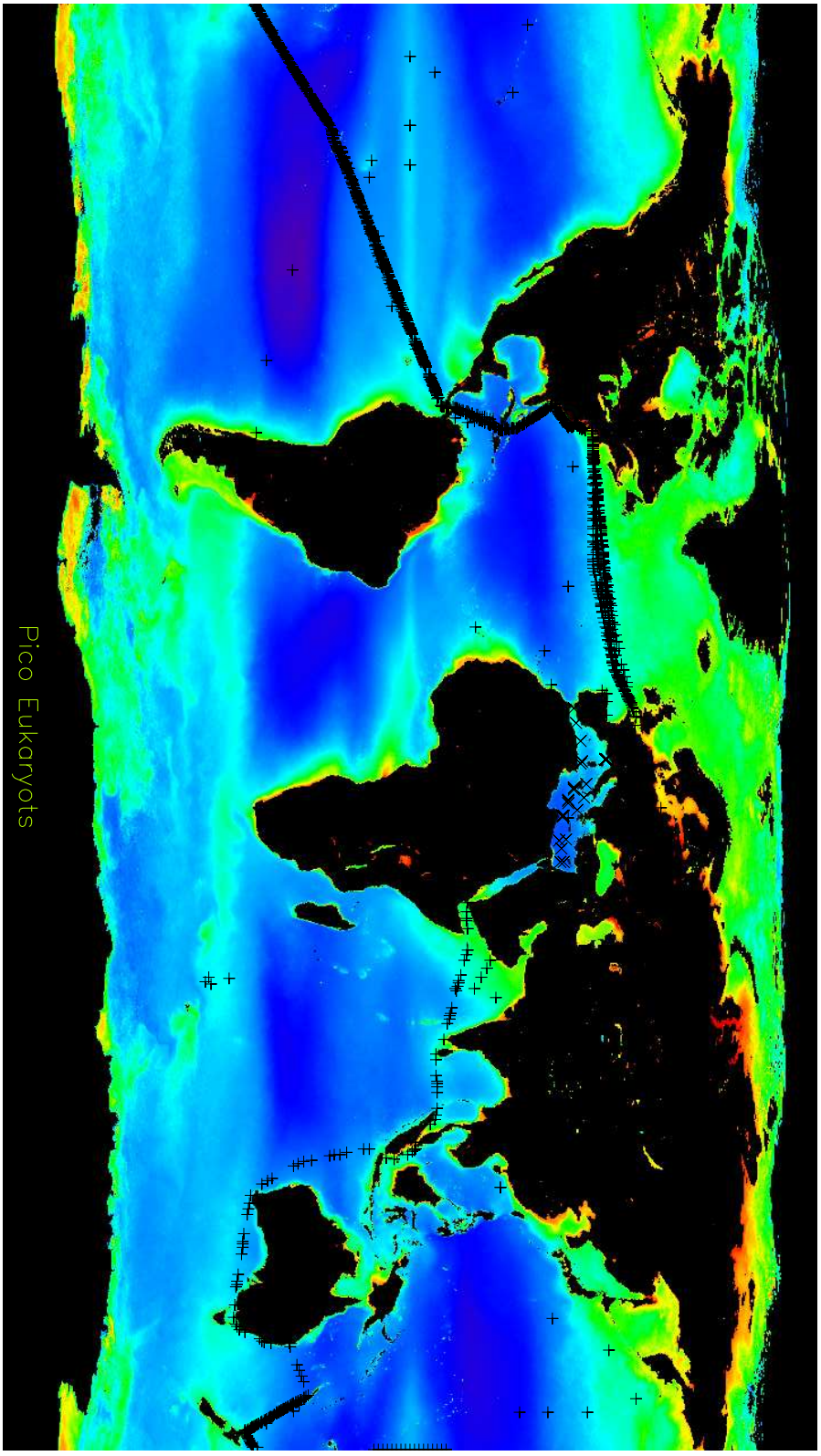

Figure 9.73: Station location for *picoeukaryots* global data.

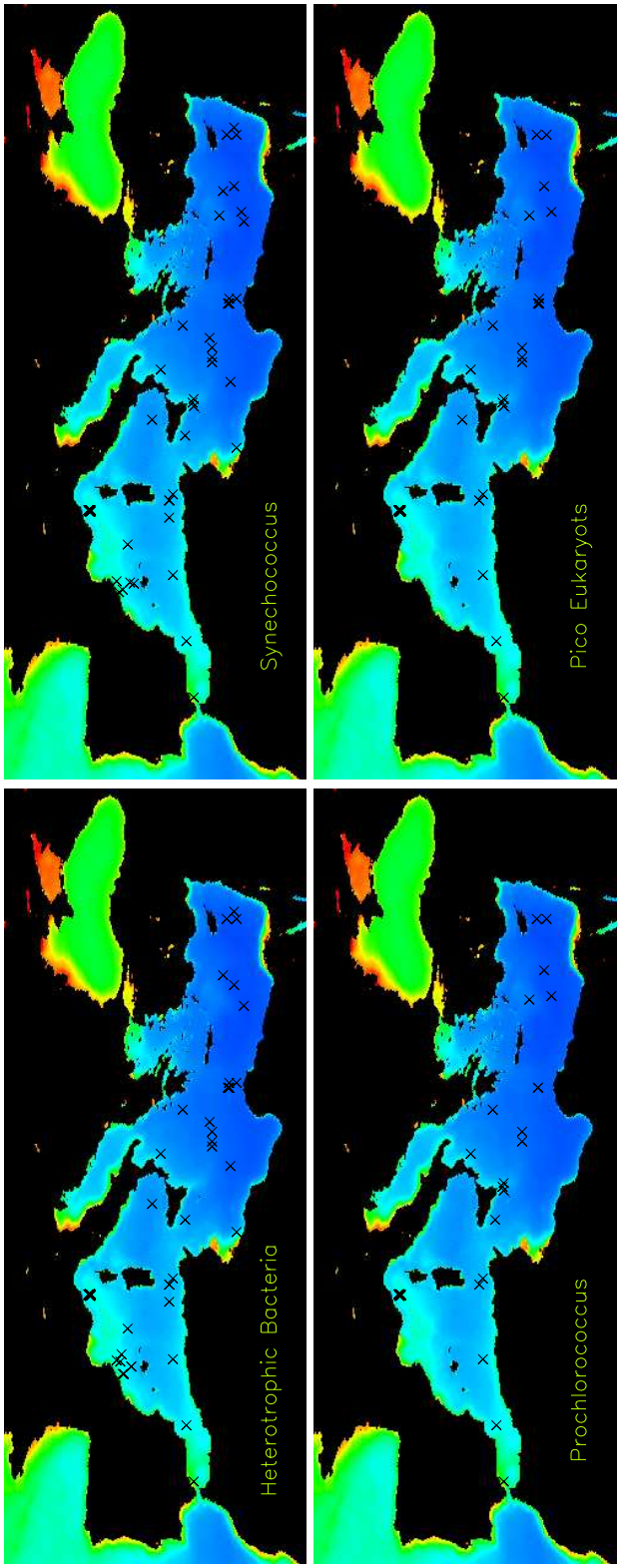

Figure 9.74: Station location for picoplankton and heterotrophic bacteria Mediterranean data.

Acknowledgments

This study was supported by ASI-SYMPLEX, ASTAPLAN and VECTOR projects. I wish to thank the coordinator and the lecturers of the "Scienze ed Ingegneria del Mare" for their time spent for the Ph.D. course activities. The Zoological Station of Naples is acknowledged for giving me the opportunity to frequent the Ph.D. courses and logistical support. There I met friendly colleagues with whom I shared time, space and fun, thank you. I also have to thank David Antoine for letting me conclude this work while starting a new job with his group. A special thank is due to crew and captains on board the N/O *Urania* and M/N *Vettoria* for their invaluable help at Sea. I also thank the duty chiefs of the cruises and the responsible of the projects for inviting me to join their missions, and for creating always a good atmosphere on board with colleagues. I warmly thank Jean-Francois Berthon who accepted to referee this work and who gave me useful suggestions to improve its quality, and my co-tutor Vincenzo Saggiomo for sharing data and scientific equipment over the years. Finally my best thanks goes to my supervisor Maurizio Ribera d'Alcalà for giving me freedom till the point I needed, and for redirecting me to the right way when too much freedom might me get lost.

Bibliography

Aas, E. Refractive index of phytoplankton derived from its metabolite composition. *Journal of Plankton Research*, 18(12):2223, 1996.

Agawin, N. S. R. and S. Agusti. Abundance, frequency of dividing cells and growth rates of Synechococcus sp.(cyanobacteria) in the stratified Northwest Mediterranean Sea. *Journal of Plankton Research*, 19(11):1599, 1997.

Agawin, N. S. R., C. M. Duarte and S. Agusti. Nutrient and Temperature Control of the Contribution of Picoplankton to Phytoplankton Biomass and Production. *Limnology and Oceanography*, 45(3):591–600, 2000.

Aguirre-Gomez, R., A. R. Weeks and S. R. Boxall. The identification of phytoplankton pigments from absorption spectra. *Journal of Remote Sensing*, 22:315–338, 2001.

Ahn, Y. U. H., A. Bricaud and A. Moel. Light backscattering efficiency and related properties of some phytoplankters. *Deep-sea research. Part A. Oceanographic research papers*, 39(11-12):1835–1855, 1992.

Allali, K., A. Bricaud, M. Babin, A. Morel and P. Chang. A New Method for Measuring Spectral Absorption Coefficients of Marine Particles. *Limnology and Oceanography*, 40(8):1526–1532, 1995.

Alvain, S., C. Moulin, Y. Dandonneau and F. M. Breon. Remote sensing of phytoplankton groups in case 1 waters from global SeaWiFS imagery. *Deep-sea research. Part 1*, 52(11):1989–2004, 2005.

Andre, J. M., C. Navarette, J. Blanchot and M. H. Radenac. Picophytoplankton dynamics in the equatorial Pacific- Growth and grazing rates from cytometric counts. *Journal of Geophysical Research*, 104(C2):3369–3380, 1999.

Antoine, D., A. Morel and J. M. André. Algal pigment distribution and primary production in the eastern Mediterranean as derived from coastal zone color scanner observations. *Journal of Geophysical Research*, 100(C8):16193–16210, 1995.

Antoine, D. and D. Nobileau. Recent increase of Saharan dust transport over the Mediterranean Sea, as revealed from ocean color satellite (SeaWiFS) observations. *Journal of Geophysical Research*, 111(D12), 2006.

Austin, R. W. *Optical Aspects of Oceanography*, chapter The remote sensing of spectral radiance from below the ocean surface, pages 317–344. London, Academic Press, 1974.

Azam, F., T. Fenchel, J. G. Field, J. S. Gray, L. A. Meyer-Reil and F. Thingstad. The ecological role of water-column microbes in the sea. *Marine Ecology Progress Series*, 10(3):257–263, 1983.

Azov, Y. Eastern Mediterranean–A marine desert?. *Marine Pollution Bulletin*, pages 225–232, 1991.

Balch, W. M., J. Vaughn, J. Novotny, D. T. Drapeau, R. Vaillancourt, J. Lapierre and A. Ashe. Light Scattering by Viral Suspensions. *Limnology and Oceanography*, 45(2):492–498, 2000.

Balch, W. M., J. M. Vaughn, J. F. Novotny, D. T. Drapeau, J. I. Goes, E. Booth, J. M. Lapierre, C. L. Vining, A. Ashe and J. M. Vaughn Jr. Fundamental Changes in Light Scattering Associated with Infection of Marine Bacteria by Bacteriophage. *Limnology and Oceanography*, 47(5):1554–1561, 2002.

Barlow, R. G., J. Aiken, P. M. Holligan, D. G. Cummings, S. Maritorena and S. Hooker. Phytoplankton pigment andabsorption characteristics along meridional transects in the Atlantic Ocean. *Deep-Sea Research*, 1(47):637–660, 2002.

Barnard, A. H., W. S. Pegau and J. R. V. Zaneveld. Global relationships of the inherent optical properties of the oceans. *Journal of Geophysical Research*, 103(C11):24955–24968, 1998.

Behrenfeld, M. J., E. Boss, D. A. Siegel and D. M. Shea. Carbon-based ocean productivity and phytoplankton physiology from space. *Global Biogeochemical Cycles*, 19(1), 2005.

Behrenfeld, M. J. and P. G. Falkowski. Photosynthetic Rates Derived from Satellite-Based Chlorophyll Concentration. *Limnology and Oceanography*, 42(1):1–20, 1997.

Berman, T., Y. Azov and D. Townsend. *Marine Phytoplankton and Productivity*, chapter Understanding oligotrophic oceans: can the eastern Mediterranean be a useful model. Springer Verlag, Berlin, 1984a.

Berman, T., D. W. Townsend, S. Z. El Sayed, C. C. Trees and Y. Azov. Optical transparency, chlorophyll and primary productivity in the eastern Mediterranean near the Israeli coast. *Oceanologica Acta*, 7(3):367–372, 1984b.

Bidigare, R. R., J. H. Morrow and D. A. Kiefer. Derivative analysis of spectral absorption by photosynthetic pigments in the western Sargasso Sea. *Journal of Marine Research*, 47(2):323–341, 1989.

Binder, B. J., S. W. Chisholm, R. J. Olson, S. L. Frankel and A. Z. Worden. Dynamics of picophytoplankton, ultraphytoplankton and bacteria in the Central Equatorial Pacific. *Deep-Sea Research(Part II, Topical Studies in Oceanography)*, 43(4):907–931, 1996.

Blanchot, J., J.-M. André, C. Navarette, J. Neveux and M.-H. Radenac. Picophytoplankton in the equatorial Pacific: vertical distributions in the warm pool and in the high nutrient low chlorophyll conditions. *Deep Sea Research Part I: Oceanographic Research Papers*, 48(1):297–314, 2001.

Bosc, E., A. Bricaud and D. Antoine. Seasonal and interannual variability in algal biomass and primary production in the Mediterranean Sea, as derived from 4 years of SeaWiFS observations. *Global Biogeochemical Cycles*, 18:GB1005, doi:10.1029/2003GB002034, 2004.

Boss, E., D. Stramski, T. Bergmann, W. S. Pegau and M. R. Lewis. Why should we measure the optical backscattering coefficient? *Oceanography*, 17:44–49, 2004.

Bratbak, G., O. H. Haslund, M. Heldal, A. Naess and T. Roeeggen. Giant marine viruses?. *Marine ecology progress series. Oldendorf*, 85(1):201–202, 1992.

Bricaud, A., M. Babin, A. Morel and H. Claustre. Variability in the chlorophyll-specific absorption coefficients of natural phytoplankton: Analysis and parameterization. *Journal of Geophysical Research*, 100(C7):13321–13332, 1995.

Bricaud, A., A. L. Bedhomme and A. Morel. Optical properties of diverse phytoplanktonic species: Experimental results and theoretical interpretation. *Journal of Plankton Research*, 10(5):85l–873, 1988.

Bricaud, A., E. Bosc and D. Antoine. Algal biomass and sea surface temperature in the Mediterranean Basin. Intercomparison of data from various satellite sensors, and implications for primary production estimates. *Remote Sensing of Environment*, 81:163–178, 2002.

Bricaud, A., H. Claustre, J. Ras and K. Oubelkheir. Natural variability of phytoplanktonic absorption in oceanic waters: Influence of the size structure of algal populations. *Journal of Geophysical Research*, 109(C11010):doi:10.1029/2004JC002419, 2004.

Bricaud, A. and A. Morel. Light attenuation and scattering by phytoplanktonic cells: a theoretical modeling. *Applied Optics*, 25(4):571–580, 1986.

Bricaud, A., A. Morel, M. Babin, K. Allali and H. Claustre. Variations of light absorption by suspended particles with chlorophyll a concentration in oceanic (case 1) waters: analysis and implications for bio-optical models. *Journal of Geophysical Research*, 103(C13):31033, 1998.

Bricaud, A., A. Morel and L. Prieur. Absorption by dissolved organic matter of the sea (yellow substance) in the UV and visible domains. *Limnology and Oceanography*, 26(1):43–53, 1981.

Brown, C. W. and J. A. Yoder. Coccolithophorid blooms in the global ocean. *Journal of Geophysical Research*, 99(C4):7467–7482, 1994.

Brown, O. B. and H. R. Gordon. Size-refractive index distribution of clear coastal water particulates from light scattering. *Applied Optics*, 13(12):2874, 1974.

Brown, S. L., M. R. Landry, R. T. Barber, L. Campbell, D. L. Garrison and M. M. Gowing. Picophytoplankton dynamics and production in the Arabian Sea during the 1995 Southwest Monsoon-the southwest and northeast monsoon, 1992-1993. *Deep Sea Research Part II: Topical Studies in Oceanography*, 46(8):1745–1768, 1999.

Brown, S. L., M. R. Landry, J. Neveux and C. Dupouy. Microbial community abundance and biomass along a 180 transect in the equatorial Pacific during an El Niño-Southern Oscillation cold phase. *Journal of Geophysical Research*, 108(C12), 2003.

Brunet, C., R. Casotti, V. Vantrepotte, F. Corato and F. Conversano. Picophytoplankton diversity and photoacclimation in the Strait of Sicily (Mediterranean Sea) in summer. I. Mesoscale variations. *Aquatic microbial ecology*, 44(2):127–141, 2006.

Bruyant, F., M. Babin, B. Genty, O. Prasil, M. J. Behrenfeld, H. Claustre, A. Bricaud, L. Garczarek, J. Holtzendorff, M. Koblizek, L. Garczareck and F. Partensky. Diel variations in the photosynthetic parameters of Prochlorococcus strain PCC 9511: Combined effects of light and cell cycle. *Limnology & Oceanography*, 50(3):850–863, 2005.

Buck, K. R., F. P. Chavez and L. Campbell. Basin-wide distributions of living carbon components and the inverted trophic pyramid of the central gyre of the North Atlantic Ocean, Summer 1993. *Aquatic Microbial Ecology*, 10(3):283–298, 1996.

Cai, Y. M., X. R. Ning, C. G. Liu and Q. Hao. Distribution Pattern of Photosynthetic Picoplankton and Heterotrophic Bacteria in the Northern South China Sea. *Journal of Integrative Plant Biology*, 49(3):282–298, 2007.

Calvo-Díaz, A., X. A. G. Morán, E. Nogueira, A. Bode and M. Varela. Picoplankton community structure along the northern Iberian continental margin in late winter–early spring. *Journal of Plankton Research*, 26(9):1069–1081, 2004.

Campbell, L., H. Liu, H. A. Nolla and D. Vaulot. Annual variability of phytoplankton and bacteria in the subtropical North Pacific Ocean at Station ALOHA during the 1991-1994 ENSO event. *Deep-Sea Research(Part I, Oceanographic Research Papers)*, 44(2):167–192, 1997.

Carder, K. L., F. R. Chen, Z. P. Lee, S. K. Hawes and D. Kamykowski. Semianalytic Moderate-Resolution Imaging Spectrometer algorithms for chlorophyll a and absorption with bio-optical domains based on nitrate-depletion temperatures. *Journal of Geophysical Research*, 104(C3):5403–5422, 1999.

Caron, D. A., H. G. Dam, P. Kremer, E. J. Lessard, L. P. Madin, T. C. Malone, J. M. Napp, E. R. Peele, M. R. Roman and M. J. Youngbluth. The contribution of microorganisms to particulate carbon and nitrogen in surface waters of the Sargasso Sea near Bermuda. *Deep Sea Research I*, 42(6):943–972, 1995.

Casotti, R., A. Landolfi, C. Brunet, F. D'Ortenzio, O. Mangoni, M. Ribera d'Alcaá and M. Denis. Composition and dynamics of the phytoplankton of the Ionian Sea (eastern Mediterranean). *Journal of Geophysical Research*, 108:1–20, 2003.

Cavender-Bares, K. K., E. L. Mann, S. W. Chisholm, M. E. Ondrusek and R. R. Bidigare. Differential Response of Equatorial Pacific Phytoplankton to Iron Fertilization. *Limnology and Oceanography*, 44(2):237–246, 1999.

Christaki, U., A. Giannakourou, F. Van Wambeke and G. Gregori. Nanoflagellate predation on auto-and heterotrophic picoplankton in the oligotrophic Mediterranean Sea. *Journal of Plankton Research*, 23(11):1297, 2001.

Ciotti, A. M., M. R. Lewis and J. J. Cullen. Assessment of the relationships between dominant cell size in natural phytoplankton communities and the spectral shape of the absorption coefficient. *Geophysical Research Letters*, 47(2):404–417, 2002.

Clark, D. K. MODIS Algorithm Theoretical Basis Document, Bio-Optical Algorithms-Case 1 Waters, version 1.2. 1997.

Claustre, H. The Trophic Status of Various Oceanic Provinces as Revealed by Phytoplankton Pigment Signatures. *Limnology and Oceanography*, 39(5):1206–1210, 1994.

Claustre, H. and S. Maritorena. The many shades of ocean blue. *Science*, 302(5650):1514–1515, 2003.

Claustre, H., A. Morel, S. Hooker, M. Babin, D. Antoine, K. Oubelkheir, A. Bricaud, K. Leblanc, B. Quéguiner and S. Maritorena. Is desert dust making oligotrophic waters greener? *Geophysical Research Letters*, 29(10):107–111, 2002.

Cleveland, J. S. Regional models for phytoplankton absorption as a function of chlorophyll a concentration. *Journal of Geophysical Research*, 100(C7):13333–13344, 1995.

Cleveland, J. S. and M. J. Perry. Quantum yield, relative specific absorption and fluorescence in nitrogen-limited Chaetoceros gracilis. *Marine Biology*, 94(4):489–497, 1987.

Colella, S. *La produzione primaria nel Mar Mediterraneo da satellite: sviluppo di un modello regionale e sua applicazione ai dati SeaWiFS, MODIS e MERIS*. Ph.D. thesis, Università degli Studi di Napoli - Federico II, 2006.

Dandonneau, Y., A. Vega, H. Loisel, Y. Penhoat and C. Menkes. Ocean Science: Oceanic Rossby Waves Acting As a "Hay Rake" for Ecosystem Floating By-Products. *Science*, pages 1548–1550, 2003.

Devred, E., S. Sathyendranath, V. Stuart, H. Maass, O. Ulloa and T. Platt. A two-component model of phytoplankton absorption in the open ocean: Theory and applications. *Journal of Geophysical Research*, 111(C03011):doi:10.1029/2005JC002880, 2006.

D'Ortenzio, F. *Space and time occurrence of algal blooms in the Mediterranean: their significance for the trophic regime of the basin*. Ph.D. thesis, Open University of London, UK, 2003.

D'Ortenzio, F., S. Marullo, M. Ragni, M. R. d'Alcalá and R. Santoleri. Validation of empirical SeaWiFS algorithms for chlorophill-a retrieval in the Mediterranean Sea. A case study for oligotrophic seas. *Remote Sensing of Environment*, 82:79–94, 2002.

Du, H., N. Jiao, Y. Hu and Y. Zeng. Diversity and distribution of pigmented heterotrophic bacteria in marine environments. *FEMS Microbiology Ecology*, 57(1):92–105, 2006.

Duarte, C. M., S. Agust, H. Kennedy and D. Vaque. The Mediterranean climate as a template for Mediterranean marine ecosystems: the example of the northeast Spanish littoral. *Progress in Oceanography*, 44(1):245–270, 1999.

Duarte, C. M., S. Agusti, M. P. Satta and D. Vaque. Partitioning Particulate Light Absorption: A Budget for a Mediterranean Bay. *Limnology and Oceanography*, 43(2):236–244, 1998.

Ducklow, H. Bacterial biomass in warm-core Gulf Stream ring 82-B: Mesoscale distributions, temporal changes and production. *Deep-Sea Research*, 33:1789–1812, 1986.

Ducklow, H. W. The bacterial component of the oceanic euphotic zone. *FEMS Microbiology Ecology*, 30(1):1–10, 1999.

Duysens, L. M. N. The flattening effect of the absorption spectra of suspension as compared to that of solutions. *Biochim. Biophys. Acta*, 19:1–12, 1956.

Ferrari, G. M. The relationship between chromophoric dissolved organic matter and dissolved organic carbon in the European Atlantic coastal area and in the West Mediterranean Sea (Gulf of Lions). *Marine Chemistry*, 70(4):339–357, 2000.

Ferrari, G. M. and S. Tassan. A method using chemical oxidation to remove light absorption by phytoplancton pigments. *Journal of Phycology*, 35:1090–1098, 1999.

Fiala, M., B. Delille, C. Dubreuil, E. Kopczynska, K. Leblanc, J. Morvan, B. Quéguiner, S. Blain, C. Cailliau, P. Conan *et al.* Mesoscale surface distribution of biogeochemical characteristics associated with a frontal system in the Crozet Basin (Southern Indian Ocean) during austral summer 1999. *Marine Ecology. Progress Series*, 249:1–14, 2003.

Floge, S. A. and M. L. Wells. Variation in colloidal chromophoric dissolved organic matter in the Damariscotta Estuary, Maine. *Limnology & Oceanography*, 52(1):32–45, 2007.

Frohlich. Data on total and spectral solar irradiance: comments. *Applied Optics*, 22:3928, 1983.

Fuhrman, J. A., T. D. Sleeter, C. A. Carlson and L. M. Proctor. Dominance of bacterial biomass in the Sargasso Sea and its ecological implications. *Marine Ecology Progress Series*, 57:207–217, 1989.

Fujiki, T. and S. Taguchi. Variability in chlorophyll a specific absorption coefficient in marine phytoplankton as a function of cell size and irradiance. *Journal of Plankton Research*, 24(9):859, 2002.

Gibbs, C. Chlorophyll b interference in the fluorimetric determination of chlorophyll a and phaeopigments. *Aust. J. Mar. Freshwater Res.*, 30:597–606, 1979.

Gitelson, A., A. Karnieli, N. Goldman, Y. Z. Yacobi and M. Mayo. Chlorophyll estimation in the Southeastern Mediterranean using CZCS images: adaptation of an algorithm and its validation. *Journal of Marine Systems*, 9(3-4):283–290, 1996.

Gordon, H. R. *Suspended solids in water*, chapter Mie-theory models of light scattering by ocean particulates, pages 73–86. Plenum Press, 1974.

Gordon, H. R. and W. M. Balch. MODIS detached coccolith concentration. Technical report, MODIS algorithm theoretical basis document 19., 1999.

Gordon, H. R., O. B. Brown, R. H. Evans, J. W. Brown, R. C. Smith, K. S. Baker and D. K. Clark. A semianalytic radiance model of ocean color. *Journal of Geophysical Research*, 93(D9):10909–10924, 1988.

Gordon, H. R., O. B. Brown and M. M. Jacobs. Computed relationships between the inherent and apparent optical properties of a flat homogeneous ocean. *Applied Optics*, 14(2):417–427, 1975.

Gordon, H. R., D. K. Clark, J. W. Brown, O. B. Brown, R. H. Evans and W. W. Broenkow. Phytoplankton pigment concentrations in the Middle Atlantic Bight: comparison between ship determinations and Coastal Zone Color Scanner estimates. *Applied Opttics*, 22:20–36, 1983.

Gordon, H. R., D. K. Clark, J. L. Mueller and W. A. Hovis. Phytoplankton pigments derived from the Nimbus-7 CZCS: initial comparisons with surface measurements. *Science*, 210:63–66, 1980.

Gordon, H. R. and A. Y. Morel. *Remote assessment of ocean color for interpretation of satellite visible imagery: A review.* Springer Verlag, New York, 1983.

Gower, J., C. Hu, G. Borstad and S. King. Ocean Color Satellites Show Extensive Lines of Floating Sargassum in the Gulf of Mexico. *Geoscience and Remote Sensing, IEEE Transactions on*, 44(12):3619–3625, 2006.

Gran, H. H. and T. Braarud. *A Quantitative Study of the Phytoplankton in the Bay of Fundy and the Gulf of Maine:(including Observations on Hydrography, Chemistry and Turbidity).* Woods Hole Oceanographic Institution, 1935.

Grob, C., O. Ulloa, H. Claustre, Y. Huot, G. Alarcón and D. Marie. Contribution of picoplankton to the total particulate organic carbon (POC) concentration in the eastern South Pacific. *Biogeosciences Discussions*, 4(3):1461–1497, 2007.

Heinänen, A., M. Raateoja, E. Lahdes and J. M. Leppänen. Relationships between bacterioplankton, chl a and temperature in Antarctic surface waters in summer. *Polar Biology*, 18(1):62–69, 1997.

Hoepffner, N. and S. Sathyendranath. Effect of pigment composition on absorption properties of phytoplankton. *Marine Ecology Progress Series*, 73:11–23, 1991.

Hoepffner, N. and S. Sathyendranath. Determination of the major groups of phytoplankton pigments from the absorption spectra of total particulate matter. *Journal of Geophysical Research*, 98:789–803, 1993.

Højerslev, N. K. and E. Aas. Spectral light absorption by yellow substance in the Kattegat-Skagerrak area. *Oceanologia*, 43(1):39–60, 2001.

Holm-Hansen, O., C. J. Lorenzen, R. W. Holmes and J. D. H. Strickland. Fluorimetric determination of chlorophyll. *J. Cons. Perm. Int. Explor. Mer*, 30:3–15, 1965.

Hooker, S. B. and A. Morel. Platform and Environmental Effects on Above-Water Determinations of Water-Leaving Radiances. *Journal of Atmospheric and Oceanic Technology*, 20(1):187–205, 2003.

Hu, C., Z. Lee, E. Muller-Karger, L. Carder and J. J. Walsh. Ocean color reveals phase shift between marine plants and yellow substance. *Geoscience and Remote Sensing Letters*, 3(2):262– 266, 2006.

Van de Hulst, H. C. *Light Scattering by Small Particles.* Light Scattering by Small Particles, New York: John Wiley & Sons, 1957, 1957.

Iglesias-Rodrıg, M. D., C. W. Brown, S. C. Doney, J. Kleypas, D. Kolber, Z. Kolber, P. K. Hayes and P. G. Falkowski. Representing key phytoplankton functional groups in ocean carbon cycle models: Coccolithophorids. *Global Biogeochemical Cycles*, 16(4):1100, 2002.

Iluz, D., Y. Z. Yacobi and A. Gitelson. Adaptation of an algorithm for chlorophyll-a estimation by optical data in the oligotrophic Gulf of Eilat. *International Journal of Remote Sensing*, 24(5):1157–1163, 2003.

Jeffrey, S. W., R. F. C. Mantoura and T. Bjørnland. *Phytoplankton pigments in oceanography: guidelines to modern methods*, chapter Data for the identification of 47 key phytoplankton pigments, pages 449–559. SCOR-UNESCO, 1997.

Jiao, N. and I. H. Ni. Spatial variations of size-fractionated Chlorophyll, Cyanobacteria and Heterotrophic bacteria in the Central and Western Pacific. *Hydrobiologia*, 352(1):219–230, 1997.

Kirk, J. T. O. A theoretical analysis of the contribution of algal cells to the attenuation of light within natural waters. I. General treatments of suspensions of living cells. *New Phytol.*, 75:1–20, 1975.

Kirk, J. T. O. Spectral absorption properties of natural waters: Contribution of the soluble and particulate fractions to light absorption in some inland waters of south-eastern Australia. *Aust. J. Mar. Freshwater Res*, 31:287–296, 1980.

Kirk, J. T. O. *Light and Photosynthesis in Aquatic Ecosystems*. Cambridge University Press, 1983.

Kirk, J. T. O. Dependance of relationship between IOP of water on solar altitude. *Limnology and Oceanography*, 29(2):350, 1984.

Kishino, M., N. Okami and S. Ichimura. Estimation of the spectral absorption coefficients of Phytoplankton in the sea. *Bull. Mar. Sci.*, 37:620–633, 1985.

Kokorin, A. M., O. V. Kopelevich and K. S. Shifrin. Refractive indexes of marine bacteria in the visible spectral band. *Oceanology C/C OF OKEANOLOGIIA*, 34(1):37–37, 1994. English Translation.

Kopelevich, O. P., T. P. Rodionov and T. P. Stupakova. Effect of bacteria on optical characteristics of ocean water. *Oceanology*, 27:696–700, 1987. English Translation.

Lacombe, H., J. C. Gascard, J. Gonella and J. P. Bethoux. Response of the Mediterranean to the water and energy fluxes across its surface, on seasonal and interannual scales. *Oceanologica Acta*, 4:247–255, 1981.

Lee, Z. P., Darecki, M., K. L. Carder, C. O. Davis, D. Stramski and W. J. Reha. Diffuse attenuation coefficient of downwelling irradiance: An evaluation of remote sensing methods. *Journal of Geophysical Research*, 110(C02017):doi:10.1029/2004JC002573, 2005a.

Lee, Z. P., K. P. Du and R. Arnone. A model for the diffuse attenuation coefficient of downwelling irradiance. *Journal of Geophysical Research*, 110(C02016):doi:10.1029/2004JC002275, 2005b.

Leong, S. C. Y. and S. Taguchi. Optical characteristics of the harmful dinoflagellate Alexandrium tamarense in response to different nitrogen sources. *Harmful Algae*, 4(2):211–219, 2005.

Li, W. K. W. Primary Production of Prochlorophytes, Cyanobacteria, and Eucaryotic Ultraphytoplankton: Measurements from Flow Cytometric Sorting. *Limnology and Oceanography*, 39(1):169–175, 1994.

Li, W. K. W. Composition of ultraphytoplankton in the central North Atlantic. *Marine ecology progress series*, 122(1):1–8, 1995.

Li, W. K. W., P. M. Dickie, B. D. Irwin and A. M. Wood. Biomass of bacteria, cyanobacteria, prochlorophytes and photosynthetic eukaryotes in the Sargasso Sea. *DEEP-SEA RES.(A OCEANOGR. RES. PAP.).*, 39(3):501–519, 1992.

Li, W. K. W. and W. G. Harrison. Chlorophyll, bacteria and picophytoplankton in ecological provinces of the North Atlantic. *Deep Sea Research Part II: Topical Studies in Oceanography*, 48(10):2271–2293, 2001.

Li, W. K. W., T. Zohary, Y. Z. Yacobi and A. M. Wood. Ultraphytoplankton in the eastern Mediterranean Sea: towards deriving phytoplankton biomass from flow cytometric measurements of abundance, fluorescence and light scatter. *Mar. Ecol. Prog. Ser*, 102:79–87, 1993.

Loisel, H., E. Bosc, D. Stramski, K. Oubelkheir and P. Y. Deschamps. Seasonal variability of the backscattering coefficient in the Mediterranean Sea based on Satellite SeaWiFS imagery. *Geophysical Research Letters*, 28(22):4203–4206, 2001.

Loisel, H. and A. Morel. Light scattering and chlorophyll concentration in case 1 waters: A reexamination. *Limnology and Oceanography*, 43(5):847–858, 1998.

Loisel, H. and D. Stramski. Estimation of the inherent optical properties of natural waters from the irradiance attenuation coefficient and reflectance in the presence of Raman scattering. *Appl. Opt*, 39:3001–3011, 2000.

Longhurst, A. Seasonal cycles of pelagic production and consumption. *Progress in Oceanography*, 36(2):77–167, 1995.

Longhurst, A., S. Sathyendranath, T. Platt and C. Caverhill. An estimate of global primary production in the ocean from satellite radiometer data. *Journal of Plankton Research*, 17(6):1245–1271, 1995.

Manizza, M., C. Le Quéré, A. J. Watson and E. T. Buitenhuis. Bio-optical feedbacks among phytoplankton, upper ocean physics and sea-ice in a global model. *Geophysical Rresearch Letters*, 32:L05603, 2005.

Marzeion, B., A. Timmermann, R. Murtugudde and F. F. Jin. Biophysical Feedbacks in the Tropical Pacific. *Journal of Climate*, 18(1):58–70, 2005.

Megard, R. O. and T. Berman. Effects of Algae on the Secchi Transparency of the Southeastern Mediterranean Sea. *Limnology and Oceanography*, 34(8):1640–1655, 1989.

Mie, G. Beiträge zur Optik trüber Medien, speziell kolloidaler Metallösungen. *Annalen der Physik*, 330(3):377–445, 1908.

Mitchell, B. G., A. Bricaud, K. Carder, C. J., G. M. Ferrari, R. Gould, M. Kahru, M. Kishino, H. Maske, T. Moisan, L. Moore, N. Nelson, D. Phinney, R. Reynolds, H. Sosik, D. Stramski, S. Tassan, C. Trees, A. Weidemann, K. Wieland and A. Vodacek. Determination of spectral absorption coefficients of particles, dissolved material and phytoplankton for discrete water samples. Technical Report Technical Memorandum 2000–209966, Greenbelt, MD NASA Goddard Space Flight Center, 2000.

Mobley, C. D. *Light and Water: Radiative Transfer in Natural Waters*. Academic, San Diego, California, 1994.

Mobley, C. D. and D. Stramski. Effects of Microbial Particles on Oceanic Optics: Methodology for Radiative Transfer Modeling and Example Simulations. *Limnology and Oceanography*, 42(3):550–560, 1997.

Moran, S. B. and K. O. Buesseler. Short residence time of colloids in the upper ocean estimated from 238 U–234 Th disequilibria. *Nature*, 359(6392):221–223, 1992.

Moran, X. A. G., J. M. Gasol, C. Pedros-Alio and M. Estrada. Partitioning of phytoplanktonic organic carbon production and bacterial production along a coastal-offshore gradient in the NE Atlantic during different hydrographic regimes. *Aquatic Microbial Ecology*, 29(3):239–252, 2002.

Morel, A. *Optical Aspects of Oceanography*, chapter Optical properties of pure water and pure sea water, pages 1–24. Academic Press, New York, 1974.

Morel, A. Optical Modeling of the Upper Oean in Relation to its Biogenous Matter Content (Case I Waters). *Journal of Geophysical Research*, 93(C9):10749–10768, 1988.

Morel, A. Light and marine photosynthesis: a spectral model with geochemical and climatological implications. *Progress in Oceanography*, 26:263, 1991.

Morel, A. Consequences of a Synechococcus Bloom Upon the Optical Properties of Oceanic (Case 1) Waters. *Limnology and Oceanography*, 42(8):1746–1754, 1997.

Morel, A. and Y. H. Ahn. Optical efficiency factors of free-living marine bacteria: Influence of bacterioplankton upon the optical properties and particulate organic carbon in oceanic waters. *Journal of Marine Research*, 48(1):145–175, 1990.

Morel, A., D. Antoine and B. Gentili. Bidirectional reflectance of oceanic waters: accounting for Raman emission and varying particle scattering phase function. *Applied Optics*, v1(30):6289–6306, 2002.

Morel, A. and J. F. Berthon. Surface Pigments, Algal Biomass Profiles, and Potential Production of the Euphotic Layer: Relationships Reinvestigated in View of Remote-Sensing Applications. *Limnology and Oceanography*, 34(8):1545–1562, 1989.

Morel, A. and A. Bricaud. Theoretical results concerning light absorption in a discrete medium, and application to specific absorption of phytoplankton. *Deep Sea Research*, 28(11):1375, 1981.

Morel, A., H. Claustre, D. Antoine and B. Gentili. Natural variability of bio-optical properties in Case 1 waters: attenuation and reflectance within the visible and near-UV spectral domains, as observed in South Pacific and Mediterranean waters. *Biogeosciences Discussions*, 4(4):2147–2178, 2007a. ISSN 1810-6277.
URL `http://www.biogeosciences-discuss.net/4/2147/2007/`

Morel, A. and B. Gentili. Diffuse reflectance of ocean waters:its dependence on sun angle as influenced by the molecular scattering contribution. *Applied Optics*, 30:4427–4438, 1991.

Morel, A. and B. Gentili. Diffuse reflectance of oceanic waters. III. Implication of bidirectionality for the remote-sensing problem. *Applied Optics*, 35(24):4850–4862, 1996.

Morel, A., B. Gentili, H. Claustre, M. Babin, A. Bricaud, J. Ras and F. Tièche. Optical properties of the" clearest" natural waters. *Limnology & Oceanography*, 52(1):217–229, 2007b.

Morel, A. and S. Maritorena. Bio-optical properties of oceanic waters: a reappraisal. *Journal of Geophysical Research*, 106(C4):7163–7180, 2001.

Morel, A. and L. Prieur. Analysis of variations in ocean color. *Limnology and oceanography*, 22(4):709, 1977.

Moutin, T., T. F. Thingstad, F. Van Wambeke, D. Marie, G. Slawyk, P. Raimbault and H. Claustre. Does Competition for Nanomolar Phosphate Supply Explain the Predominance of the Cyanobacterium Synechococcus? *Limnology and Oceanography*, 47(5):1562–1567, 2002.

Mueller, J. L. SeaWiFS algorithm for the diffuse attenuation coefficient, K(490), using water-leaving radiances at 490 and 555 nm. In Hooker, S. B. and E. R. Firestone, editors, *SeaWiFS postlaunch calibration and validation analyses: Part 3*, volume 11, pages 24–27. NASA, Greenbelt: NASA Goddard Space Flight Center, 2000.

Mueller, J. L. and R. E. Lange. Bio-Optical Provinces of the Northeast Pacific Ocean: A Provisional Analysis. *Limnology & Oceanography*, 34(8):1572–1586, 1989.

Murtugudde, R., J. Beauchamp, C. R. McClain, M. R. Lewis and A. Busalacchi. Effects of Penetrative Radiation on the Upper Tropical Ocean Circulation. *Journal of Climate*, 15(5):470–486, 2002.

Neckel, H. and D. Labs. The solar radiation between 3300 and 12500 A. *Solar Physics*, 90:205–258, 1984.

Nelson, D. M. and W. O. Smith Jr. Sverdrup Revisited: Critical Depths, Maximum Chlorophyll Levels, and the Control of Southern Ocean Productivity by the Irradiance-Mixing Regime. *Limnology and Oceanography*, 36(8):1650–1661, 1991.

Nelson, N. B., C. A. Carlson and D. K. Steinberg. Production of chromophoric dissolved organic matter by Sargasso Sea microbes. *Marine Chemistry*, 89:273–287, 2004.

Nelson, N. B., D. A. Siegel and A. F. Michaels. Seasonal dynamics of colored dissolved material in the Sargasso Sea-Implications for biogeochemistry and remote sensing. *Deep Sea Research Part I: Oceanographic Research Papers*, 45(6):931–957, 1998.

Neveux, J. and M. Panouse. Spectrofluorometric determination of chlorophylls and pheophytins. *Arch. Hydrobiol.*, 109(4):567–581, 1987.

Nobileau, D. and D. Antoine. Detection of blue-absorbing aerosols using near infrared and visible(ocean color) remote sensing observations. *Remote Sensing of Environment*, 95(3):368–387, 2005.

O'Reilly, J. E., S. Maritorena, D. A. Siegel, M. C. O'Brien, D. Toole, B. G. Mitchell, M. Kahru, F. P. Chavez, P. Strutton, G. F. Cota, S. B. Hooker, C. R. McClain, K. L. Carder, F. Muller-Karger, L. Harding, A. Magnuson, D. Phinney, G. F. Moore, J. Aiken, K. R. Arrigo, R. Letelier and M. Culver. *SeaWiFS Postlaunch Technical Report Series, Vol. II. SeaWiFS postlaunch calibration and validation analyses: part 3.*, chapter Ocean color chlorophyll a algorithms for SeaWiFS, OC2, and OC4: Version 4, pages 9–23. Greenbelt, MD: NASA Goddard Space Flight Center, 2000.

Oubelkheir, K., H. Claustre, A. Sciandra and M. Babin. Bio-optical and biogeochemical properties of different trophic regimes in oceanic waters. *Limnology and Oceanography*, 50(6):1795–1809, 2005.

Pane, L., L. Radin, G. Franconi and A. Carli. The carotenoid pigments of a marine Bacillus firmus strain. *Boll. Soc. Ital. Biol. Sper.*, 72(11-12):303–8, 1996.

Pedros-Alio, C., J. I. Calderon-Paz, N. Guixa-Boixereu, M. Estrada and J. M. Gasol. Bacterioplankton and phytoplankton biomass and production during summer stratification in the northwestern Mediterranean Sea. *Deep Sea Research Part I: Oceanographic Research Papers*, 46(6):985–1019, 1999.

Pegau, W. S., D. Gray, and J. R. V. Zaneveld. Absorption and attenuation of visible and near-infrared light in water: dependence on temperature and salinity. *Applied Optics*, 36:6035–6046, 1997.

Piskozub, J. Effect of ship shadow on in-water irradiance measurements. *Oceanologia*, 46(1):103–112, 2004.

Pope, R. M. and E. S. Fry. Absorption spectrum (380–700 nm) of pure water. II. Integrating cavity measurements. *Applied Optics*, 36:8710–8723, 1997.

Preisendorfer, R. W. Application of radiative transfer theory to light measurements in the sea. *Union Geodetic and Geophysical International*, 10:11–29, 1961.

Preisendorfer, R. W. *Hydrological Optics.* 1976.

Preisendorfer, R. W. and C. D. Mobley. Albedos and Glitter Patterns of a Wind-Roughened Sea Surface. *Journal of Physical Oceanography*, 16(7):1293–1316, 1986.

Prieur, L. *Transfer radiatife dans les eaux der mer.* Ph.D. thesis, Univ. Pierre et Marie Curie, Paris, 1976.

Prieur, L. and S. Sathyendranath. An optical classification of coastal and oceanic waters based on the specific spectral absorption of phytoplankton pigments, dissolved organic matter, and other particulate materials. *Limnology and Oceanography*, 26(4):671–689, 1981.

Rabitti, S., G. Civitarese and M. Ribera d'Alcalá. Data Report Cruise POEM-BC-October 1991-Ionian Basin and Sicily Channel: II. Chemical and Biological Data. Technical report, Tech. Report No. 13/94 Venice: Istituto di Biologia del Mare, CNR, 1994.

Ragni, M. and M. Ribera d'Alcalá. Light as an information carrier underwater. *Journal of Plankton Research*, 26(4):433–443, 2004.

Ragni, M. and M. Ribera d'Alcalá. Circadian variability in the photobiology of Phaeodactylum tricornutum: pigment content. *Journal of Plankton Research*, 29(2):141–156, 2007.

Robarts, R. D., T. Zohary, M. J. Waiser and Y. Z. Yacobi. Bacterial abundance, biomass, and production in relation to phytoplankton biomass in the Levantine Basin of the southeastern Mediterranean Sea. *Marine Ecology Progress Series*, 137(1):273–281, 1996.

Robinson, A. R. and M. Golnaraghi. The Physical and dynamical oceanography of the Mediterranean sea. In Malanotte-Rizzoli, P. and A. R. Robinson, editors, *Ocean Processes in Climate Dynamics: Global and Mediterranean Examples.*, pages 255–306. NATO-ASI, Kluwer Academic Publishers, Dordrecht, The Netherlands, 1995.

Roesler, C. S., M. J. Perry and K. L. Carder. Modeling in Situ Phytoplankton Absorption from Total Absorption Spectra in Productive Inland Marine Waters. *Limnology and Oceanography*, 34(8):1510–1523, 1989.

Sarmiento, J. L., R. Slater, R. Barber, L. Bopp, S. C. Doney, A. C. Hirst, J. Kleypas, R. Matear, U. Mikolajewicz, P. Monfray, V. Soldatov, S. A. Spall and R. Stouffer11. Response of ocean ecosystems to climate warming. *Global Biogeochemical Cycles*, 18(3), 2004.

Sathyendranath, S., L. Lazzara and L. Prieur. Variations in the Spectral Values of Specific Absorption of Phytoplankton. *Limnology and Oceanography*, 32(2):403–415, 1987.

Sathyendranath, S. and T. Platt. Analytic model of ocean color. *Applied optics*, 36(12):2620, 1997.

Sathyendranath, S., L. Watts, E. Devred, T. Platt, C. Caverhill and H. Maass. Discrimination of diatoms from other phytoplankton using ocean-colour data. *Marine Ecology Progress Series*, 272:59–68, 2004.

Selph, K. E., J. Shacat and M. R. Landry. Microbial community composition and growth rates in the NW Pacific during spring 2002. *Geochemistry Geophysics Geosystems*, 6(12):doi:10.1029/2005GC000983, 2005.

Seritti, A., D. Russo, C. Santinelli, L. Nannicini, E. Murru and B. B. Manca. Vertical distribution of DOC in the Ionian Sea. In *Ocean biogeochemistry: a new paradigm JGOFS open science conference, Bergen, Norway.* 2000.

Siegel, D. A., S. Maritorena, N. B. Nelson and M. J. Behrenfeld. Independence and interdependencies among global ocean color properties: Reassessing the bio-optical assumption. *Journal of Geophysical Research*, 110(C7):C07011, 2005a.

Siegel, D. A., S. Maritorena, N. B. Nelson, M. J. Behrenfeld and C. R. McClain. Colored dissolved organic matter and its influence on the satellite-based characterization of the ocean biosphere. *Geophysical Research Letters*, 32:L20605, 2005b.

Siegel, D. A., S. Maritorena, N. B. Nelson, D. A. Hansell and M. Lorenzi-Kayser. Global distribution and dynamics of colored dissolved and detrital organic materials. *Journal of Geophysical Research*, 107(C12):3228, 2002.

Simis, S. G. H., M. Tijdens, H. L. Hoogveld, H. J. Gons and O. Journals. Optical changes associated with cyanobacterial bloom termination by viral lysis. *Journal of Plankton Research*, 27(9):937–949, 2005.

Smith, R. C. and K. S. Baker. The Bio-Optical State of Ocean Waters and Remote Sensing. *Limnology and Oceanography*, 23(2):247–259, 1978.

Smith, R. C. and K. S. Baker. Optical properties of the clearest natural waters (200–800 nm). *Applied Optics*, 20:177–184, 1981.

Smyth, T. J., G. H. Tilstone and S. B. Groom. Integration of radiative transfer into satellite models of ocean primary production. *Journal of Geophysical Research*, 110(C10), 2005.

Steinberg, D. K., N. B. Nelson, C. A. Carlson and A. Prusak. Production of chromophoric dissolved organic matter(CDOM) in the open ocean by zooplankton and the colonial cyanobacterium Trichodesmium spp. *Marine Ecology Progress Series*, 267:45–56, 2004.

Stomp, M., F. de Jongh, A. J. Veraart, D. Gerla, M. Rijkeboer, B. W. Ibelings, U. I. A. Wollenzien and L. J. Stal. Adaptive divergence in pigment composition promotes phytoplankton biodiversity. *Nature*, 432:104–107, 2004.

Stramska, M. and D. Stramski. Effects of a nonuniform vertical profile of chlorophyll concentration on remote-sensing reflectance of the ocean. *Applied Optics*, 44(9):1735–1747, 2005.

Stramski, D., E. Boss, D. Bogucki and K. J. Voss. Progress in Oceanography. *Progress in Oceanography*, 61:27–56, 2004.

Stramski, D., A. Bricaud and A. Morel. Modeling the inherent optical properties of the ocean based on the detailed composition of the planktonic community. *Appl. Opt*, 40(18):2929–2945, 2001.

Stramski, D. and D. A. Kiefer. Light scattering by microorganisms in the open ocean. *Progress in Oceanography*, 28(4):343–383, 1991.

Stramski, D. and D. A. Kiefer. Can heterotrophic bacteria be important to marine light absorption? *Journal of Plankton Research*, 20(8):1489, 1998.

Stramski, D. and C. D. Mobley. Effects of Microbial Particles on Oceanic Optics: A Database of Single-Particle Optical Properties. *Limnology and Oceanography*, 42(3):538–549, 1997.

Stramski, D., R. A. Reynolds, M. Kahru and B. G. Mitchel. Estimation of Particulate Organic Carbon in the Ocean from Satellite Remote Sensing. *Science*, 285:239–242, 1999.

Stramski, D. and J. Tegowski. Effects of intermittent entrainment of air bubbles by breaking wind waves on ocean reflectance and underwater light field. *Journal of Geophysical Research. C. Oceans*, 106:31345–31360, 2001.

Stramski, D. and S. B. Wozniak. On the role of colloidal particles in light scattering in the ocean. *Limnology & Oceanography*, 50(5):1581–1591, 2005.

Stumpf, R. P., M. E. Culver, P. A. Tester, M. Tomlinson, G. J. Kirkpatrick, B. A. Pederson, E. Truby, V. Ransibrahmanakul and M. Soracco. Monitoring Karenia *brevis blooms* in the Gulf of Mexico using satellite ocean color imagery and other data. *Harmful Algae*, 2(2):147–160, 2003.

Subramaniam, A., C. W. Brown, R. R. Hood, E. J. Carpenter and D. G. Capone. Detecting Trichodesmium blooms in SeaWiFS imagery. *Deep-Sea Research II*, 49(1-3):107–121, 2002.

Suttle, C. A. Viruses in the sea. *Nature*, 437(7057):356–361, 2005.

Sverdrup, H. U. On Conditions for the Vernal Blooming of Phytoplankton. *ICES Journal of Marine Science*, 18(3):287, 1953.

Sweeney, C., A. Gnanadesikan, S. M. Griffies, M. J. Harrison, A. J. Rosati and B. L. Samuels. Impacts of Shortwave Penetration Depth on Large-Scale Ocean Circulation and Heat Transport. *Journal of Physical Oceanography*, 35(6):1103–1119, 2005.

Tassan, S. and G. M. Ferrari. An alternative approach to absorption measurments of acquatic particles retained on filters. *Limnology and Oceanography*, 40(8):1358–1368, 1995a.

Tassan, S. and G. M. Ferrari. Measurement of light absorption by aquatic particles retained on filters: determination of the optical pathlength amplification by the 'trasmittance-reflectance' method. *Journal of Plankton Research*, 20(9):1699–1709, 1998.

Tassan, S. and G. M. Ferrari. A sensitivity analysis of the'Transmittance-Reflectance'method for measuring light absorption by aquatic particles. *Journal of Plankton Research*, 24(8):757, 2002.

Terrill, E. J., W. K. Melville and D. Stramski. Bubble entrainment by breaking waves and their influence on optical scattering in the upper ocean. *Journal of Geophysical Research*, 108:16, 2001.

Thurman, E. M. *Organic geochemistry of natural waters*. Kluwer Academic, 1985.

Trees, C. C., R. R. Bidigare, D. M. Karl and V. H. L. Fluorometric Chlorophyll a: Sampling, Laboratory Methods, and Data Analysis Protocols. In Fargion, G. and J. Mueller, editors, *Ocean Optics Protocols for Satellite Ocean Color Sensor Validation, Revision 2*, number Technical Memorandum 2000–209966, page 184. NASA, Greenbelt, MD NASA Goddard Space Flight Center, 2000.

Tyrrell, T., P. M. Holligan and C. D. Mobley. Optical impacts of oceanic coccolithophore blooms. *Journal of Geophysical Research*, 104(C2):3223–3242, 1999.

Vaillancourt, R. D., C. W. Brown, G. R. R. L. and B. W. M. Light backscattering properties of marine phytoplankton: relationships to cell size, chemical composition and taxonomy. *Journal of Plankton Research*, 26(2):191–212, 2004.

Vesk, M. and S. W. Jeffrey. Effect of blue-green light on photosynthetic pigments and chloroplast structure in unicellular marine algae from six classes. *J. Phycol*, 13:280–288, 1977.

Vidussi, F., J. C. Marty and J. Chiaverini. Phytoplankton pigment variations during the transition from spring bloom to oligotrophy in the Mediterranean Sea. *Deep-Sea Research*, 1(47):423–445, 2000.

Volpe, G., R. Santoleri, V. Vellucci, M. Ribera d'Alcalá, S. Marullo and F. D'Ortenzio. The colour of the Mediterranean Sea: Global versus regional bio-optical algorithms evaluation and implication for satellite chlorophyll estimates. *Remote Sensing of Environment*, 107(4):625–638, 2007.

Voss, K. J. A spectral model of the beam attenuation coefficient in the ocean and coastal areas. *Limnology and Oceanography*, 37(3):501–509, 1992.

Wells, M. L. Marine colloids: a neglected dimension. *Nature*, 391(6667):530, 1998.

Werdell, P. J. and S. W. Bailey. An improved in-situ bio-optical data set for ocean color algorithm development and satellite data product validation. *Remote Sensing of Environment*, 98(1):122–140, 2005.

Williams, N. MEETING BRIEFS: The Mediterranean Beckons to Europe's Oceanographers. *Science*, 279(5350):483–484, 1998.

Worden, A. Z. and B. J. Binder. Application of dilution experiments for measuring growth and mortality rates among Prochlorococcus and Synechococcus populations in oligotrophic environments. *Aquatic Microbial Ecology*, 30(2):159–174, 2003.

Yentsch, C. S. Measurement of Visible Light Absorption by Particulate Matter in the Ocean. *Limnology and Oceanography*, 7(2):207–217, 1962.

Zaneveld, J. R. V. Penetration of ultraviolet radiation into natural waters. In *Impacts of climatic change on the biosphere, Vol. 1, Ultraviolet Radiation Effects, CIAP Monograph.*, volume 5, pages 2–108. vol. 5, Natl. Tech. Inf. Serv., Springfield, Va., 1975.

Zaneveld, J. R. V., J. C. Kitchen and C. Moore. The scattering error correction of reflecting-tube absorption meters. In *SPIE*, volume 2258, pages 44–55. 1994.

Zepp, R. G., T. V. Callaghan and D. J. Erickson. Effects of increased solar ultraviolet radiation on biogeochemical cycles. *Ambio*, 24(3):181–7, 1995.

Zhang, X., M. Lewis and B. Johnson. Influence of bubbles on scattering of light in the ocean. *Appl. Opt*, 37(27):6525–6536, 1998.

Zhang, X., M. Lewis, M. Lee, B. Johnson and G. Korotaev. The Volume Scattering Function of Natural Bubble Populations. *Limnology and Oceanography*, 47(5):1273–1282, 2002.

Zohary, T. and R. D. Robarts. Experimental Study of Microbial P Limitation in the Eastern Mediterranean. *Limnology and Oceanography*, 43(3):387–395, 1998.

Contents

List of Tables

List of Figures